MATHEMATISCH-NATURWISSENSCHAFTLICHE FAKULTÄT

INSTITUT FÜR BIOCHEMIE UND BIOLOGIE

DISSERTATION

ZUM ERWERB DES AKADEMISCHEN GRADES

doctor rerum naturalium

Impact of microcystin on the non-canonical localization of RubisCO in the toxic bloom-forming cyanobacterium *Microcystis aeruginosa* PCC7806

vorgelegt von

Tino Barchewitz

Potsdam, 23.09.2020

Betreuerin: Prof. Dr. Elke Dittmann

2. Gutachter: Prof. Dr. Hans-Peter Grossart

3. Gutachterin: Prof. Dr. Ilka Axmann

Published online on the
Publication Server of the University of Potsdam:
https://doi.org/10.25932/publishup-50829
https://nbn-resolving.org/urn:nbn:de:kobv:517-opus4-508299

Erklärung

Hiermit erkläre ich, die vorliegende Arbeit eigenständig verfasst und keine anderen als die angegebenen Hilfsmittel und Quellen benutzt zu haben.

Potsdam, den 23. September 2020

……

Contents

SUMMARY

Cyanobacteria are an abundant bacterial group and are found in a variety of ecological niches all around the globe. They can serve as a real threat for eukaryotes like fish or mammals and can restrict the use of lakes or rivers for recreational purposes or as a source of drinking water, when they form blooms at the air-water interphase. One of the most abundant bloom-forming cyanobacteria is *Microcystis aeruginosa* PCC7806 that is found all around the world occurring is blooming events.

In the first part of the study, the role and possible dynamics of RubisCO during the establishment and maintenance of a dense bloom were examined. Therefore, low-light adapted *M. aeruginosa* cultures were shifted to high-light irradiation and its response was analyzed on the protein and peptide level via immunoblotting, immunofluorescence microscopy and with high performance liquid chromatography (HPLC). It was revealed that large amounts of RubisCO were located outside of carboxysomes under the applied high-light stress. RubisCO aggregated mainly underneath the cytoplasmic membrane. There it forms a putative Calvin-Benson-Bassham (CBB) super complex. This complex could be part of an alternative carbon-concentrating mechanism (CCM) in *M. aeruginosa*.

Furthermore, the relocalization of RubisCO was delayed in the microcystin-deficient mutant Δ*mcyB* and RubisCO was more evenly distributed over the cell in comparison to the wild type. The data in this study are in line with previous work about microcystin and its role as a protector against protein degradation through binding to the respective protein. Since Δ*mcyB* is not harmed in its growth, possibly other produced cyanopeptides as aeruginosin or cyanopeptolin also play a role in the stabilization of RubisCO and the putative CBB complex, especially in the microcystin-free mutant.

In the second part of this work, the possible role of microcystin as an extracellular signaling peptide during the diurnal cycle was studied. HPLC analysis showed a strong increase of extracellular microcystin in the wild type when the population entered nighttime and it resumed into the next day as well. Together with the increase of extracellular microcystin, a strong decrease of protein-bound intracellular microcystin

was observed via immunoblot analysis. Interestingly, the signal of the large subunit of RubisCO (RbcL) also diminished when high amounts of microcystin were present in the surrounding medium. Microcystin addition experiments to *M. aeruginosa* WT and Δ*mcyB* cultures support this observation, since the immunoblot signal of both subunits of RubisCO and CcmK, a shell protein of carboxysomes, diminished after the addition of microcystin. In addition, the fluctuation of cyanopeptolin during the diurnal cycle indicates a more prominent role of other cyanopeptides besides microcystin as a signaling peptide, intracellularly as well as extracellularly.

This work gives new insights into the processes, which take place during the adaptation of *M. aeruginosa* to high-light conditions. The hypothesized alternative CCM located underneath the cytoplasmic membrane gives *M. aeruginosa* an advantage over other cyanobacteria, which only possess the canonical carboxysome-based CCM. Furthermore, the presented results strengthen the idea of microcystin as a signaling molecule as the main extracellular function instead of the toxic effect against other organisms.

1. Introduction

1.1 Cyanobacteria – ecological role and bloom formation

Cyanobacteria are gram-negative bacteria with an autotrophic mode of live and their evolutionary history dates back around 2.6 billion years (Schirrmeister *et al.*, 2016; Shih *et al.*, 2017). The name “cyanobacteria” originates from the blue-greenish color of the bacteria, which is primarily caused by phycocyanobilins, the characteristic photosynthetic antennae pigment in cyanobacteria. Chlorophyll is the pigment found in photosynthetic reaction centers of cyanobacteria, which closely resemble reaction centers in chloroplasts of plants. It is considered that chloroplasts evolved from an endosymbiotic cyanobacterium in a plant cell (McFadden, 1999; Hohmann-Marriott and Blankenship, 2011). Furthermore, cyanobacteria are considered responsible for the oxygenation of the Earth’s atmosphere (“The Great Oxygenation”), which enabled multicellular life on Earth due to their ability to perform oxygenic photosynthesis.

Cyanobacteria occur in a variety of habitats all around the world. They are found in terrestrial habitats such as soil, bare or partly moistened rocks, deserts or even Antarctic rocks, where they form or are part of biofilms and microbial mats (Gaysina *et al.*, 2018). In these habitats, cyanobacteria play a major part in maintaining microbial mats, because of the increased tolerance against desiccation and water stress. Another important ecological role of cyanobacteria is their function as nitrogen fixers. Cyanobacteria are only one of a few groups of organisms which can convert the atmospheric nitrogen into bioavailable forms of nitrogen for other organisms (Whitton and Potts, 2006). Due to this ability, they are often found in symbioses with higher plants (e.g. legumes) and fungi (lichens). Besides terrestrial habitats, cyanobacteria also occur in marine environments as well as in freshwater habitats for example ponds, lakes, or rivers. There, they appear as planktonic cells or biofilms. In biotechnological approaches, cyanobacteria are often used as primary producers. Cyanobacteria possess a large and versatile secondary metabolome, which characterizes them as a rich source of bioactive compounds with antibacterial, antiviral or antifungal effects (Kajiyama *et al.*, 1998; Jaki *et al.*, 2000; Abed *et al.*, 2009). Several cyanobacterial

genera produce polyhydroxyalkanoates (PHA), which are used as bioplastics. Hydrogen gas produced by cyanobacteria is an alternative energy source to replace fossil fuel resources (Abed *et al.*, 2009; Al-Haj *et al.*, 2016). However, a feature of cyanobacteria that is often in focus of research and the public, is their ability to form blooms on top of water surfaces.

A cyanobacterial bloom (CyanoHAB) is characterized as a visible discoloration of the water caused by cyanobacteria. It can be either macroscopically visible colonies of cyanobacteria in the whole waterbody or a cyanobacterial scum on top of the water surface (Figure 1A-C). Typical bloom-forming genera are *Aphanizomenon*, *Cylindrospermopsis*, *Dolichospermum*, *Microcystis*, *Nodularia*, *Planktothrix* and *Trichodesmium* (Huisman *et al.*, 2018). Studies from Lake Taihu (China), one of the major studies sites of cyanobacterial blooms worldwide, showed a strong correlation between nitrogen and phosphorus loading in the lake and the occurrence of CyanoHABs. The more nitrogen/phosphorus, the higher the concentration of cyanobacteria in the lake (Xu *et al.*, 2017). This increased load of nutrients causes a switch from mesotrophic to hypertrophic conditions.

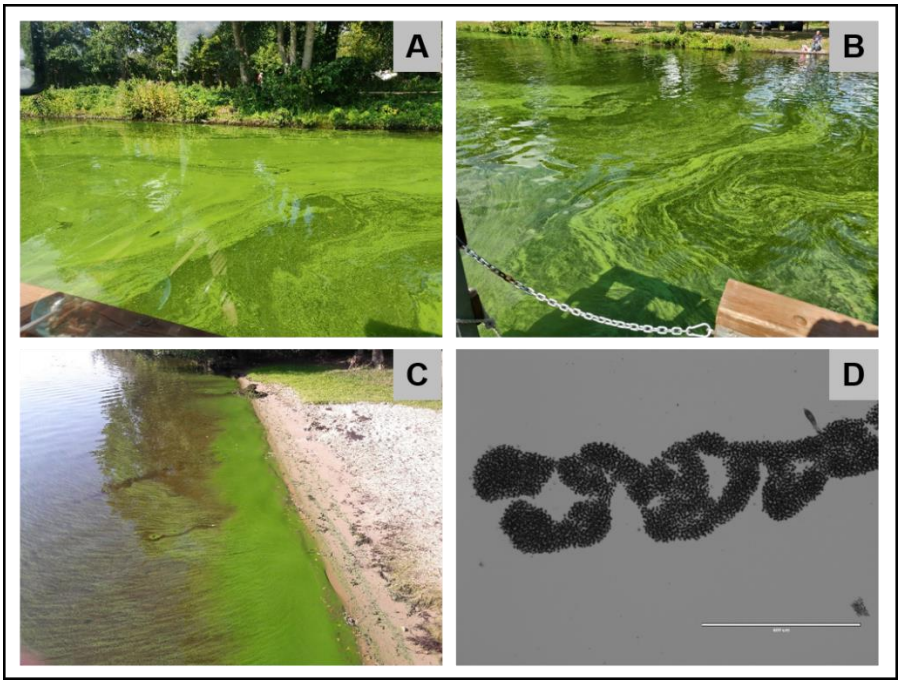

Figure 1. Cyanobacterial blooms. **(A-B)** Microcystis aeruginosa bloom in the river Havel near Potsdam (Caputher Gemünde), Germany, 21st of August 2019. **(C)** M. aeruginosa bloom at the shore of river Havel, Potsdam, Germany, 30th of August 2017. **(D)** Microscopic picture of M. aeruginosa culture from the bloom in image C.

Several traits of cyanobacteria give them an advantage over eukaryotic phytoplankton. Many of bloom-forming cyanobacteria are nitrogen-fixing bacteria (*Aphanizomenon*, *Cylindrospermopsis*, *Dolichospermum*, *Nodularia*), which enables them to use atmospheric nitrogen. The carbon-concentrating-mechanism (CCM) of cyanobacteria gives them an advantage especially under CO_2-limited conditions. Furthermore, since several bloom-forming genera possess gas vesicles (*Aphanizomenon*, *Microcystis*, *Trichodesmium*) and build a large mat on top of the water surface, they shade other organisms and consume most of the atmospheric CO_2. The gas vesicles also allow them to change their position in the water column to adapt to the best light and nutrient conditions (Huisman *et al.*, 2018). It is to notice, that one bloom is mostly dominated by only one cyanobacterium. All these blooms have in common, that a large variety of heterotrophic bacteria are associated with one bloom. Heterotrophic bacteria are organisms, which use organic material as their nutrients. The composition of this bacterial community appears quite dynamic, depending on the environmental conditions rather than the dominating cyanobacterium. Especially, the organic matter pool dynamics seem to have a large influence on the composition of the microbial community. Often, the associated bacteria of cyanobacteria are comprised of stable and dominant taxa (Woodhouse *et al.*, 2018; Cook *et al.*, 2020). Members of the phyla *Proteobacteria*, *Bacteroidetes*, *Actinobacteria* and *Firmicutes* are often found in cyanobacterial blooms (Katri A. Berg *et al.*, 2009; Li *et al.*, 2018).

The occurrence of blooms often has direct and indirect effects on the environment. Indirect effects of the dense structure of a bloom are an increased turbidity of the underneath water which influences other photosynthetically active or living organisms in their growth. In addition, the taste and smell of a CyanoHAB can affect recreational purposes of lakes or rivers. The produced compounds of the cyanobacteria often cause direct effects of blooms. Several produced secondary metabolites can be harmful or even toxic to other organisms. CyanoHABs can stress or even cause death of fish, birds or mammals due to released toxins or oxygen depletion because of the dense growth (Carmichael, 2001; Rabalais *et al.*, 2010). Another direct threat of cyanobacterial blooms is the influence on water management, especially in lakes or water reservoirs, which are used for drinking water. Especially because of their direct threat to other organisms and water management, cyanobacterial toxins and the major producing bloom-forming strains are extensively studied.

1.2 *Microcystis aeruginosa*

Microcystis aeruginosa is one of the main toxic bloom-forming cyanobacterial species worldwide. It is a single-cell cyanobacterium and is mainly found in freshwater, where it was originally isolated (Braakman water reservoir, The Netherlands) (Frangeul *et al.*, 2008). Some strains can as well be found in brackish water (Tanabe *et al.*, 2018; des Aulnois *et al.*, 2019). Although *M. aeruginosa* is a single-celled organism, in nature it most often occurs as cell colonies. The taxonomy of the different *Microcystis* species is mainly based on the different colony morphotypes. Since the classification based on morphological features does not reassemble genomic studies, the current taxonomy of *Microcystis* species can be challenged (Xiao *et al.*, 2018).

A well-known appearance of *M. aeruginosa* in rivers and lakes is in form of a bloom (Figure 1). The formation of colonies or even blooms has many advantages for a single-cell bacterium like *M. aeruginosa*: adaptation to varying light conditions, persistent growth under nutrient stress and protection from mechanical as well as chemical stresses (Xiao *et al.*, 2018). Since the growth of a cyanobacterial blooms inhibits the growth of other organisms in the direct vicinity, the formation of a bloom also increases the biomass of *M. aeruginosa* in relation to the surrounding organisms. Another feature of *M. aeruginosa*, which supports the formation of a bloom, is the existence of gas vesicles. These enable the cell to change their height in the water column, thus they can be in optimal spot of the water column depending on light conditions, nutrient availability, etc. (Walsby, 1994).

When *M. aeruginosa* is growing in a bloom, it is always exposed to other organisms. Secondary metabolites produced by *M. aeruginosa* can play an important part in direct interactions with other microorganisms. Several studies display *M. aeruginosa* can inhibit the growth of competing green eukaryotic algae through allelopathic interactions. Released linoleic acid by *M. aeruginosa* inhibits the growth of *Chlorella vulgaris*, a model green alga. Secreted nitric oxide of *C. vulgaris* stimulates the positive feedback loop of linoleic acid production (Song *et al.*, 2017). Even non-toxic *M. aeruginosa* strains can affect the growth of green algae, which also shows the allelopathic interaction is not solely based on the secretion of toxic peptides by *M. aeruginosa* (Bittencourt-Oliveira *et al.*, 2014). Taken together, the interaction with other microorganisms clearly supports the growth of *M. aeruginosa* in comparison to

monocultures of it (Zhang *et al.*, 2019). Furthermore, *M. aeruginosa* can synthesize and excrete several small peptides as secondary metabolites which makes *M. aeruginosa* blooms a direct threat for the environment and a major study field for research. One of the most known and best studied peptides of *M. aeruginosa* is the cyclic hepatotoxin microcystin. In addition, *M. aeruginosa* PCC 7806 can produce two other lesser studied small peptides: cyanopeptolin and aeruginosin. Most of the experiments in this work were performed with *Microcystis aeruginosa* PCC 7806. In the following work, *M. aeruginosa* refers to *M. aeruginosa* PCC 7806, if not stated otherwise.

1.3 Cyanopeptides of *M. aeruginosa*

Cyanobacteria are a phylum with a large secondary metabolome including a variety of non-ribosomal oligopeptides, which are called cyanopeptides. Due to their effect on the environment and water management (Janssen, 2019), microcystins are by far the most studied cyanopeptides. However, cyanobacteria can produce many other small peptides, which also can act as toxins or fulfill intracellular functions. The produced peptides are a concern for water management since they are released directly into the surface waters when cells release the toxin actively or passively via cell lysis (Flores and Caixach, 2015). The synthesis of such oligopeptides is a very energy costly process since most of them are produced non-ribosomally. The non-ribosomal peptide synthetases (NRPS) and the polyketide synthases (PKS), where the oligopeptides are synthesized, are large multienzyme machineries. They are organized in a modular structure, which means that every module is responsible for the synthesis of one amino acid (Keatinge-Clay, 2017; Süssmuth and Mainz, 2017). Furthermore, every module is made up of several proteins. For the synthesis of a second oligopeptide in one cell, other enzymes and modules are needed. This makes the biosynthesis of non-ribosomal oligopeptides very costly for the cell and therefore it is of special interest, why *M. aeruginosa* for example, produces even three different oligopeptides. In the following, the three oligopeptides microcystin, cyanopeptolin and aeruginosin of *M. aeruginosa* are introduced and characterized.

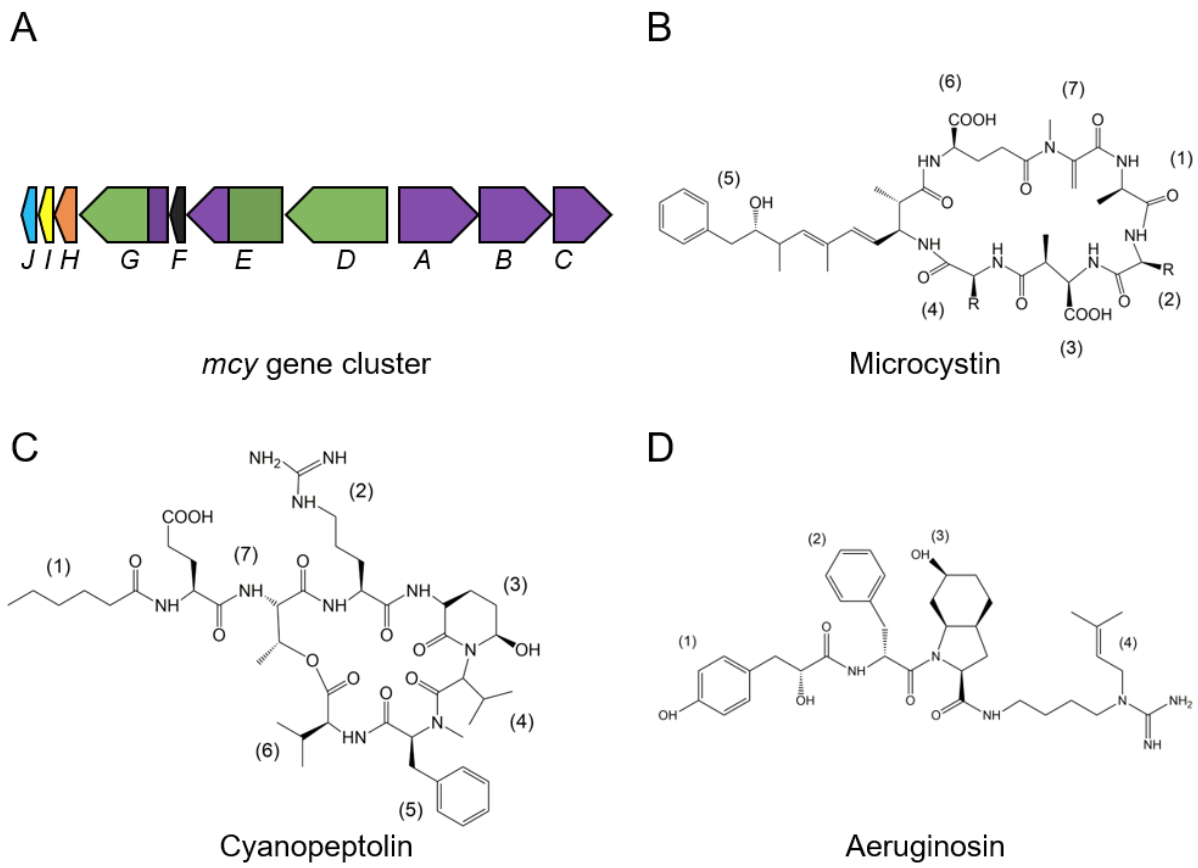

Figure 2. Structures of the cyanopeptides microcystin, cyanopeptolin and aeruginosin and the gene cluster for microcystin biosynthesis. After *Tillett* et al*., 2000* and *Janssen, 2019*. **(A)** Mcy gene cluster for MC synthesis after *Tillett* et al*., 2000*. The purple bars represent peptide synthetase genes and the orange bars polyketide synthase genes. The black bar shows aspartate racemase genes, the orange bar ABC transporters genes, the yellow bar dehydrogenase genes, and the blue bar thioesterase genes. **(B)** General structure of microcystins. (1) Ala, (2) variable position 2, (3) N-methyl-Asp, (4) variable position 4, (5) Adda, (6) Glu, (7) N-methyl-dehydro-Ala. **(C)** Example structure of cyanopeptolin. (1) fatty acid, (2) Arg, (3) Ahp, (4) Leu, (5) methyl-Phe, (6) Val, (7) Thr. **(D)** Example structure of aeruginosin. (1) Hpla, (2) Ile, (3) Choi, (4) Arg.

1.3.1 Microcystin

Microcystins (MC) are cyclic heptapeptides, which possess several unusual amino acids. One characteristic amino acid for microcystins is 9-methoxy-2,6,8-trimethyl-10-phenyldeca-4(E),6(E)-dienoic acid (ADDA). Every microcystin shares the structure cyclo(-D-Ala-L-**2**-D-MeAsp-L-**4**-Adda-D-Glu-Mdha), whereas (2) and (4) are variable L-amino acids (Figure 2B). *M. aeruginosa* PCC 7806 produces MC-LR and [D-Asp3] microcystin-LR. These microcystin types contain leucine (L) in position 2 and arginine (R) in position 4. Additionally, [D-Asp3]MC-LR has a demethylated D-MeAsp to Asp (Carmichael *et al.*, 1988). Not only *Microcystis* is capable of producing microcystin, but also other cyanobacterial genera like *Dolichospermum*, *Oscillatoria* and *Planktothrix*

produce microcystins (Huisman *et al.*, 2018). Microcystins are synthesized non-ribosomally via a mixed nonribosomal peptide synthetase/polyketide synthase (NRPS/PKS) pathway. The biosynthesis pathway and by this the involved genes differ between the different genera (Christiansen *et al.*, 2003). The following biosynthesis is shown such as the example of *M. aeruginosa* PCC 7806 displays (Figure 2A). In general, two operons (*mcyA-C* and *mcyD-J*) are involved in this process, which is a cascade of 48 sequential catalytic reactions (Tillett *et al.*, 2000). McyA-C are three NRPS modules, McyD a PKS and McyE and G hybrid enzymes of NRPS/PKS modules. These catalytic domains perform 45 out of the 48 catalytic reactions, including the incorporation of the precursors phenylpropionate, malonyl-CoA, S-adenosyl-L-methionine, glutamate, serine, alanine, leucine, D-methyl-isoaspartate, and arginine. Also, the monofunctional proteins carry out O-methylation (McyJ), epimerization (McyF), dehydration (McyI), and localization (McyH). The assembly of MC starts with the synthesis of ADDA at the hybrid cluster McyG, where a phenylalanine-derived phenylpropionate starter unit gets activated (Tillett *et al.*, 2000; Rastogi *et al.*, 2014). Furthermore, in the synthesis of ADDA also McyJ, McyD, McyE and McyF are involved. After the synthesis of ADDA, the full oligopeptide is produced by the remaining modules McyE, McyA, McyI, McyB and McyC. Afterwards, the peptide is released. Intra- and extracellular functions of MC are presented in a later chapter (1.4).

1.3.2 Cyanopeptolin

Cyanopeptolin is another oligopeptide produced by *M. aeruginosa* and other bloom-forming cyanobacterial genera such as *Anabaena* or *Planktothrix*. Examinations of the biosynthesis gene clusters revealed that these genes evolved independently from each other within each genus (Rounge *et al.*, 2007). They all have in common that cyanopeptolin is produced via an NRPS (Tooming-Klunderud *et al.*, 2007). A study of the Great Lake Basin in the U.S. showed that cyanopeptolin occurred on a comparable level such as microcystin in drinking water treatment plants (Beversdorf *et al.*, 2018). The lack of available standards of cyanopeptolin or other cyanopeptides hinders the quantification of small peptides besides microcystin on a regular basis. Cyanopeptolins are hexapeptides with a characteristic Ahp moiety (3-amino-6-methoxy-2-piperidone). Furthermore, they are depsipeptides with a β-lactone ring and carry a fatty acid. Only (3) Ahp and (7) Threonine are shared by all cyanopeptolins; the other amino acids are

variable between the different forms (Figure 2C) (Janssen, 2019). Cyanopeptolins inhibit the human serine proteases trypsin or chymotrypsin (Bister *et al.*, 2004; Von Elert *et al.*, 2005). Additionally, cyanopeptolins act as toxins against the grazing crustacean *Thamnocephalus platyurus* to prevent the cyanobacterium from getting eaten (Gademann *et al.*, 2010). Another toxic effect was shown with zebrafish embryos, where cyanopeptolin acts as a neurotoxin since it affects DNA damage repair and regulation of the circadian rhythm (Faltermann *et al.*, 2014). Transcriptomic analyses of *M. aeruginosa* in a diurnal cycle show that cyanopeptolin biosynthesis genes are transcribed only during day time as other secondary metabolites (Straub *et al.*, 2011). Light intensity, temperature and phosphorus limitation influence the cyanopeptolin production in *M. aeruginosa* as well the salinity in brackish-water strains (Tonk *et al.*, 2009; des Aulnois *et al.*, 2019). Unfortunately, there is a lack of studies about the physiology role of cyanopeptolins and especially about a possible intracellular role.

1.3.3 Aeruginosin

The third produced cyanopeptide of *M. aeruginosa* is aeruginosin. As cyanopeptolins, they are also synthesized by the bloom-forming cyanobacterium *Planktothrix*. Aeruginosins are produced by an NRPS, but the gene clusters differ largely within the individual producing organisms. A structural difference between aeruginosins and microcystins / cyanopeptolins is the structure as a linear peptide. Characteristic for the tetrapeptide aeruginosin is the unusual (4-hydroxy)phenyl lactic acid (Hpla), 2-carboxy-6-hydroxyoctahydroindole (Choi) moieties and an arginine derivative at the C terminus (Figure 2D) (Ishida *et al.*, 1999). An effect aeruginosins have in common with several other cyanopeptides of *M. aeruginosa*, excluding microcystin, is the inhibition of human serine proteases like thrombin or trypsin (Murakami *et al.*, 1994; Kodani *et al.*, 1998). The physiological role of aeruginosin besides the toxic effect is still unknown. It appears that the expression of the biosynthesis genes is linked to the diurnal cycle of *M. aeruginosa* since the genes are only expressed during day time (Straub *et al.*, 2011).

1.4 Intra- and extracellular functions of microcystin

Microcystins are a severe threat to other organisms since they inhibit eukaryotic protein phosphatases. This can lead to liver and kidney damage, gastroenteritis or tumor promotion in mammals (Huisman *et al.*, 2018). All effects of the toxin on the environment require the release of the toxin from the producing cell. Large parts of the free MC in a bloom result from cell lysis, even though *M. aeruginosa* is able to actively secrete MC (Cordeiro-Araújo and Bittencourt-Oliveira, 2013; Rastogi *et al.*, 2014). The role of MC as a signaling molecule is described in a later chapter (see 1.8). Even though MC acts as a toxin, several points indicate the toxic function of MC is not the main or original function of it. Since MC-producing bacteria existed before eukaryotes evolved, the original function of MC cannot be the inhibition or killing of other eukaryotes (Rantala *et al.*, 2004). In addition, the strong phenotype of MC-deficient mutants further indicate that MC has an important role for the producing cyanobacterium itself (Zilliges *et al.*, 2011). These potential functions will be illustrated hereafter.

A general feature of microcystin is the bond to a variety of different proteins (Table 1). The methylene group of the Mdha moiety of MC interacts with thiol groups of cysteines via Michael addition, which leads to the binding of MC to the protein. It is not clearly resolved, if the binding of MC to cysteines of the targeted protein is reversible or not. It seems that the reversibility depends on several parameters. A higher pH of the culture could lead to a reversible conjugation of MC with other proteins as well as temperature or the pool of free and protein bound MC may influence the reversibility of the conjugation (Zilliges *et al.*, 2011; Miles *et al.*, 2016). In general, the major part of intracellular MC can be found in the protein-bound fraction and not as free MC. This is true for laboratory cultures and field samples (Meissner *et al.*, 2013; Wei *et al.*, 2016) The binding of MC to proteins is enhanced under stress conditions such as high-light irradiation, oxidative stress or increased temperatures (Dziallas and Grossart, 2011; Zilliges *et al.*, 2011). Especially, enzymes involved in photosynthesis and carbon metabolism are binding partners of microcystin: small and large subunits of RubisCO, phosphoribulokinase, phosphoglycerate kinase, aldolase or G3P dehydrogenase. Additionally, MC also binds for example to the ATP synthase subunit alpha (ATP biosynthesis), 60 kDa chaperonin (protein folding and assembly) and glutathione

reductase (biosynthesis of cofactors) (Zilliges *et al.*, 2011; Wei *et al.*, 2016). Experiments with *M. aeruginosa* under various stress conditions as high-light irradiation, hydrogen peroxide treatment or depletion of iron show an increased protein-binding of MC. This binding leads to a lower sensitivity to proteases or oxidative stress of the bound protein (Zilliges *et al.*, 2011). The interaction of MC with several enzymes of photosynthesis already suggests that MC is directly involved into key process of carbon uptake and photosynthesis.

Table 1. Binding partners of microcystin. Shown are binding partners of MC and to which metabolic pathway they belong. Data from *Zilliges* et al*., 2011; Wei* et al*., 2016*.

MC binding partner	**Category**
Small subunit of RubisCO (RbcS)	Photosynthesis
Large subunit of RubisCO (RbcL)	Photosynthesis
Phosphoribulokinase (PRK)	Photosynthesis
Phosphoglycerate kinase	Photosynthesis
Fructose-bisphosphate aldolase	Photosynthesis
Glyceraldehyde-3-phosphate dehydrogenase	Photosynthesis
Phycocyanin alpha subunit	Photosynthesis
Phycocyanin beta subunit	Photosynthesis
Allophycocyanin alpha subunit	Photosynthesis
Glutathione reductase	Biosynthesis cofactors
60 kDa chaperonin	Protein folding, assembly
ATP synthase alpha subunit	ATP biosynthesis
Acetyl-CoA-acetyltransferases	Transferase for acetylation

1.5 CO_2 adaptation of *M. aeruginosa* and the role of microcystin

To assess the physiological role of microcystin, several studies were performed with the *M. aeruginosa* wild type and an MC-deficient mutant strain Δ*mcyB* (Dittmann *et al.*, 1997). A crucial challenge of cyanobacteria and therefore *M. aeruginosa,* is to adapt to different inorganic carbon (CO_2) conditions since CO_2 is the principal carbon source of *Microcystis*. Two independent studies examined the response of the *M. aeruginosa* WT and the MC-free mutant Δ*mcyB* to different CO_2 concentrations (Jähnichen *et al.*, 2007; Van De Waal *et al.*, 2011). The results show clearly the WT has an advantage over Δ*mcyB* under low carbon conditions, thus the WT outcompetes Δ*mcyB* under these conditions. Surprisingly, at high CO_2 concentrations the MC-deficient mutant outcompetes the WT and has a growth advantage. These studies indicate that MC clearly interferes with inorganic carbon adaptation and may play a key role in the adaptation to different CO_2 conditions with a supporting effect under carbon limitation.

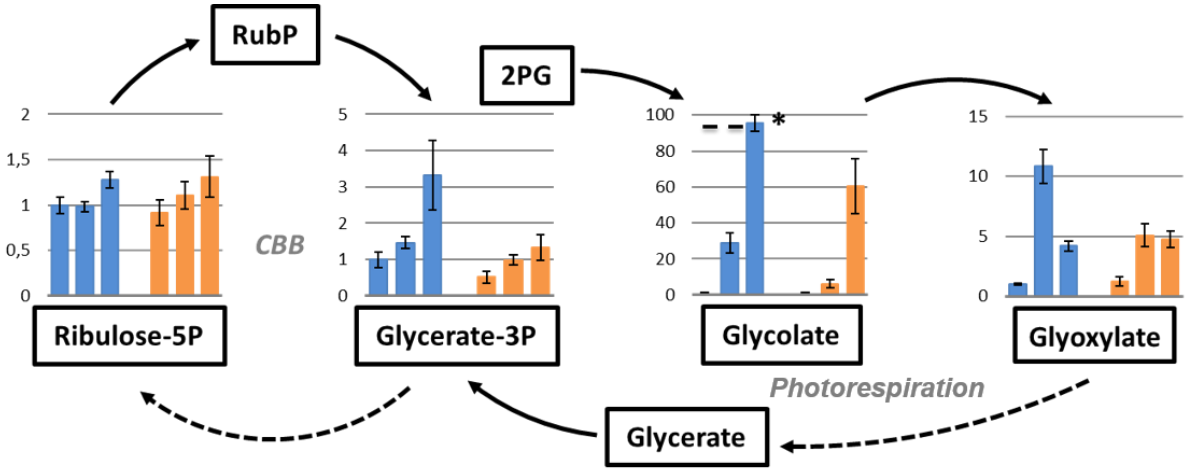

Figure 3. Steady-state levels of key metabolites of Calvin-Benson-Bassham cycle (CBB) and photorespiration. Data from *Meissner* et al.*, 2015*. Blue bars show data of M. aeruginosa WT and orange bars of M. aeruginosa ΔmcyB. For both strains, levels after 0 h high-light (250 µmol photons m^{-2} s^{-1}; HL), 1 h and 4 h HL are shown from left to right for each metabolite. The glycolate level after 4 h HL in the WT is marked with an asterisk to indicate the high value. RubP: Ribulose-1,5-bisphosphate, Glycerate-3-P: Glycerate-3-phosphate, Ribulose-5P: Ribulose-5-phosphate, 2PG: 2-phosphoglycerate.

Another interesting study shows that both strains, the WT and the MC-deficient Δ*mcyB*, differ significantly in their metabolic response to high-light stress (Figure 3) (Meissner *et al.*, 2015). MC may influence the fitness of *M. aeruginosa* strongly under light stress. Furthermore, the study revealed strong differences between *M. aeruginosa* and the model cyanobacterium *Synechocystis* sp. PCC 6803. The *M. aeruginosa* WT dispalys a faster accumulation of glycogen in comparison to Δ*mcyB* during high-light irradiation.

The accumulated glycogen is used as ballast to actively sink towards deeper water layers as an adaptation to changing light conditions. In turn, the MC-deficient mutant accumulates general stress markers such as trehalose and sucrose indicating the stabilizing role of MC. Microcystin also influences the oxygenation reaction of RubisCO, which results in a faster accumulation of glycolate in the wild type in comparison to Δ*mcyB* (Figure 3). *Synechocystis* PCC 6803 shows a considerably lower rate of photorespiration then *M. aeruginosa*. This difference cannot be explained solely by the stabilizing effect of MC, because also the MC-deficient mutant shows a pronounced accumulation of 2-phosphoglycolate (2-PG). However, the wild type produces 2-PG even faster and at a higher rate, which hints an important role of MC in photorespiration (Meissner *et al.*, 2015). The insensitivity of *M. aeruginosa* to oxygen fixation products of the carboxylase activity of RubisCO is potentially an advantage over other cyanobacteria. This phenotype could also be observed with a carboxysome-deficient mutant of *Synechocystis* PCC 6803, where oxygenase products of RubisCO accumulated inside of the cell (Hackenberg *et al.*, 2012). Furthermore, these results strongly indicate that *M. aeruginosa* probably adapts differently to changing carbon conditions than other cyanobacteria. MC plays a major role in this process by interfering with key enzymes of photosynthesis and the CBB cycle like RubisCO.

1.6 The Calvin-Benson-Bassham cycle, photorespiration and RubisCO

1.6.1 Calvin-Benson-Bassham cycle

In the Calvin-Benson-Bassham (CBB) cycle, CO_2 is the carbon source for the synthesis of glucose. The fixation of CO_2 is achieved by the carboxylation of Ribulose-1,5-bisphosphate (RuBP) as the first step of the CBB cycle (Figure 4). This reaction is catalyzed by the ribulose-1,5-bisphosphate carboxylase/oxygenase (RubisCO) (Farazdaghi, 2009). Since this step is a crucial part of photosynthesis and carbon metabolism and RubisCO shows a slow reactivity, it is considered one of the most abundant proteins on the earth (Ellis, 1979). The resulting intermediate (3-keto-2-carboxyarabinitol 1,5-bisphosphate) of the carbon fixation step is immediately split into 2 molecules of 3-phosphoglycerate (3-PGA). After the phosphorylation of 3-PGA to glyceraldehyde-3-phosphate (G3P), which is energy consuming, G3P is used for

different pathways. It can be used as an immediate nutrient source; to synthesize glucose via glycolysis; or for longtime carbon storage in the form of glycogen. The remaining G3P is used to regenerate RuBP. Since one CO_2 molecule generates two molecules of G3P and five molecules of G3P are necessary for regeneration of RuBP, three molecules of CO_2 need to be fixed for the net gain of one G3P molecule (Raines, 2003).

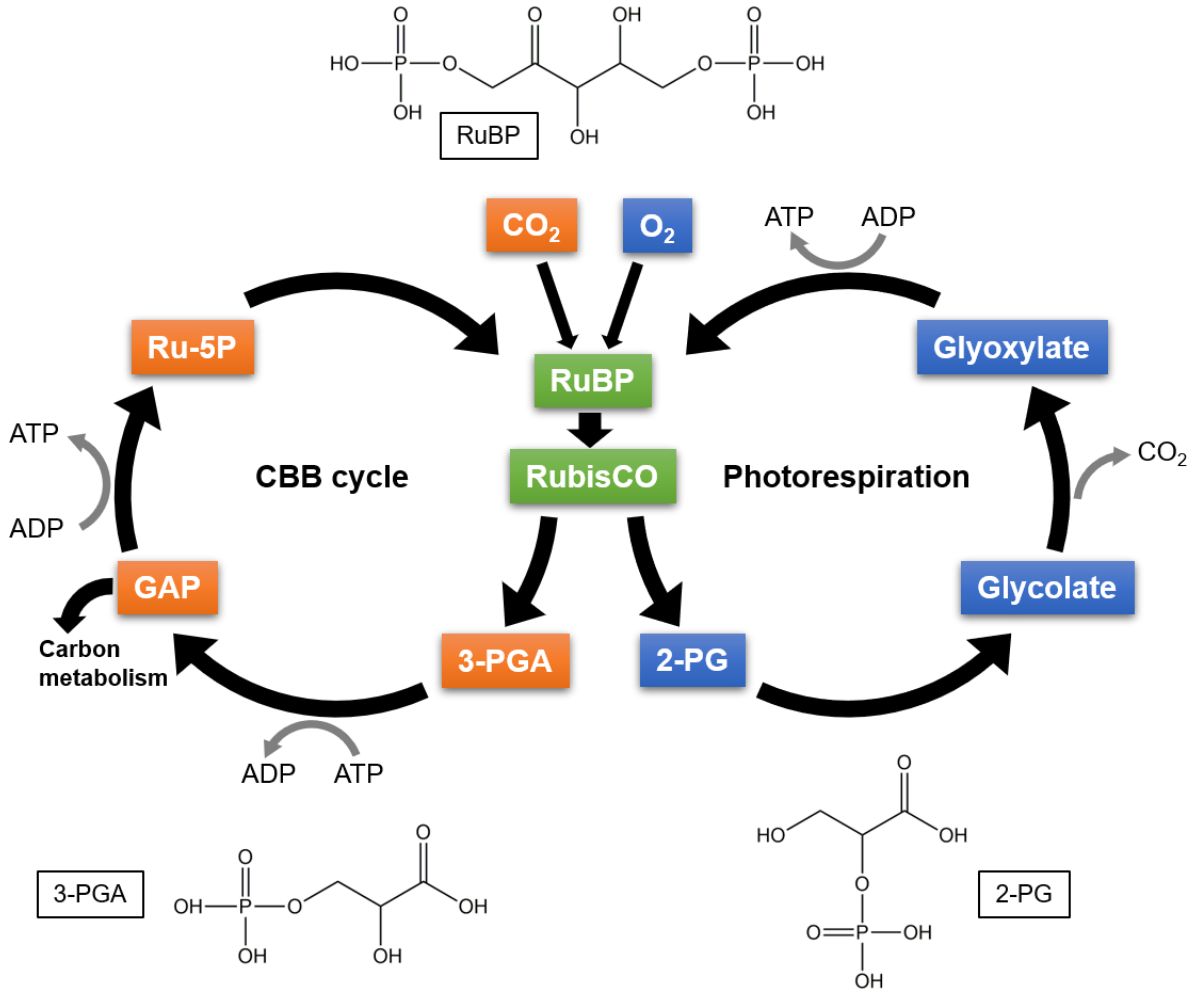

Figure 4. Scheme of CBB cycle and photorespiration. The Calvin-Benson-Bassham (CBB) cycle is the left cycle, the photorespiration pathway the left cycle. Energy consumption, energy gain and loss of CO_2 are marked with gray arrows. Additionally, the structures of RuBP, 3-PGA and 2-PG are displayed. RuBP: Ribulose-1,5-bisphosphate, 3-PGA: 3-phosphoglycerate, GAP: Glyceraldehyde-3-phosphate, Ru-5P: Ribulose-5-phosphate, 2-PG: 2-phosphoglycerate. This figure was inspired by *Xu* et al.*, 2015*

1.6.2 Photorespiration

One feature of RubisCO, which by itself interferes with the carbon fixation, is the oxygenase activity of the enzyme. Besides catalyzing the carboxylation of RuBP, RubisCO also catalyzes the oxygenation of RuBP. The following pathway is called photorespiration, because oxygen and energy are consumed and CO_2 is generated as

one of the products, as in the cellular respiration (Orf *et al.*, 2016) (Figure 4). In brief, the oxygenation of one molecule of RuBP leads to one molecule of 3-PGA (used in the CBB cycle) and one molecule of 2-PG (Hagemann *et al.*, 2013). 2-PG and also the following products of photorespiration, glycerate and glyoxylate, are thought to be intracellular toxins (Campbell and Ogren, 1990). For instance, enzymes of the CBB cycle are inhibited by 2-PG (Igamberdiev and Kleczkowski, 1977; Husic *et al.*, 1987). Even though energy and carbon are consumed during this process, photorespiration is not a “wasteful” pathway. Studies in land plants show photorespiration is linked to nitrogen assimilation and that engineered plants with a modified pathway are inhibited in their growth (Rachmilevitch *et al.*, 2004; Bloom *et al.*, 2010). Furthermore, photorespiration is a significant source of hydrogen peroxide (H_2O_2), which is the main contributor to the controlling of the redox homeostasis of a cell (Foyer *et al.*, 2009).

1.6.3 RubisCO

Depending on the function and composition of the enzyme there are different types of RubisCO (Table 2). Form I and II have photosynthetic functions, whereas form III and IV have non-photosynthetic functions. Form I is found in autotrophic proteobacteria, eukaryotic algae, higher plants and cyanobacteria. It consists of two subunits: the large subunit RbcL and the small subunit RbcS. A fully assembled Form I RubisCO contains of 4 RbcL dimers and 8 RbcS units (L_8S_8) (Badger and Price, 2003). Since different Form I RubisCOs exist, based on the large subunit type, it is classified into Form 1A, B, C and D. This grouping led to the classification of cyanobacteria into two big phylogenetic groups: α-cyanobacteria (Form 1A RubisCO) and β-cyanobacteria (Form 1B RubisCO) (Badger *et al.*, 2002). Form II RubisCO is simpler and is comprised of two identical large subunits or pluralities of it ($(L_2)_n$); it can be found in Dinoflagellates and some proteobacteria (Morse *et al.*, 1995). The non-photosynthetically active Form III is presented in some archaea and fulfills the function of RuBP regeneration (Tabita *et al.*, 2007). Lastly, Form IV RubisCO is also called RubisCO-like protein, since it is structurally similar to other RubisCO types but involved in the sulfur metabolism (Hanson and Tabita, 2001).

Table 2. RubisCO types. All known RubisCO forms are shown, with their typical subunit composition (L: large subunit; S: small subunit), if the RubisCO form shows a RubisCO activity (+: possesses RubisCO activity; -: does not possess RubisCO activity) and the phylogenetic distribution of the RubisCO form.

RubisCO type	Subunit composition	RubisCO activity	Phylogenetic distribution
Form I-A	L_8S_8	+	α-Cyanobacteria, Proteobacteria, Green algae, Plants
Form I-B	L_8S_8	+	β-Cyanobacteria, Proteobacteria, Green algae, Plants
Form I-C	L_8S_8	+	Chloroflexi, Proteobacteria
Form I-D	L_8S_8	+	Non-green algae, Proteobacteria
Form II	$(L_2)_n$	+	Dinoflagellates, Proteobacteria
Form III	$(L_2)_n$	+	Archaea
Form IV	variable	-	Archaea, Bacteria, Algae

1.7 Carbon concentrating mechanism (CCM) in cyanobacteria

Different mechanisms and pathways exist in plants and cyanobacteria to favor the carboxylation reaction of RubisCO over the oxygenation reaction. All these methods are summarized under the term “carbon concentrating mechanisms” (CCM). The so-called C_4 plants pre-fix CO_2 as phosphoenolpyruvate (PEP), resulting in the organic acid oxaloacetic acid. Subsequently, this compound is transported to another specialized cell, where RubisCO is located, and is decarboxylated. The released CO_2 is fixed by RubisCO and enters the CBB cycle. Through this physical separation of initial carbon fixation and RubisCO, an increased supply of CO_2 to RubisCO is achieved to favor the carboxylation over the oxygenation reaction (Williams *et al.*, 2013). Eukaryotic algae achieve an increased intracellular CO_2 concentration by actively importing inorganic carbon (CO_2 and hydrogen carbonate HCO_3^-). Inside of the cell, CO_2 is concentrated in microcompartments (pyrenoids) where RubisCO is packed into it. Carbonic anhydrases dehydrate the accumulated HCO_3^- to free the CO_2 for fixation by RubisCO (Yamano and Fukuzawa, 2009).

The CCM of aquatic cyanobacteria is quite like the CCM of eukaryotic algae. The initial step also involves the active import of dissolved CO_2 and HCO_3^- into the cell (Figure

5A). Three HCO_3^- importers and two CO_2 importers are known, although not all cyanobacteria possess all carbon uptake transporters. The hydrogen carbonate importers are located at the plasma membrane and display different substrate affinities. SbtA is a high-affinity Na^+/HCO_3^- symporter (Price *et al.*, 2011); BicA a medium- to low-affinity Na^+-dependent transporter (Price and Howitt, 2011); and BCT1 a high-affinity ABC transporter (Omata *et al.*, 2002). The CO_2 uptake complexes contain a carbonic anhydrase (CA), which hydrates the through diffusion accumulated CO_2 directly to HCO_3^- to increase the intracellular hydrogen carbonate pool. NDH-I_3 and NDH-I_4 are located in the thylakoid membrane (Shibata *et al.*, 2001; Maeda *et al.*, 2002). It is to note, that not all cyanobacteria possess all importers. *M. aeruginosa* PCC 7806 for example lacks the high-affinity HCO_3^- importer SbtA but owns the four other importers. A lot of other *Microcystis* strains lack the medium-to-low HCO_3^- importer BicA or only have the incomplete gene for it (Sandrini *et al.*, 2014). Furthermore, the adaptation to different carbon concentrations happens mainly on the level of the importers. Under elevated carbon conditions all importers are downregulated or remain constant and under low concentrations all importers are upregulated. This shows that only the activity of the importing system is regulated, but not the distribution or availability of single importers (Sandrini *et al.*, 2015).

Once the inorganic carbon is imported into the cell in the form of HCO_3^-, another step follows in the CCM of cyanobacteria. Since RubisCO cannot fix hydrogen carbonate, it needs to be converted back to CO_2. This step is carried out in a specific bacterial microcompartment (BMC) of the cyanobacterial cell, the carboxysome. Besides the carboxysome other BMCs exist in bacteria. Most of them are grouped together under the name of metabolosomes. Aldehyde oxidation or other metabolic pathways take place there, which benefit from the spatial separation from the cytosol. In cyanobacteria, RubisCO is packed densely into the carboxysome. The accumulated HCO_3^- inside of the cytoplasm is dehydrated by a CA and imported into the carboxysome in the form of CO_2 (Figure 5B) (Cot *et al.*, 2008; Long *et al.*, 2011). This elevated concentration of CO_2 leads to a saturation of RubisCO with carbon dioxide to favor the carboxylation over the oxygenation reaction. The selectively permeable protein shell of the carboxysomes prevents the permeation of molecular oxygen and the leakage of CO_2 while being permeable for hydrogen carbonate and fixation products of RubisCO (Benjamin D. Rae *et al.*, 2013). The RubisCO type, which is

packed into the carboxysomes, also determines the type of the carboxysome. Carboxysomes with RubisCO Form 1A are called α-carboxysomes, with RubisCO Form 1B they are called β-carboxysomes (Badger and Price, 2003). In general, marine cyanobacteria like *Prochlorococcus* or *Synechococcus* have α-carboxysomes and freshwater/coastal cyanobacteria like *Microcystis*, *Synechocystis* or *Nostoc* have β-carboxysomes. Outside of cyanobacteria, some other bacteria also carry carboxysomes: some sulfur-oxidizing bacteria like *Thiobacillus* and *Halothiobacillus* or nitrifying bacteria of the genera *Bradyrhizobium* (B. D. Rae *et al.*, 2013).

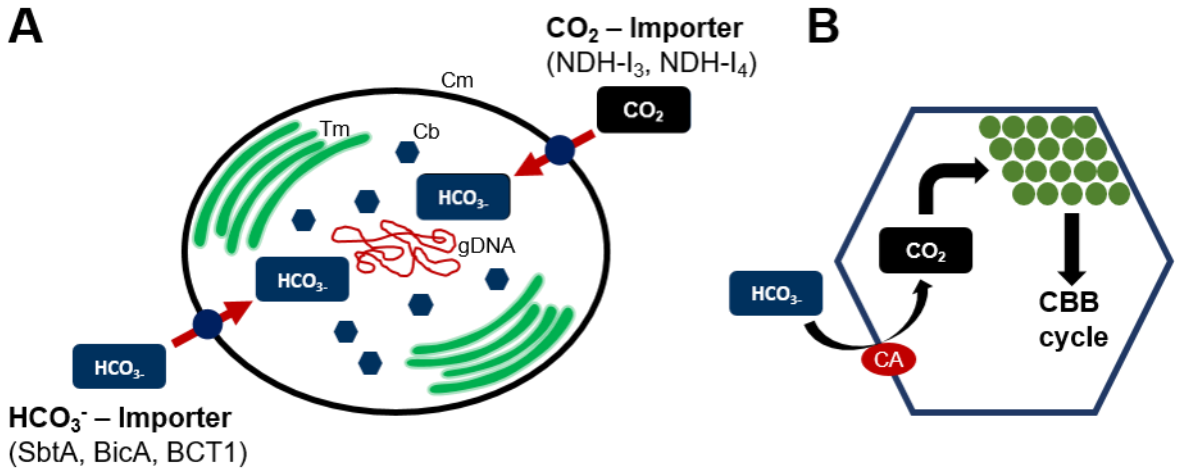

Figure 5. Carbon-concentrating mechanism (CCM) in cyanobacteria. **(A)** HCO_3^- and CO_2 are imported into the cyanobacterial cell by the respective importers, indicated in the figure. CO_2 gets transformed into HCO_3^- while getting imported. Cm: cytoplasmic membrane, Tm: thylakoid membrane, Cb: carboxysome, gDNA: genomic DNA. **(B)** The accumulated HCO_3^- in the cytosol is transported into the carboxysome and gets transformed into CO_2, catalyzed by carbonic anhydrases (CA). In the carboxysome, CO_2 is fixed by RubisCO (green dots) and enters the Calvin-Benson-Bassham (CBB) cycle.

Both types of carboxysomes have a similar structure. The outer shell consists out of hexameric and trimeric units. At the intersection of these units, small pores are created, which are believed to be the spots where metabolite exchange takes place (Benjamin D. Rae *et al.*, 2013). On the inside, RubisCO is densely packed to perform CO_2 fixation. Apart from that, the involved proteins in the assembly of carboxysomes are different, depending on the type. Shell proteins of α-carboxysomes can be grouped into two categories: small size proteins (CsoS1A-E and CsoS4A-B) and larger shell-associated proteins (CsoS2A-B and CsoSCA). The small proteins form flattened, regularly hexagonal hexamers (CsoS1A-C) or trimers (CsoS1D). The gaps between these parts are closed by the other small proteins CsoS4A and CsoS4B, thus preventing leakage

of CO_2 from the carboxysome. The larger proteins CsoS2A-B attach to the shell and interact with it. The exact function of these proteins is still not clear, but it appears that they play a crucial role in RubisCO organization (Heinhorst *et al.*, 2006). CsoSCA is the carboxysomal CA and binds to the shell.

The β-carboxysome is built with different proteins and has a different shell structure, since it consists of an outer shell and an inner shell. The outer shell layer is formed by hexameric shell facets of CcmK2, CcmK3 and CcmK4 with CcmL pentamers located at the vertices between the shell facets. CcmO faces the edge of the shell facets. The inner shell layer is mainly formed by CcmM. CcmM has two isoforms: CcmM58 and CcmM35, each with distinct functions. CcmM58 recruits the carbonic anhydrase CcaA and links RubisCO to the inner shell layer through small subunit-like domains (SSLD). Paracrystalline arrays of RubisCO in the carboxysomal lumen are formed through the interlinking function of CcmM35. Additionally, CcmN acts as a bridge between the outer shell protein CcmK2 and CcmM (Sutter *et al.*, 2019). The assembly of a fully functional carboxysome starts from the core (Figure 6). CcmM58 aggregates some RubisCO molecules by replacing RbcS with its SSLD and CcmM35 links the aggregates with the inner shell layer. This so-called procarboxysome is encapsulated with CcmK, CcmO and CcmL. The fully assembled carboxysomes are evenly distributed inside of a cell to limit the distance the imported HCO_3^- needs to diffuse before entering the carboxysome (Faulkner *et al.*, 2017; Kerfeld *et al.*, 2018).

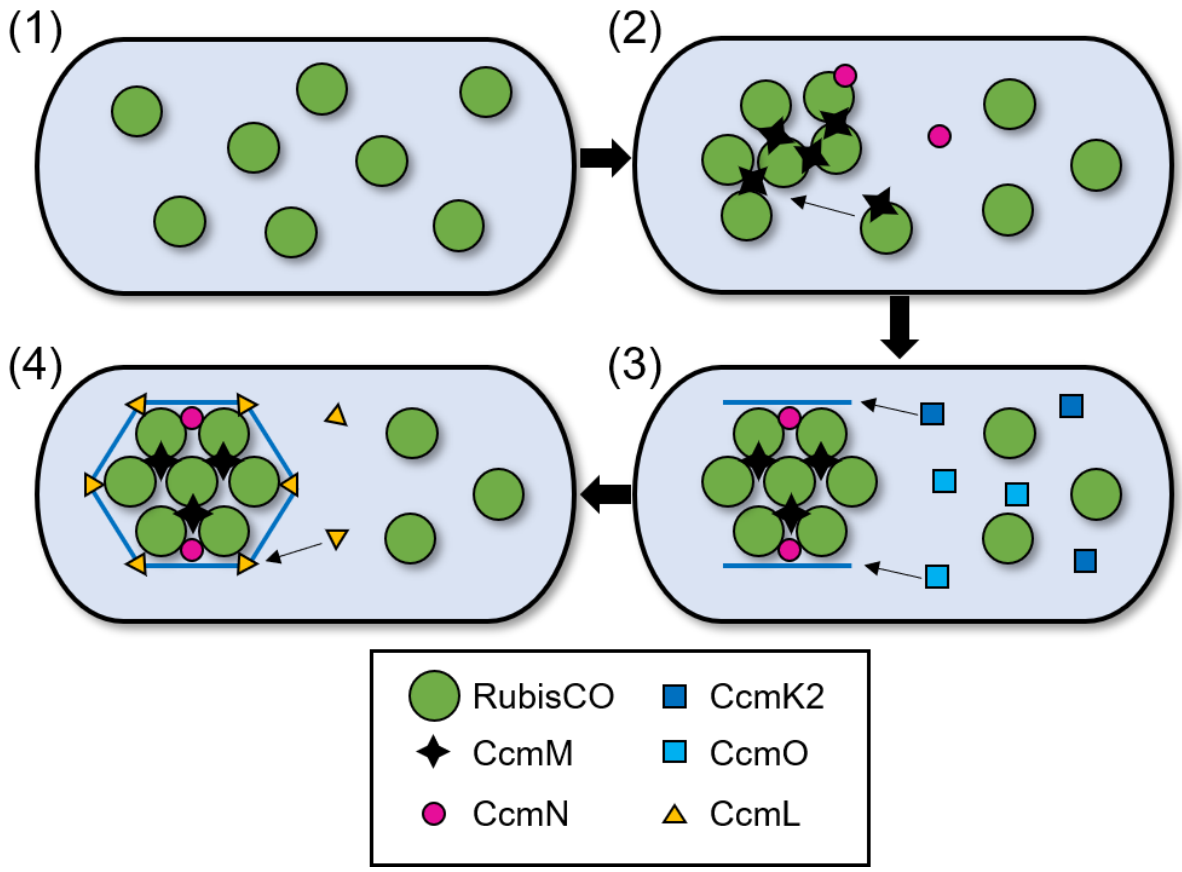

Figure 6. Assembly of a β-carboxysome in β-cyanobacteria like *M. aeruginosa*. **(1)** RubisCO exist in the cell as a soluble protein. **(2)** Formation of procarboxysome (PC). RubisCO is aggregated by CcmM, CcmN binds to the aggregates as well. **(3)** Start of encapsulation of the procarboxysome. The shell proteins CcmK2 and CcmO bind to the PC and encapsulate it. CcmN mediates the binding of the shell proteins to the inner proteins. **(4)** Fully assembled carboxysome. The shell facets build by CcmK2 and CcmO are closed at the vertices by CcmL. Figure inspired by *Cameron* et al.*, 2013*.

1.8 Extracellular signaling in bacteria and *M. aeruginosa*

The intracellular role of MC is already described in a previous chapter (cf. 1.4). However, small amounts of MC and other peptides are always detected in the supernatant of a *M. aeruginosa* culture. For example MC does not only act extracellularly as a toxin to inhibit other organisms, it can also affect the producing cells itself (Kaplan *et al.*, 2012). The presence of extracellular MC in a non-microcystin producing *M. aeruginosa* culture leads to the downregulation of the transcription of secondary metabolite genes (Makower, Schuurmans, Groth, Zilliges, Hans C P Matthijs, *et al.*, 2015). Another addition experiment with the supernatant of toxic *M. aeruginosa* showed an autoinduction effect on the MC-producing strain, which is leading to elevated MC production (Schatz *et al.*, 2007). This is an indicator, that MC can also serve as signaling molecule for *M. aeruginosa* to initiate intracellular

processes such as a change of the secondary metabolome as an adaptation to changing conditions. MC may act as an infochemical to indicate cells in a population when larger amounts of cells lyse and by this release large amounts of MC or other bioactive compounds. Co-culturing experiments of toxic and non-toxic *M. aeruginosa* strains also showed that both strains benefit from each other, further strengthen the hypothesis of a possible role of MC and other oligopeptides as signaling molecules (Briand *et al.*, 2016).

Bacteria occur in nature rarely as single cells. They grow in colonies, mats, biofilms or in case of cyanobacteria often in blooms. These cell aggregates are mostly heterogeneous, which means they are composed out of different cell types of the same species or a mixture with different species or both simultaneously. The growth and reaction to changing environmental conditions does not always happen randomly, the cells of one species or even different species can communicate and organize their response to each other. This cell-cell communication is carried out by small molecules. These are secreted by cells and can be detected by other cells which leads to the activation of intracellular processes. This concept of bacterial cell-cell communication is called quorum sensing (QS). In general, it triggers changes in a bacterial population through population-density dependent signaling. When the intracellularly produced signaling molecule reaches a certain threshold in the population, it activates a coordinated change in gene expression in the population (Figure 7) (Abisado *et al.*, 2018). Different signaling molecules (so-called autoinducers) are existing in QS systems: gram-positive bacteria often use short oligopeptides and gram-negative bacteria as cyanobacteria use acyl-homoserine lactone (AHL).

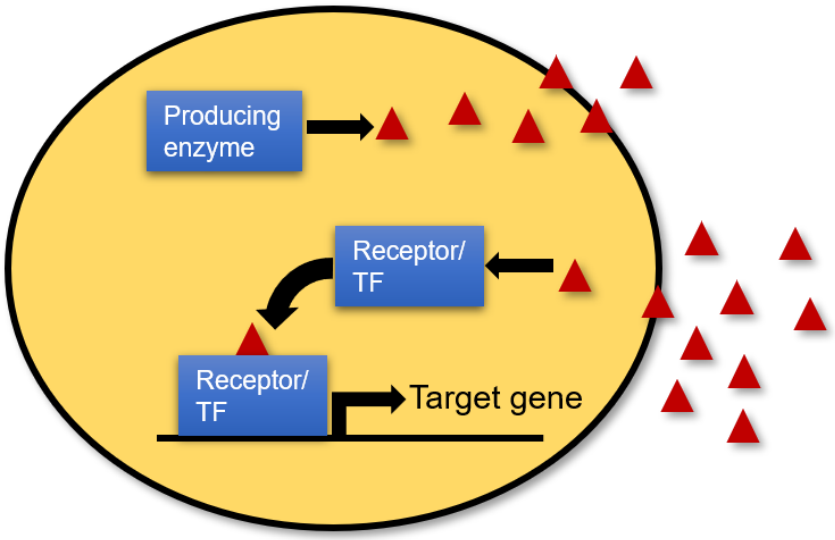

Figure 7. Basic principal of quorum sensing. One enzyme produces the signaling molecule (red triangles), which freely diffuses through the membrane into the surrounding medium. When a certain threshold of the signaling molecule is reached, it binds to a receptor protein. It gets activated and acts as a transcription factor (TF) to initiate the transcription of the target gene. Figure inspired by *Ng and Bassler, 2009*.

Studies about QS in cyanobacteria are limited but there are some data available which suggest QS also plays an important role in cyanobacteria. Culturing experiments with *Microcystis* and *Radiocystis* showed cellular density had a significant effect on peptide production. Cultures with a higher cellular density possessed also higher cellular quotas of several cyanopeptides, for instance microcystin, aeruginosin or cyanopeptolin in comparison to low cellular density cultures (Pereira and Giani, 2014). Furthermore, even for *Gloeothece* PCC 6909 (unicellular planktonic cyanobacterium) and *M. aeruginosa* the production and release of AHLs was reported. The produced AHL had a clear effect on the proteome of *Gloeothece*, including the upregulation of RubisCO (Sharif *et al.*, 2008). In *M. aeruginosa* self-produced AHL-addition to planktonic cultures lead to an earlier and thicker formation of biofilm-like structures (Zhai *et al.*, 2012).

As indicated earlier in this chapter, extracellular signaling and quorum sensing is not only a communication between members of the same species. It plays also a major role in cooperative and competitive interspecific microbial interactions (West *et al.*, 2006). Also, for cyanobacteria it is reported that QS-based interactions exist in nature. The marine cyanobacterium *Trichodesmium* shows an increased activity of alkaline phosphatases (APases) when exposed to AHLs of isolated heterotrophic bacteria from

Trichodesmium colonies. The heterotrophs use these APases for the acquisition of phosphate from dissolved-organic phosphorus molecules (Van Mooy *et al.*, 2012).

In nature, cyanobacteria never occur as an axenic culture. In blooms or even colonies, they are always associated with heterotrophic bacteria. Field samples of cyanobacteria always contain other microorganisms which grow together with the cyanobacteria. Since they share the same ecological niche, they also interact with each other. Like with QS systems, these interspecies interactions in a colony or bloom can be beneficial for both organisms, or one organism gets exploited or even inhibited. Research about interaction networks is challenging, because a large variety of organisms can contribute to a single network. Several studies show that the heterotrophic bacterial community is often dominated by members of the phyla of Proteobacteria, Flavobacteria and Bacteroidetes. A lot of isolated strains show positive growth effects on the cyanobacterium (Katri A Berg *et al.*, 2009; Zheng *et al.*, 2020).

Various interactions are based on the interchange of nutrients. Samples of the marine cyanobacterium *Synechococcus* show that the cyanobacterium had an increased organic matter biosynthesis and release metabolism. The isolates of the phylum Flavobacteria displayed preferences for initial degradation of complex compounds and biopolymers (Zheng *et al.*, 2020). The Alphaproteobacterium *Rhizobium* sp. MK23 showed a strong growth promotion of *M. aeruginosa*. When co-cultured with *M. aeruginosa*, the cyanobacterium was more resistant to H_2O_2 stress (Kim *et al.*, 2019). In another study, the cyanobacterium *Synechococcus* provide scavenging functions for reactive oxygen species in co-culture with the heterotroph *Shewanella putrefaciens* (Beliaev *et al.*, 2014). These results also indicate an important role of the heterotrophs in the adaptation of cyanobacteria to harsher environmental conditions. A large-scale study about the *M. aeruginosa* microbiome in different lakes in four continents furthermore strengthen the synergistic effects of the heterotrophs and *M. aeruginosa* (Cook *et al.*, 2020).

1.9 Aim of the study

This study aims to further understand the impact of MC and other peptides on the inorganic carbon adaptation of *M. aeruginosa* PCC 7806. Specifically, the study intents to analyze how the protein binding of MC affetcs the functionality of the protein binding partners *in vivo*. Since previous high-light shift experiments revealed differences in the metabolomic adaptation of the *M. aeruginosa* WT and the MC-deficient mutant Δ*mcyB* in comparison to the model cyanobacterium *Synechocystis* sp., this study aimed to uncover the underlying mechanistic basis of these deviations. As several studies pointed to distinctive features of the carbon concentrating mechanism (CCM) of *M. aeruginosa* compared to other cyanobacteria, this study addressed the question to what extend the subcellular localization of RubisCO and carboxysome dynamics differ in *M. aeruginosa* and whether the protein binding of MC contributes to these dynamics. Former experiments already suggest a more prominent role of microcystin in the adaptation to different physiological conditions.

The second part of the study is focused on the role of microcystin as a signaling peptide. Previous addition experiments with microcystin showed that extracellular MC influenced in particular the secondary metabolome, but also the growth of *M. aeruginosa* itself. Data about the direct influence of extracellular MC on the carbon metabolism and the CCM are still missing. This work aims to give further understanding of the role of extracellular MC as a regulator of the CCM of *M. aeruginosa*.

2. Materials and methods

2.1 Cultivation conditions

Non-axenic and axenic *Microcystis aeruginosa* PCC 7806 wild type and Δ*mcyB* mutant were cultivated in BG-11 medium (Rippka *et al.*, 1979) either on plate or in liquid medium. When cultivated on plate, agar with a final concentration of 0.7 % was added to the medium. Chloramphenicol with a final concentration of 5 µg ml^{-1} was added to BG-11 either in agar plates or the liquid medium when the Δ*mcyB* mutant (Dittmann *et al.*, 1997) was cultivated.

To maintain the strains, they were cultivated at 23° C under continuous illumination at 10 µmol photons m^{-2} s^{-1}. The non-axenic *M. aeruginosa* strains were grown without agitation; the axenic strains were agitated on an orbital shaker with 95 rpm (Shaker DOS-10L; neoLab Migge, Heidelberg, Germany). No external aeriation was used. This state of the culture was defined as low-light-adapted cultures and will be referred to when mentioning growth under low-light conditions. Continuous cultivation was performed by dilution of the culture once per month with fresh BG-11 medium. To monitor the axenic state of *M. aeruginosa*, some cell material was transferred onto an R2A agar plate (R2A-Agar; Carl Roth, Karlsruhe, Germany) when the culture was diluted. The agar plate was incubated for 3 days at room temperature. An empty agar plate without any visible growth of microorganisms confirmed the axenic state of that culture. The growth of cyanobacteria was monitored by measuring the optical density at 750 nm.

2.2 Protein extraction

2.2.1 Total protein extraction

All the following steps were performed on ice or pre-cooled centrifuges. The cell pellet of the sample to extract proteins from was resuspended in 500 µl of native or thylakoid extraction buffer (Table 3) in a 1.5 ml reaction tube. The sample was sonicated with the Sonopuls mini20 (Bandelin, Berlin, Germany) for 90 s (50 % amplitude, 3 s on/off pulse). Phenylmethylsulfonyl fluoride (PMSF) was added at a final concentration of 1

mM. Subsequently, a slow centrifugation step (2000*g* for 2 min) was performed to get rid of intact cells from the sonication step. Followed by a long centrifugation step of the supernatant (21,000*g* for 15 min). The resulting supernatant was transferred into a new reaction tube and is the cytosolic protein fraction (cytosolic fraction) of the sample. The remaining pellet of that long centrifugation is the membrane-associated protein fraction (membrane fraction) because all cellular membranes were collected in the pellet. To detach proteins from the membranes, another round of sonication was performed. The pellet was resuspended in 500 µl of native or thylakoid extraction buffer and sonicated for 60 s (50 % amplitude, 3 s on/off pulse). Either the sample was centrifuged again (21,000*g* for 15 min) to get rid of the membranes from the detached proteins (supernatant), or the sonicated sample was transferred directly into a new reaction tube and stored at -20° C until use.

2.2.2 Thylakoid membrane extraction

The extraction method of thylakoid membranes from *M. aeruginosa* is based on the method described by Gandini et al. 2017. All following steps were performed on ice and pre-cooled centrifuges. The cell pellet of 100 ml *M. aeruginosa* culture grown under low-light or higher light (50 µmol photons m^{-2} s^{-1}) conditions was resuspended in 1 ml homogenization buffer (HB) (Table 3). To break up the cells in a glass bead mill (Mixer Mill MM2; Retsch, Haan, Germany), a mixture of glass beads (0.10 mm and 0.18 mm), which equates half the volume of the cell suspension (0.5 ml) was added to the sample. 4 cycles of 3 min shaking (shaking frequency 100 min^{-1}) and 3 min resting on ice were performed, followed by a centrifugation step (13,000*g* for 1 min) to get rid of unbroken cells and cell debris. The supernatant was transferred into a fresh reaction tube for a long centrifugation step (21,000*g* for 1 h). Subsequently, the supernatant was discarded, and the pellet was washed twice with 1 ml Tricine buffer (Table 3) (13,000*g* for 15 min). After resuspension of the pellet with 1 ml Tricine buffer, 50 µl glycerol was added to the sample to store it at -20° C until use.

To prepare the sample for running in the Blue Native PAGE (see 2.3.1), β-DM (n-Dodecyl β-D-maltoside) was added at a final concentration of 1 % (v/v). After incubation at room temperature for at least 10 min the sample was centrifuged (16,000*g* for 10 min), and the supernatant was transferred into a new reaction tube ready to be used for Blue Native PAGE.

Table 3. Recipes of the needed buffers for total protein extraction and thylakoid membrane extraction. The left column shows the compounds of the buffer and the right column the used concentration (conc.).

Compound	**Conc.**	**Compound**	**Conc.**
Native extraction buffer		*Homogenization buffer (HB)*	
HEPES	50 mM	Sucrose	0.4 M
EDTA	0.1 mM	NaCl	10 mM
EGTA	0.1 mM	$MgCl_2$ x 6 H_2O	5 mM
$MgSO_4$	1 mM	Tricine pH 7.9	20 mM
Triton X-100	0.5 % (v/v)	Freshly added:	
Glycerol	20 % (v/v)	Na-ascorbate	10 mM
		NaF	10 mM
Thylakoid extraction buffer		*Tricine buffer*	
HEPES	50 mM	Tricine	5 mM
$MgCl_2$ x 6 H_2O	5 mM	Freshly added: NaF	10 mM
$CaCl_2$ x 2 H_2O	25 mM		
Glycerol	10 % (v/v)		
Set pH to 7.0 (with NaOH)			

2.3 Protein gel electrophoresis and immunoblotting

2.3.1 Protein gel electrophoresis

Different gel electrophoresis types were used to separate proteins. Bis-Tris gels (recipe from BiteSize Bio based on NuPAGE from Invitrogen) were used for denaturing and native gels (Table 4). The recipe for the Blue Native (BN) gels differed from the Bis-Tris gels and is shown in Table 4 as well. The used polyacrylamide concentration depended on the targeted protein, with higher polyacrylamide concentrations used for smaller proteins and *vice versa*. Different loading dyes were used depending on the gel type. The same loading dye was used for denaturing and native Bis-Tris gels (5x concentrated; 250 mM Tris pH 6.8, 0.1 % Bromophenol blue, 50 % glycerol, 10 % SDS, 500 mM 2-mercaptoethanol) with the removal of SDS and 2-mercaptoethanol for native gels. The recipe for the BA loading dye differed (10x concentrated; 5 % Coomassie G-250, 200 mM Bis-Tris pH 7.0, 75 % Sucrose, 1 M Amino-caproic acid) When running an SDS-PAGE the sample with the added loading dye was heated to 95° C for 10 min

to support the denaturation of proteins. All protein samples were centrifuged for 1 min at 13,000*g* to remove possible cell debris before loading on the gel.

Table 4. Recipes of Bis-Tris and BN gels. The left column shows the recipes for the running gel, stacking gel and the 5x gel buffer of Bis-Tris gels. The right column shows the recipes for the running gel, stacking gel and the 6x gel buffer of BN gels.

Compound	**Volume**	**Compound**	**Volume**
Bis-Tris gel (10 %)		*Blue Native gel (7 %)*	
5x gel buffer	1 ml	6x gel buffer	0.83 ml
40 % acrylamide	1.25 ml	30 % acrylamide	1.12 ml
H_2O	2.70 ml	H_2O	3.03 ml
10 % APS	50 µl	10 % APS	15.48 µl
TEMED	5 µl	TEMED	4.6 µl
Stacking gel for Bis-Tris		*Stacking gel for BN*	
5x gel buffer	0.4 ml	6x gel buffer	0.21 ml
40 % acrylamide	0.25 ml	30 % acrylamide	0.25 ml
H_2O	1.35 ml	H_2O	1.04 ml
10 % APS	20 µl	10 % APS	8 µl
TEMED	5 µl	TEMED	3 µl
5x gel buffer		*6x gel buffer*	
Bis Tris	373.5 g l^{-1}	Amino-caproic acid	393.5 g l^{-1}
Adjust pH to 6.5-6.8 with HCl		500 mM Bis-Tris pH 7.0	60 %

Different protein concentrations of the samples resulting from different cell concentrations when sampled were normalized using the optical density of the respective samples. The sample with the lowest OD_{750} value was used as the reference for the other samples. With 15 µl being the reference volume, the applied sample volume on the gel corresponded to the OD_{750} value ratio. 3.5 µl of protein ladder (PageRuler Plus Prestained; Thermo Fisher Scientific, Waltham, MA) was used for every protein gel. The used running parameters of the gel differed between SDS, Native, and Blue Native PAGE. SDS gels were run at a constant voltage of 180 V for 40 min; Native gels at 180 V for 30 min; Blue Native gels at 50 V over-night 4° C. Furthermore, the used running buffers also differed between the gel types. SDS and native PAGE were run in a MOPS running buffer (10.46 g l^{-1} MOPS, 6.06 g l^{-1} Tris, 1 g l^{-1} SDS, 0.3 g l^{-1} EDTA) with the removal of SDS from the buffer when running a native

PAGE. The BN system needed a cathode (50 mM Tricine, 15 mM Bis-Tris, 0.2 % Coomassie G-250, pH adjusted to 7.0) and an anode running buffer (50 mM Bis-Tris, pH adjusted to 7.0). Images were taken with the ChemiDoc XRS+ Imaging System (Bio-Rad).

When the sample from the Blue Native PAGE was used for a 2nd dimension SDS-PAGE, the sample lane was cut out from the 1st dimension gel and was placed horizontally on top of the gel for 2nd dimension PAGE. Furthermore, on both ends of the cut out-lane, a filter paper with 4 µl of protein ladder pipetted on it was placed. The gel piece and the filter papers were sealed with 0.8 % agarose (made with MOPS running buffer). The gel was run at a constant voltage of 180 V for 40 min.

2.3.2 Immunoblotting

The applied method for immunoblotting was used irrespective of the gel type in the gel electrophoresis. The protein gel was blotted with a wet blot electrophoresis apparatus (Mini-Protean, Bio-Rad, Hercules, CA) onto a nitrocellulose membrane (Amersham Protein Premium 0.45 µm MC; GE Healthcare, Chicago, IL) as described previously (Towbin *et al.*, 1979). The transfer buffer (14.42 g l^{-1} Glycin, 3.03 g l^{-1} Tris) contained 20 % methanol (v/v) for more efficient blotting. After blotting, the membrane was blocked with 1 % polyvinylpyrrolidone (PVP) K-30 in Tris-buffered saline with 0.1 % (v/v) Tween-20 (TBS-T; 6.06 g l^{-1} Tris, 8.77 g l^{-1} NaCl, pH set to 7.4, add 0.1 % Tween-20) and was washed subsequently one time for 5 min at 4° C with TBS-T. The primary antibody was incubated in TBS-T overnight at 4° C. All used primary antibodies, and the applied dilution for immunoblotting can be viewed in Table 5. Afterward, the membrane was washed with TBS-T to remove unbound primary antibodies, and the secondary antibody (horseradish peroxidase HRP-conjugate) was applied in TBS-T and incubated for at least 1 h at 4° C. All used secondary antibodies and the applied dilution can be seen in Table 5. The membrane was washed 4 times for 5 min to remove unbound secondary antibodies and developed (SERVALight Polaris CL HRP WB Substrate Kit; Serva, Heidelberg, Germany). Images were taken with the ChemiDoc XRS+ Imaging System (Bio-Rad).

Table 5. Primary and secondary antibodies used for immunoblotting. The left column shows the primary antibodies, their animal origin, and the applied dilution. CcmK, CPS-CP12, and RbcS are from Pineda antibody service (Berlin, Germany). The remaining antibodies are from Agrisera (Vännas, Sweden). The right column shows the secondary antibodies, their origin, and the applied dilution. Both antibodies are from Agrisera.

Antibody	**Origin**	**dilution**	**Antibody**	**Origin**	**dilution**
Primary antibodies			*Secondary antibodies*		
CcmK	Rabbit	1:10,000	Mouse	Rabbit	1:10,000
CBS-CP12	Rabbit	1:5,000	Rabbit	Goat	1:10,000
FtsZ	Rabbit	1:5,000			
Microcystin	Mouse	1:10,000			
PEP carboxylase	Rabbit	1:10,000			
Prk	Rabbit	1:5,000			
RbcL	Rabbit	1:10,000			
RbcS	Rabbit	1:10,000			

2.4 Extraction of peptides for HPLC analysis

Peptide extraction from *M. aeruginosa* (including microcystin) is based on a methanol extraction. To analyze the intracellular peptides, the pellet was resuspended with 10 ml of 75 % methanol and subsequently shook for 5 min at 3200 rpm (Vortex Genie 2; Scientific Industries, Bohemia, NY). After sonication for 10 min (70 % amplitude, 3 s on/off pulse), the sample was centrifuged for 10 min (21,000*g*, 10 min, 4° C). The supernatant was transferred to a new reaction tube, and the pellet was resuspended with fresh 10 ml of 75 % methanol. The extraction was repeated, and both supernatants were pooled. To concentrate and purify the extracted peptides, the sample was diluted with water to a concentration of methanol of approx. 5 % and run over a C-18 cartridge (Sep-Pak Plus C18 cartridge; Waters, Milford, MA). In the final step, the sample was eluted with 2 ml of 100 % methanol and dried in a vacuum concentrator (RVC 2-25 CDplus; Christ, Osterode am Harz, Germany) afterward. When analyzing the extracellular peptides of an *M. aeruginosa* culture, the supernatant of the sample of interest was loaded directly on the C-18 cartridge and was processed like the pellet fraction. The sample was resolved with 200 µl of 60 % methanol and filtered (Acrodisc 4 mm with 0.45 µm membrane; Pall Life Sciences, Port Washington, NY) before 10 –

50 µl of it was loaded on the high-performance liquid chromatograph Prominence LC-20AD (Shimadzu, Kyoto, Japan) to analyze the peptides. The extracts were separated on a Symmetry Shield RP18 Column (100Å, 3.5 µm, 4.6 mm x 100 mm) with a mobile phase containing 0.05 % Trifluoroacetic acid. As a guard column a Symmetry Shield RP18 Sentry Guard Cartridge (100Å, 3.5 µm, 3.9 mm x 20 mm) was used (both columns from Waters). The compounds were eluted at 1 ml min^{-1} using the following gradient of the 42 min program: 1) 70 % aqua dest., 30 % acetonitrile within 10 min to 65 % aqua dest., 35 % acetonitrile; 2) within 30 min to 30 % aqua dest., 70 % acetonitrile; 3) within 2 min to 100 % acetonitrile. When only microcystin was examined, the program was shortened to 13 min using the following gradient: 1) 70 % aqua dest., 30 % acetonitrile within 12 min to 64 % aqua dest., 36 % acetonitrile; 2) within 1 min to 100 % acetonitrile. The examination of the chromatograms and quantification of peaks was done with the LabSolutions software package (Version 5.87 SP1; Shimadzu). To collect certain compounds of the extract, like microcystin, the flow-through of the HPLC was collected with a fraction collector and dried in a vacuum concentrator to remove the acetonitrile. Afterward, the compound was resolved with 60 % methanol. It was loaded on the HPLC to check if the fraction collection was performed successfully, and quantified, if necessary.

2.5 LC-MS analysis of metabolites

To analyze and quantify metabolites of *M. aeruginosa* liquid chromatography – mass spectrometry (LC-MS) was performed. The intracellular metabolites were extracted by resuspension of the pellet fraction with 4 ml of H_2O and were subsequently sonicated for 2 min (60 % amplitude, 3 s on/off pulse). After centrifugation (21,000*g*, 10 min, 4° C), the resulting supernatant was dried in a vacuum concentrator. The supernatant of the culture-sample of interest was sterile-filtered (Rotilabo-syringe filter 0.45 µm pore size; Carl Roth) and dried without further processing when extracellular metabolites needed to be analyzed.

After resolving the dried extracts with 200 µl of H_2O and filtration (0.2 µm filter Omnifix-F; B. Braun, Melsungen, Germany), the sample was analyzed by HPLC (LC-MS-8050 system; Shimadzu) and the incorporated LC-MS/MS method package for primary metabolites (version 2, Shimadzu). To prepare the extract to be loaded onto the

system, 4 µl of extract was separated on a pentafluorophenylpropyl column (Supelco Discovery HS FS, 3 µm, 150 x 2.1 mm) with a mobile phase containing 0.1 % formic acid. Elution of the compounds was performed at 0.25 ml min^{-1} using the following gradient: 1 min 0.1 % formic acid, 95 % aqua dest., 5 % acetonitrile, within 15 min linear gradient to 0.1 % formic acid, 5 % aqua dest., 95 % acetonitrile followed by 10 min 0.1 % formic acid, 5 % aqua dest., 95 % acetonitrile. Aliquots were continuously injected in the MS/MS part and ionized via electrospray ionization. Identification and quantification of the compounds was done with the LC-MS/MS method package and the LabSolutions software package (Shimadzu) using the multiple reaction monitoring values. Standard substances (Sigma-Aldrich, St. Louis, MO) were included in all measurements and batches at varying concentrations for calibration.

2.6 Immunofluorescence microscopy

Four milliliters of *M. aeruginosa* culture were separated into two 2 ml reaction tubes and centrifuged 1 min at 10,000*g* (parameters for every following centrifugation step). When field samples were analyzed, cells were collected and concentrated by centrifugation before the described steps. To wash the cells, the pellet from one tube was resuspended with 1 ml of phosphate-buffered saline (PBS; 8.18 g l^{-1} NaCl, 0.2 g l^{-1} KCl, 1.42 g l^{-1} Na_2HPO_4, 0.25 g l^{-1} KH_2HPO_4, pH adjusted to 8.3), transferred to the other tube to re-suspend the pellet as well and was centrifuged again. For fixation, the pellet was resuspended with 1 ml of 4 % formaldehyde in PBS. The incubation time depended on the used *M. aeruginosa* strain: 30 min for the WT, 15 min for Δ*mcyB*. In both cases, it was incubated at room temperature. After two washing steps with PBS to wash away any excessive formaldehyde, which could cause artifacts during microscopy, the pellet was resuspended with 100 µl PBS and 20 µl were spread on a microscope slide each. The slides were air-dried and stored at -20° C for later use.

To start the hybridization with antibodies, the sample slides were equilibrated in PBS for 5 min at room temperature. Afterward, the slides were incubated with 2 mg ml^{-1} lysozyme in PBS with 0.3 % (v/v) Triton X-100 (PBS-TX) for 30 minutes at room temperature and washed twice with PBS-TX for 3 min. The samples were blocked with 1 % PVP K-30 in PBS-T (PBS with 0.3 % Tween-20) for at least 1 h at 4° C and washed twice with PBS-T. The primary antibody dilutions were made with PBS-T as well. All

used antibodies are shown in Table 6. After incubation of at least 1 h at room temperature, the slides were washed twice to remove unbound primary antibody, and the secondary antibody (all from Thermo Fisher Scientific) was applied to the slides (Table 6). The used secondary antibody depended on the selected primary antibody. Subsequently, the slides were washed twice, air-dried, and approx. 30 µl of 4 % propyl gallate in glycerol was dropped onto the slide and covered with a coverslip. The slides were stored at -20° C until use. Immunofluorescence images were taken with a Zeiss LSM 780 (Carl Zeiss, Oberkochen, Germany) laser scanning confocal microscope using a Plan-Apochromat 63x/1.40 oil immersion objective. Alexa Fluor 488 was excited at 488 nm (detection spectrum 493-556 nm), Alexa Fluor 546 and 568 at 561 nm (570-632 nm), and autofluorescence at 633 nm (647-721 nm). The excitation was performed simultaneously.

Table 6. Primary and secondary antibodies used for immunofluorescence microscopy. The left column shows the primary antibodies, their animal origin, and the applied dilution. CcmK, CPS-CP12, and RbcS are from Pineda antibody service. The remaining antibodies are from Agrisera. The right column shows the secondary antibodies, their excitation wavelength, and the applied dilution. All secondary antibodies are Alexa Fluor antibodies from Thermo Scientific.

Antibody	**Origin**	**dilution**	**Antibody**	**Excitation λ**	**dilution**
Primary antibodies			*Alexa Fluor*		
CcmK	Rabbit	1:200	Chicken	488 nm	1:200
CBS-CP12	Rabbit	1:200	Chicken	546 nm	1:200
Microcystin	Mouse	1:250	Mouse	405 nm	1:100
Prk	Rabbit	1:200	Mouse	488 nm	1:100
RbcL	Chicken	1:300	Mouse	568 nm	1:100
RbcS	Rabbit	1:200	Rabbit	488 nm	1:200

2.7 Electron microscopy

Transmission electron microscopy (TEM) was used to image the inside of single cells. To prepare samples, 2 ml of *M. aeruginosa* cell culture were centrifuged (13,000*g* for 2 min). The supernatant was removed, and the fixative (2.5 % glutaraldehyde, 2.0 % formaldehyde in 0.1 M Na-cacodylate buffer, pH 7.4) was added directly on the pellet without resuspension. Samples were fixed for 1-3 h at room temperature, then over-night at 4° C. After washing the cells 3 times for 10 min with 0.1 M Na-cacodylate buffer,

the cells were post-fixed for 90 min with Na-cacodylate-buffered 2 % OsO_4 at room temperature. Subsequently, cells were washed twice for 10 min in H_2O to remove the fixative. The sample was overlaid by a thin layer of 1 % low-melting agarose, dehydrated in a graded EtOH series, and acetone and embedded in low viscosity resin (Agar Scientific, Stansted, UK). Ultrathin sections stained with uranyl acetate and lead citrate were examined in a JEM 1011 (JEOL, Tokyo, Japan).

2.8 Experimental setups with *M. aeruginosa*

2.8.1 High-light experiment

Low-light adapted *M. aeruginosa* WT and Δ*mcyB* cultures were diluted with BG-11 before the experiment to an OD_{750} of 0.2 and incubated at low-light conditions until an OD_{750} of 0.45 was reached. Subsequently, the cultures were divided into 4 x 80 ml and were then transferred into the Multi-Cultivator MC 1000 (Photo Systems Instruments, Brno, Czech Republic). The cultures were illuminated at a light intensity of 250 µmol photons m^{-2} s^{-1} (defined in this work as high-light) for 4 h under continuous aeriation with ambient air. A sample of 40 ml was taken at the start of the experiment (t_0), and every hour of the 4 h high-light illumination (t_1-t_4). 1 ml was used for the measurement of the optical density at 750 nm, 4 ml for IFM (see 2.6), and the remaining 35 ml were used for the total protein extraction (see 2.2.1). The sample used for protein extraction was centrifuged (21,000*g* for 7 min, 4° C) and the pellet was stored at -20° C for later extraction. The supernatant of the centrifugation was used to measure the pH of the culture (FiveEasy Plus FP20; Mettler Toledo, Columbus, OH). The experiment was repeated three times with similar results.

2.8.2 Diurnal experiment

Before the experiment, low-light adapted *M. aeruginosa* WT and Δ*mcyB* cultures were split into 4 separate cultures (biological replicates) and diluted with fresh BG-11 medium to an OD_{750} value of 0.1 and transferred to the diurnal conditions so that the cultures can adapt to the changed culturing conditions. The setup of the diurnal cycle was 16 h of daytime (55 µmol photons m^{-2} s^{-1}) and 8 h of nighttime (no illumination). The cultures were agitated mildly on an orbital shaker with 40 rpm without external aeriation at 25° C in the AlgaeTron AG130 growth chamber (Photo Systems Instruments). The experiment itself was started after the cultures reached an OD_{750} of

0.3 (low cell density experiments) or 0.6 (high cell density experiments). The starting point for every experiment was 2 h before daytime started (t_0: 1st night). The next sampling time points were the change from night to daytime (t_2) and 2 h into daytime (t_4: 1st day). The same sampling pattern was done at the end of the 1st day and the end of the 2nd night. The sampling plan can be viewed in Figure 8 as well.

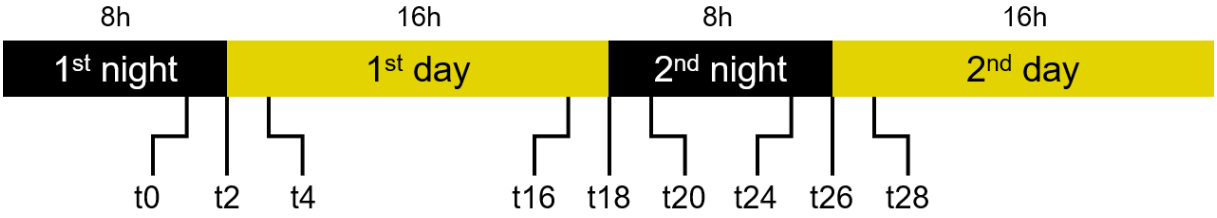

Figure 8. Diurnal cycle and sampling plan. The night phase had a duration of 8 h, the day phase of 16 h. All sampling time points are shown, and their number corresponds to the hours of the experiment running.

Every sampling time point, 28 ml of culture were taken to perform all necessary analyses. 1 m was used for OD_{750}-measurement, 2 ml for IFM (see 2.6), 10 ml for total protein extraction, 7.5 ml each for HPLC and LC-MS analysis. The samples for protein extraction were centrifuged (21,000*g* for 10 min), the supernatant was discarded, and the pellet was snap-frozen with liquid nitrogen and stored at -20° C until use (see2.2.1). Samples for HPLC and LC-MS analysis were centrifuged as well (same conditions), but the supernatant was transferred into a fresh reaction tube. Both the pellet (intracellular fraction) and the supernatant (extracellular fraction) were snap-frozen with liquid nitrogen and stored at -20° C until use (HPLC see2.4; LC-MS see 2.5).

2.8.3 Microcystin addition experiment

Addition experiments of microcystin (MC) to *M. aeruginosa* cultures were performed with the WT as well as with Δ*mcyB*. The experiments were executed with the non-axenic strains and the axenic strains. Different microcystin concentrations and variants were used: 10 and 100 ng ml^{-1} of MC-LR for the non-axenic strains and 250 ng ml^{-1} of MC-LR together with 100 ng ml^{-1} of MC-D-Asp3-LR for the axenic strains.

The experiments with *M. aeruginosa* WT and Δ*mcyB* strains were carried out in separate experiments but the method was the same. Low light-adapted cultures were diluted with fresh BG-11 medium to an OD_{750} of 0.15 and incubated under low-light conditions until an OD_{750} of 0.5 was reached. 45 ml of sample was taken from that cell

culture and was defined as the starting point of the experiment (t_0). 1 ml was used for OD_{750} measurement, 4 ml for IFM (see 2.6) and the remaining 40 ml for total protein extraction (see 2.2.1). The sample for protein extraction was centrifuged (21,000*g* for 10 min) and the cell pellet was stored at -20° C until used. After taking sample t_0 the cell culture was split into 3 x 50 ml. Culture 1 was the control culture without the addition of microcystin-LR (MC-LR), MC-LR with a final concentration of 10 ng ml^{-1} was added to culture 2 and 100 ng ml^{-1} to culture 3. All three cultures were incubated in the Multi-Cultivator MC 1000 (Photo Systems Instruments) with constant aeriation with ambient air for 2 h before sampling (t_2; sampling procedure as described for t_0). The experiment was carried out under low-light (10 µmol photons m^{-2} s^{-1}) and high-light (250 µmol photons m^{-2} s^{-1}) conditions in independent experiments.

The microcystin addition experiments of the axenic *M. aeruginosa* strains differed from the non-axenic strains. The described procedure was performed with the WT as well as with Δ*mcyB* in separate experiments. A low light-adapted cell culture was split into 2 separate cultures and diluted with fresh BG-11 medium to an OD_{750} of 0.2 and incubated under low-light conditions until an OD_{750} value of 0.35 was reached. Then a sample of 28 ml was taken of each culture (defined as t_0) and they were split into 3 x 70 ml cultures each afterward. One subset was defined as the control cultures (C = no addition of microcystins; 3 technical replicates), the other subset was the MC addition cultures (MC = MC addition; 3 technical replicates). MC-LR and MC-D-Asp3-LR, with a final concentration of 250 ng ml^{-1} and 100 ng ml^{-1} respectively, were added to these cultures. All cultures were transferred into the Algaetron growth chamber (Photo Systems Instruments) and incubated at 55 µmol photons m^2 s^{-1}, 23° C on an orbital shaker (40 rpm). Samples were taken after 2 and 4 h of incubation (t_2 and t_4). Like t_0, also at these time points 28 ml of culture were sampled. 1 ml was used for OD_{750} measurement, 2 ml for IFM (2.6), 7.5 ml for HPLC (2.4) and LC-MS analysis (2.5) each and the remaining 10 ml for total protein extraction (2.2.1). The samples used for HPLC and LC-MS analysis were centrifuged (21,000*g* for 10 min), the resulting supernatant was sterile filtrated (0.45 µm pore size) and transferred into a fresh reaction tube. Both the pellet and the supernatant were snap-frozen with liquid nitrogen and stored at -20° C until used. The sample for the protein extraction was centrifuged as well (same parameters), the supernatant was discarded, and the pellet was snap-frozen with liquid nitrogen and stored at -20° C until used.

3. Results

3.1 Dynamic subcellular localization of RubisCO and proteins of carbon fixation

Previous studies already indicate that RubisCO in cyanobacteria is not only located in carboxysomes as stated in the canonical literature (Badger and Price, 2003; B. D. Rae *et al.*, 2013). Data from model cyanobacteria like *Synechocystis* PCC 6803 and *Anabaena cylindrica* show that RubisCO besides other photosynthetic proteins can be found also outside of the carboxysomes in sufficient amounts (Cossar *et al.*, 1985; Agarwal *et al.*, 2009). Additionally, in *M. aeruginosa* the accumulation of RubisCO products, especially photorespiratory products, after high-light treatment is another indicator for a potential portion of RubisCO not associated with carboxysomes (Meissner *et al.*, 2015). To test these suggestions for the bloom-forming cyanobacterium *M. aeruginosa* PCC 7806, firstly the possible dynamics of RubisCO during 4 h of high-light irradiation was observed. Since several data show that the wild type (WT) of *M. aeruginosa* behaves differently than the microcystin (MC)-deficient mutant Δ*mcyB* in terms of growth rates and also on a metabolic level (Jähnichen *et al.*, 2007; Van De Waal *et al.*, 2011), both strains were used and compared to assess the possible physiological role of MC. Steady-state levels of the immediate products of RubisCO 3-PGA and 2-PG were examined to get a first understanding how RubisCO responds to the changing conditions. Intracellular levels of 3-PGA were 10 times higher in WT compared to the non-MC producing Δ*mcyB*, at low-light and high-light irradiation. Extracellular levels were at an extremely low level in both strains (Figure 9A). Interestingly, the concentration of 2-PG in the culture supernatant of Δ*mcyB* exceeded the intracellular concentration. The WT showed higher levels of 2-PG in the intracellular fraction then in the supernatant fraction (Figure 9B). Overall concentrations of 2-PG were rather low and differences between the two strains were neglectable. However, the examination of the immediate products of RubisCO clearly showed differences in the accumulation of carboxylase and oxygenase products between the MC-producing WT and the MC-deficient mutant Δ*mcyB*. The carboxylase products of RubisCO were

favored in the WT in comparison to Δ*mcyB*. Furthermore, measurable amounts of 2-PG in the culture supernatant indicate a direct involvement of RubisCO in this process.

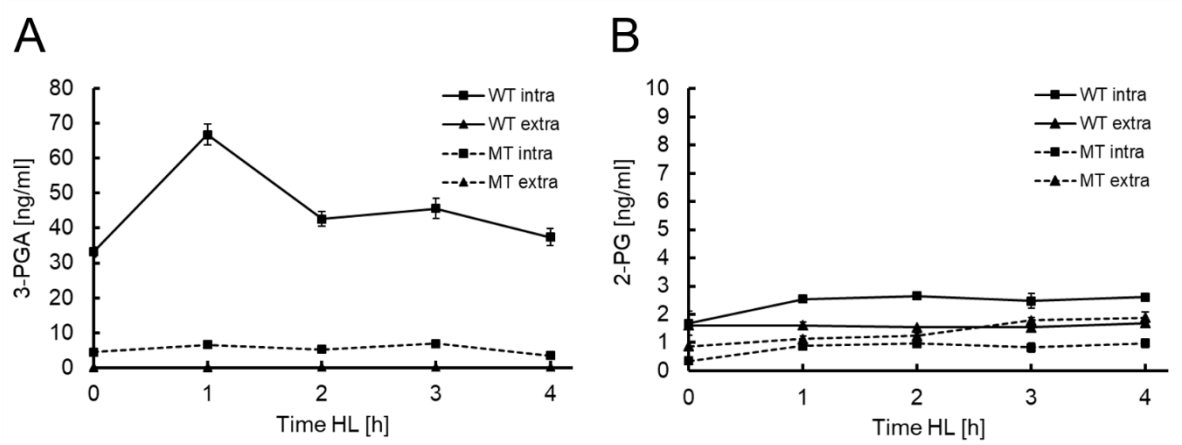

Figure 9. Steady-state levels of RubisCO products during high-light illumination of M. aeruginosa WT and ΔmcyB. Low light-adapted cultures of both WT and ΔmcyB were illuminated for 4 h with high-light (250 µmol photons m^{-2} s^{-1}). Mean values of 3 biological replicates are shown. **(A)** Intra- and extracellular steady-state levels of 3-PGA. **(B)** Intra- and extracellular levels of 2-PG.

As a next step, cellular protein extracts of the experiment were analyzed. To assess possible localization dynamics, the extracts were divided into the soluble fraction (cytosolic fraction) and the insoluble fraction (membrane-associated fraction) (Figure 10A). FtsZ, a cytosolic protein involved into cell division, confirmed a successful separation of both fractions, since it only could be detected in the cytosolic fraction (Figure 10B-C). RubisCO dynamics were studied by examining the dynamics of RbcL (large subunit of RubisCO) and RbcS (small subunit of RubisCO). The carboxysomal shell protein CcmK2 was used as an indicator for carboxysomes. Unexpectedly, RbcL showed a strong dynamic over the course of the experiment in WT. At the start of the experiment RbcL was detected in both fractions with a stronger signal in the cytosolic fraction. Already after 1 h of high-light irradiation, the signal mainly shifted towards the membrane fraction and got even more pronounced with every hour. CcmK2 was detected at the start of the high-light treatment nearly only in the cytosolic fraction as well. After 3 h the signal also shifted to the membrane fraction, indicating a possible location or assembly of carboxysomes at cellular or thylakoid membranes (Figure 10B). Especially after 1 and 2 h of the experiment, RbcL was mainly detected in the membrane fraction without the presence of carboxysomes in the fraction. This first result already suggested, that RubisCO may appear also outside of carboxysomes. The same shift of RbcL was observed in Δ*mcyB* with a delay of 1 h in comparison with

WT. However, the signal faded away after 4 h of irradiation (Figure 10C). Interestingly, RbcS does not reflect the dynamics of RbcL and was stable in both fractions over the whole experiment in both WT and Δ*mcyB*. It also seems that RbcS was more stable then RbcL in Δ*mcyB*, indicating possibly different turnover rates for the two subunits of RubisCO in *M. aeruginosa* (Figure 10C). Due to the different response to high-light conditions it is possible that the assembled RubisCO under these conditions differs from the proposed L_8S_8 complex with less RbcS used for assembly.

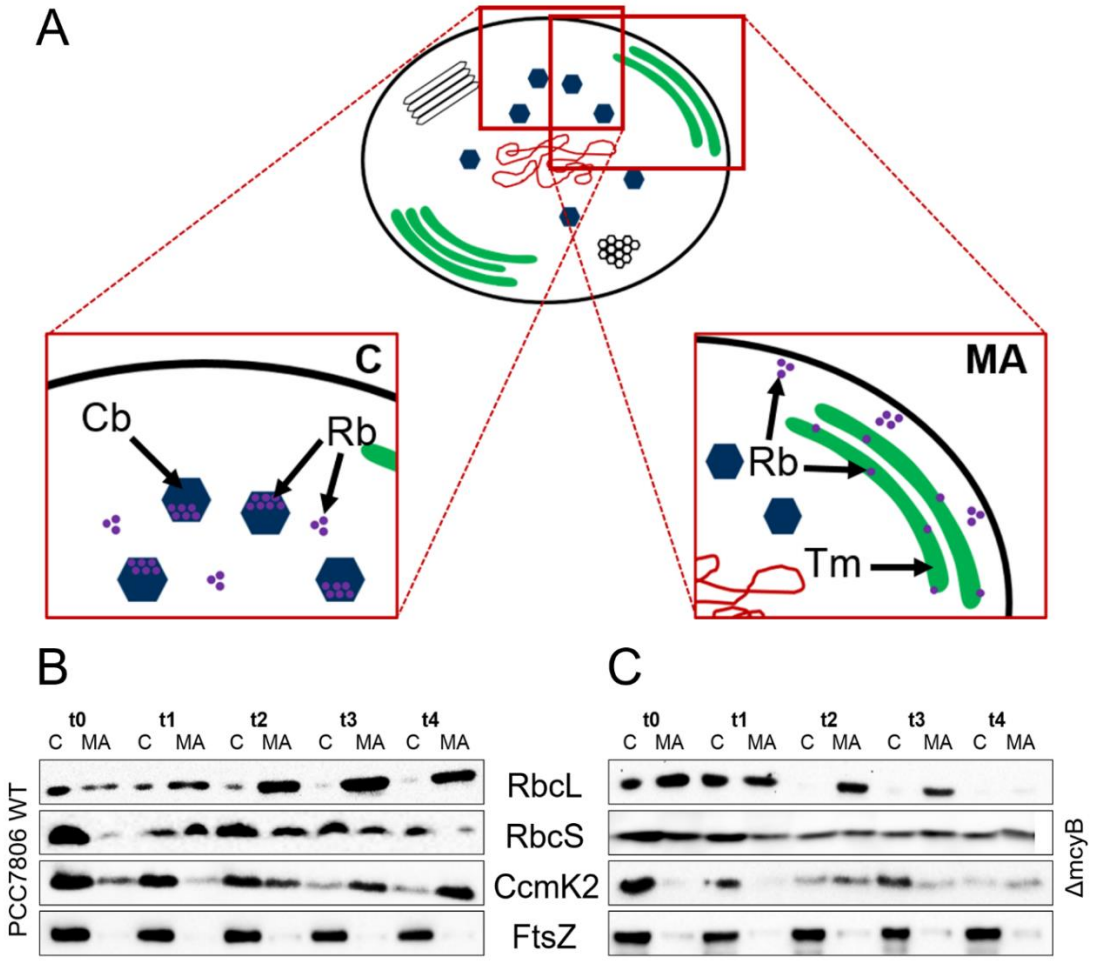

Figure 10. Dynamics of key proteins of carbon fixation during a high-light irradiation experiment in M. aeruginosa PCC7806. Low-light adapted cultures of M. aeruginosa wild type (WT) and the ΔmcyB mutant (MT) were exposed to high-light for up to 4 h. (**A)** Schematic representation of subcellular localization of RubisCO in M. aeruginosa. RubisCO (Rb) can be localized in the cytosol (C) and encapsulated in carboxysomes (Cb) or associated with membranes such as the thylakoid membrane (Tm) or the cytosolic membrane (MA). **(B-C)** Western blots showing the relocation of RbcL and CcmK from the cytosolic fraction (C) towards the membrane-associated fraction (MA) during 4 h of high-light treatment in the WT and the MT, respectively. RbcS is located both in the cytosolic (C) and the membrane-associated fraction (MA) independent of the light condition. FtsZ serves as cytosolic marker and confirms the separation of cytosolic and membrane-associated proteins.

The separation of the two subunits also raised the question, if these different RubisCO conformations are even active and show a normal activity respectively. To check the membrane associated RubisCO, the extracted membrane fraction was sonicated again to mechanically detach bound proteins and to get an understanding how tightly bound RubisCO and other proteins are to membranes. The treatment revealed that RbcL could be detached from membranes rather easily. In the remaining membrane sample (tightly bound proteins) no RbcL could be detected (Figure 11A). Furthermore, only the loose protein fraction showed RubisCO activity in comparison to the tightly bound proteins. The activity of the total membrane sample was like the loose protein fraction (Figure 11B). This first results already indicate a more dynamic role of RubisCO in *M. aeruginosa* then is was proposed for model cyanobacteria. To further evaluate the possible location of RubisCO outside of carboxysomes a microscopic evaluation was performed. Several trials were assessed to construct fluorescently labelled RubisCO *M. aeruginosa* strains, but none of the mutants were viable at any time point. Instead immunofluorescence microscopy was chosen to visualize the location of RubisCO and other proteins inside the cell and to get further insights into the high-light dynamics of *M. aeruginosa*.

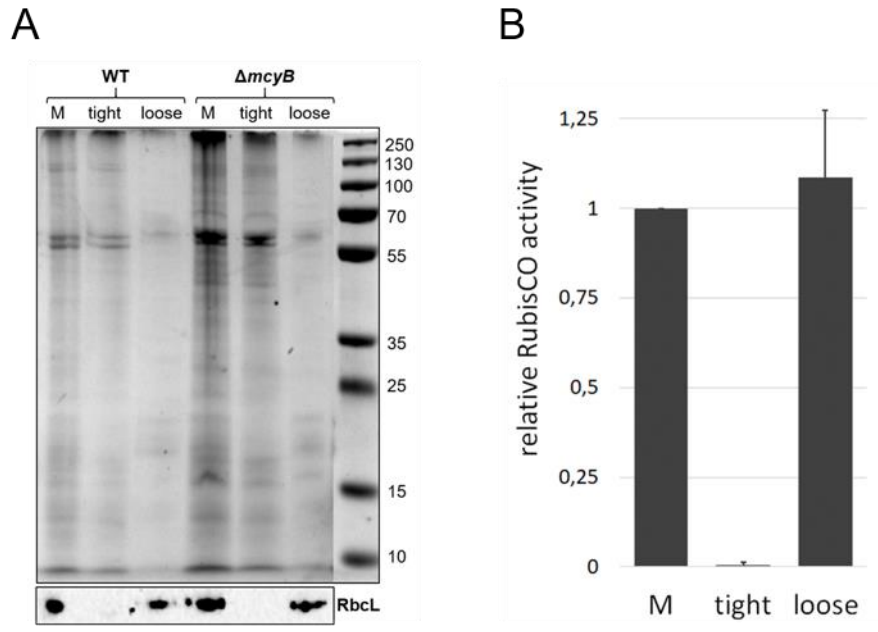

Figure 11. RbcL is loosely attached to membranes in M. aeruginosa PCC7806 and the ΔMcyB mutant. (**A)** RbcL present in the membrane fraction (M) can be completely detached from the membranes by sonication (loose fractions). The remaining membrane fractions contain proteins more tightly connected (tight fractions) but lack detectable RbcL protein. (**B)** RubisCO activity can only be detected in the whole membrane fraction (M) and in the loosely attached protein fraction.

3.2 RubisCO is located underneath the cytoplasmic membrane in *M. aeruginosa*

3.2.1 Establishment of an immunofluorescence microscopy method

Immunofluorescence microscopy (IFM) in cyanobacteria is not trivial, because of the existing pigments like chlorophyll and phycocyanin which can influence the microscopic evaluation due to autofluorescence effects. Hence, the used IFM method needs to be established or adapted to the specific strain which is used. In this study, the fixation of *M. aeruginosa* cells as a first step was a crucial part of sample preparation and success of IFM. The method of antibody hybridization was rather untouched in the establishment of the method (see 2.6 for detailed method). The first used fixative was a combination of the organic solvent methanol and acetone, a well-established fixation method for IFM. This method resulted in cells showing only unspecific signals, whether they were hybridized with the anti-RbcL antibody (α-RbcL) or not. Furthermore, only a very weak autofluorescence signal could be observed (Figure 12A). Since methanol dissolves lipids like membranes it was not suitable as a fixative to preserve the cellular structure. An important part of IFM sample preparation is that the cell needs to be made permeable for antibodies but at the same time the structure of the cell needs to be preserved in the natural state. The next tested fixatives were formaldehyde and glutaraldehyde, because both cross-link proteins and by this should preserve the structure of the cell and not dissolve membranes. Both methods resulted in intact cells with autofluorescence signals. However, glutaraldehyde displayed the same problem as the fixation with methanol/acetone. Only unspecific signals occurred, independent if the sample was hybridized with α-RbcL or not (Figure 12B). The fixation with formaldehyde showed a reliable and specific fluorescence signal of the applied antibody. Hybridizations with only the secondary antibody, which carries the fluorophore, showed no significant signal and confirmed the specificity of the applied primary antibody α-RbcL (Figure 12C). Further tests with all used secondary antibodies in this work confirmed that none of the used secondary antibodies gives a specific signal (Figure S 1). With the established method for IFM sample preparation, the samples from the high-light shift experiments could be studied to visualize the subcellular localization of RubisCO and to possibly confirm the localization outside of carboxysomes with a separate method.

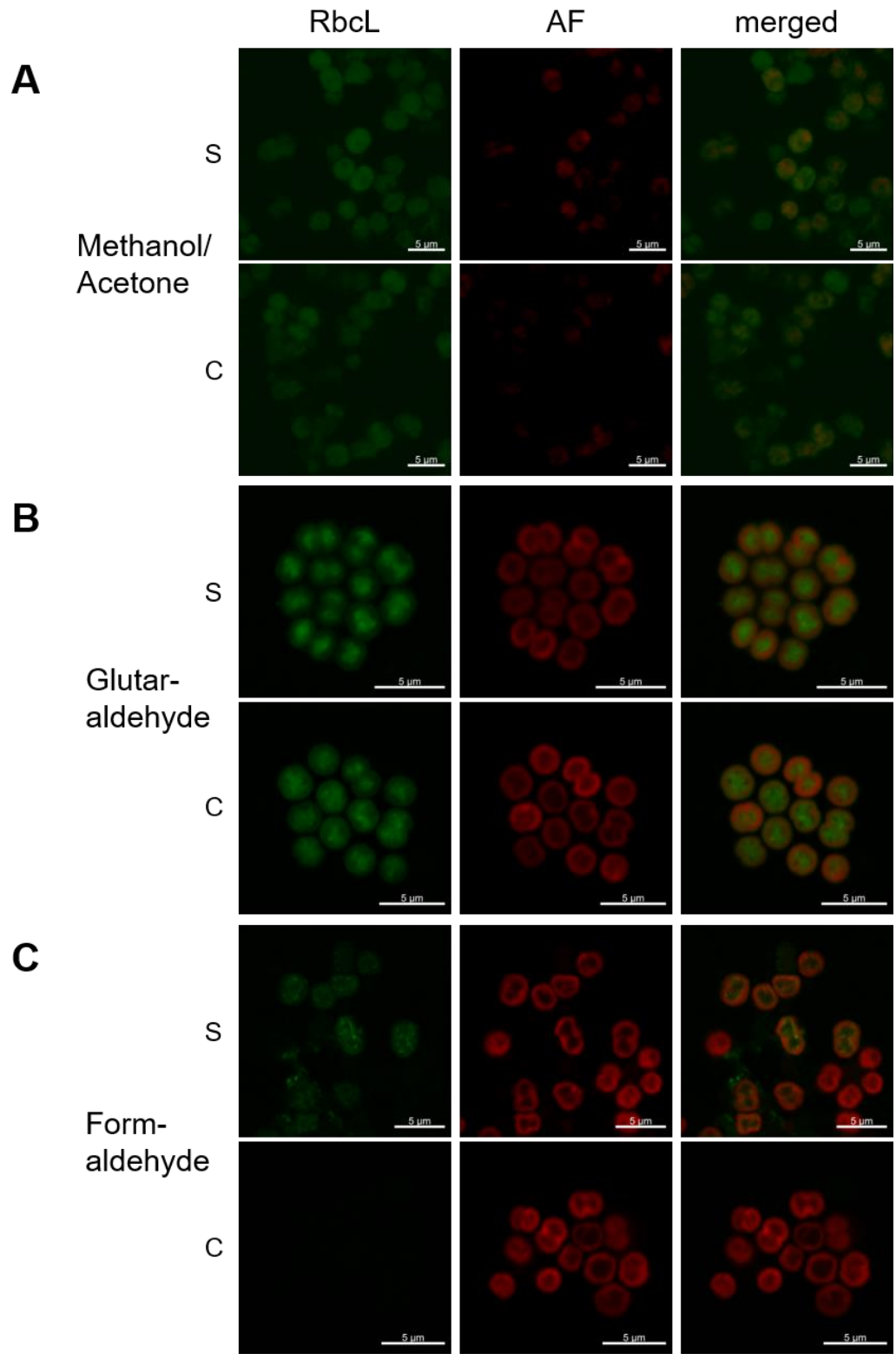

Figure 12. Test of different fixation methods for IFM imaging. M. aeruginosa WT cells were fixed with different fixatives and then hybridized with α-RbcL. **(A)** Methanol/Acetone, **(B)** Glutaraldehyde, **(C)** Formaldehyde. For every fixative, always one sample hybridized with α-RbcL and the secondary antibody (S) and one control sample hybridized only with the secondary antibody (C) is displayed. The green channel is the location of RbcL, the red channel is the phycobilisome autofluorescence (AF) and the third image is the merged image of both images.

The cells of both WT and Δ*mcyB* were hybridized with α-RbcL and α-CcmK independently at every hour of the 4 h high-light shift experiment. The antibody against CcmK (α-CcmK) was also used as marker for successful cell penetration, because carboxysomes are distinct intracellular structures. If α-CcmK gives a ring-like structure, it confirms the successful penetration of the cell and that the intracellular structure is still intact at the same time. CcmK was detected as ring-like signals primarily in the cytosolic matrix of the cells. These structures show that CcmK is involved in carboxysome formation and is an important part of carboxysomes in *M. aeruginosa*. Occasionally, CcmK was observed in the periphery of the cell. There it appeared as unstructured or undefined spots and did not form carboxysomes. This observation was true for both WT and Δ*mcyB* (Figure 13). The independent method of IFM matched generally with the results of the immunoblotting of CcmK, since the majority of CcmK appeared in the cytosolic fraction and IFM visualized this. In addition, IFM even showed signals in the periphery of the cell which most likely are the signals in the membrane-associated protein fractions in immunoblotting (Figure 10B-C). Unlike CcmK, RbcL showed a large heterogeneity between low-light and high-light conditions and during the high-light exposure. At every time point of the experiment, *M. aeruginosa* WT and Δ*mcyB* were heterogeneous cultures in terms of RbcL localization. Low light adapted-cells of both strains showed RbcL mainly located in the cytosol as a diffuse signal. In a lot of low-light cells RbcL was observed to accumulate in small spots in the cytosolic matrix which is possibly the carboxysomal RubisCO. This observation was more pronounced in Δ*mcyB* then in WT (Figure 13). In addition, for the WT some spots of RbcL were located at the cytoplasmic membrane (Figure 13A). Already after 1 h of high-light exposure, more spots were located at the cytoplasmic membrane then the cytosol in WT. This trend intensified in the next hours to the point, where in most of the cells RbcL was located exclusively at the cytoplasmic membrane in a lot of aggregates (Figure 13A). The same trend was observed in Δ*mcyB*, but it was only after 3 h of high-light treatment (Figure 13B). Since not all cells of the culture showed the subcellular relocalization of RubisCO to the cytoplasmic membrane, at all time points cells with RbcL mainly located in the cytosol were present. These results suggest that a cyanobacterial colony also under major changing environmental conditions consists of different cell types and only their ratio inside of the colony changes. MC seems to play an important role in the relocalization process, because the RubisCO dynamics in

Δ*mcyB* are lagging clearly behind the WT. Furthermore, the IFM images strengthen the hypothesis that large amounts of active RubisCO are not located inside of carboxysomes under high-light conditions. This phenomenon is not reported for any cyanobacterium until now.

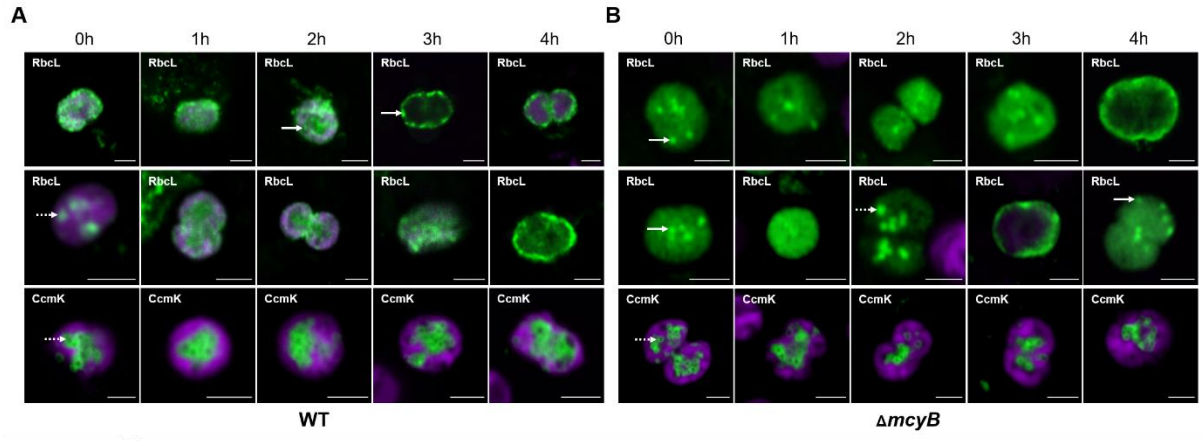

Figure 13. Immunofluorescence micrographs (IFM) visualizing the subcellular localization of RbcL and CcmK in M. aeruginosa wild type (WT) and ΔmcyB mutant during the light-shift experiment. **(A)** Immunostaining of RbcL and CcmK in M. aeruginosa WT cells with respective antibodies. **(B)** Immunostaining of RbcL and CcmK in M. aeruginosa ΔmcyB mutant cells with respective antibodies. The green fluorescence signal indicates the subcellular localization of RbcL and CcmK respectively; the purple signal reflects the autofluorescence of thylakoid-associated phycobiliproteins. In the WT, RbcL appears as spots in the cytosol or underneath the cytoplasmic membrane (arrow) or in apparent carboxysomal bodies (dashed arrow), while it shows a homogenous distribution with a few concentrated spots in the ΔmcyB mutant. CcmK signals show the characteristic carboxysome structures (arrow) inside the cytosol and some undefined structures at the cytoplasmatic membrane (dashed arrow) in both WT and in the ΔmcyB mutant strains. The scale bar in all images is 2 µm.

3.2.2 Population density is an important parameter for RubisCO dynamics

To further understand the role of protein-binding of MC in this process diurnal cultivation experiments were carried out with two different starting cell densities (OD_{750} 0.3 and 0.6). As reported in earlier studies, MC only bound to proteins at higher cell densities and only in the cytosolic fraction. Several distinct bands appeared in the immunoblot, further strengthen the theory that MC binds to several different proteins in *M. aeruginosa*. Besides a signal at 52 kDa, the size of RbcL, especially the strong band on top of the SDS gel is noticeable. It appears to be an SDS stable high mass complex, but further examination will be done in later chapter (3.4). In turn, the membrane fraction is free of protein-bound MC. At lower cell densities no protein-bound MC could be detected neither in the cytosolic fraction nor in the membrane fraction. The double-staining with α-RbcL and α-CcmK revealed a clear separation of RbcL and CcmK during daytime at higher cell densities and further underlines the

existence of RubisCO outside of carboxysomes. This experiment also showed that the relocalization process under high-light is a reversible process, because at nighttime most of RbcL is found in the cytosolic matrix and at the inner layer of the thylakoid membrane. The localization of RbcL at the thylakoid membrane is another facet of the subcellular localization of RubisCO, since low light-adapted cells of *M. aeruginosa* WT and Δ*mcyB* showed RbcL located mainly in the cytosolic matrix and not at the thylakoid membrane (Figure 13). Interestingly, at lower cell densities no dynamics of RbcL were observed. During daytime RbcL stayed at the inner layer of the thylakoid membrane and the cytosolic matrix, only a weak signal at the cytoplasmic membrane was observed. This results clearly show, that the subcellular relocalization of RubisCO is a reversible process and is depending on a certain population density.

Furthermore, the co-localization of RbcL and RbcS were tested in this experimental setup. Both, the WT and the Δ*mcyB* mutant were examined (Figure S 2). Interestingly, the two subunits of RubisCO only showed a partial overlap of it signals. In the WT, RbcL was mainly located underneath the cytoplasmic membrane, whereas RbcS was found in distinct spots in the cytoplasm and near the thylakoid membrane (Figure S 2A). In addition, the IFM images underline that the observed shift of both subunits during the high-light irradiation does not mean that both RbcL and RbcS are found in the same subcellular locations. It is to note, that the used RbcS antibody in this study was raised against the recombinant monomeric protein. This enables the possibility that the used antibody does not recognize RbcS aggregates *in situ* as well as RbcS monomers in immunoblotting analyzes. In the Δ*mcyB* mutant, RbcL and RbcS were partially overlapping. In comparison to the WT, RbcL was more distributed over the cell and RbcS was solely located in the cytosol, resembling carboxysome-like structures (Figure S 2B).

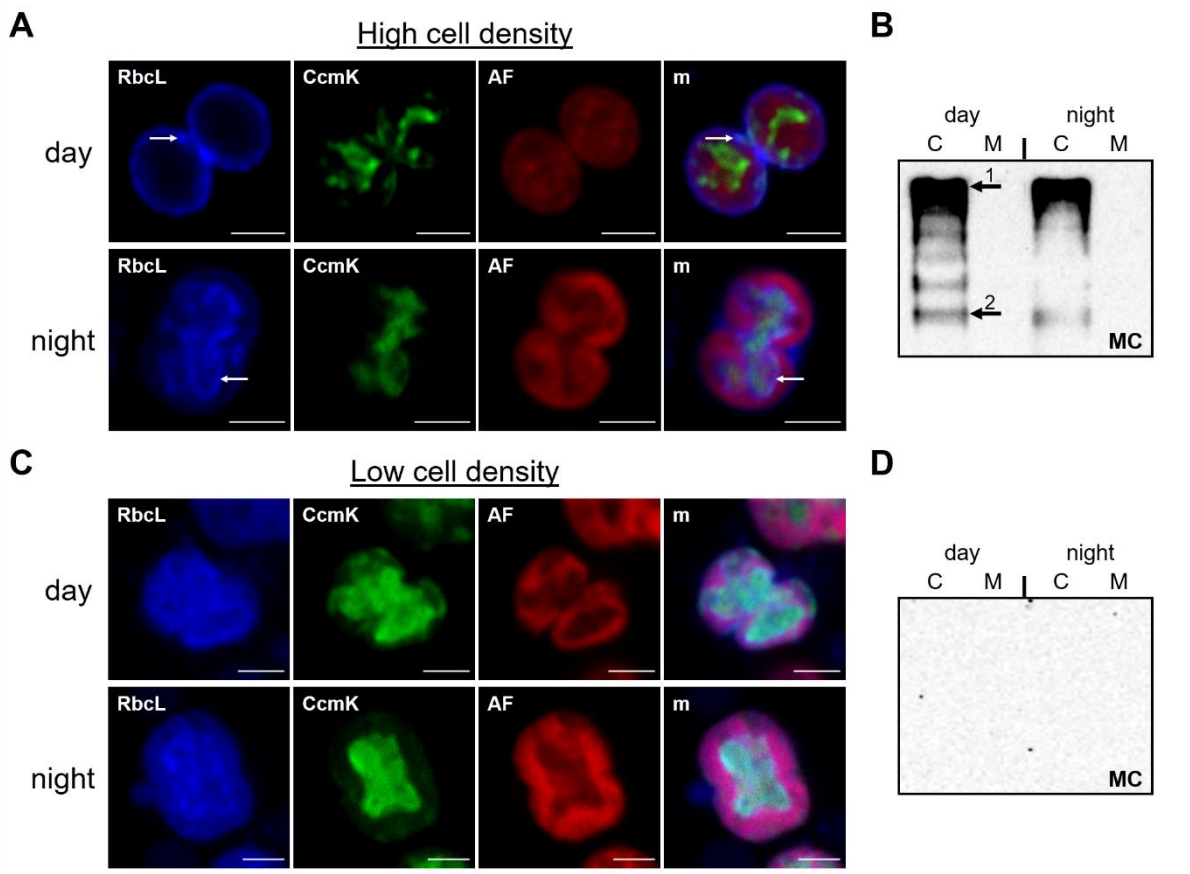

Figure 14. Co-localization of RbcL and CcmK in *M. aeruginosa* WT visualized by IFM and protein-binding of MC. Samples were taken from *M. aeruginosa* WT cultures grown in a diurnal cycle (16 h day, 8 h night; 50 µmol photons m^{-2} s^{-1}). The initial cell density was either OD_{750} 0.6 (high cell density) or 0.3 (low cell density). **(A, C)** IFM micrographs made by co-incubation with α-RbcL and α-MC from cells harvested during daytime and nighttime from high (A) and low cell density (C). The blue channel is the RbcL signal, the green channel the CcmK signal and the red channel the phycobilisome autofluorescence (AF). The image on the right side is the merged image (m) of the three fluorescence channels, which are also indicated at the top left corner of each image. The displayed arrows show the relocalization of RbcL from the cytosolic membrane (day) to the thylakoid membrane (night). The scale bar in all images is 2 µm. **(B, D)** Immunoblot hybridization of cytosolic (C) and membrane (M) protein fraction with α-MC from the same samples as in (A) and (C). The signal indicated by arrow 1 is the putative CBB super complex and the second arrow shows another distinct band at the size of RbcL (≈ 52 kDa).

Transmission electron microscopy (TEM) micrographs of *M. aeruginosa* WT and Δ*mcyB* after high-light treatment further underline the observations made with IFM imaging. Electron-dense granules were visible in both low-light and high-light cells in both WT and Δ*mcyB*. They were mostly located in the cytosol with some granules found next to the cytoplasmic membrane (Figure 15). After 3 h of high-light irradiation, both strains showed different distribution patterns of the granules. Most of the granules remained in the cytosol with some located in the thylakoid membrane area in the MC-deficient mutant. In the WT most granules were found underneath the cytoplasmic membrane (Figure 15). Since the observed distribution of the granules mirrors the

subcellular relocalization of RubisCO in the light shift experiment, it is probable that the granules are RubisCO-rich structures in the cell. The accumulation of RbcL in spots in the IFM micrographs emphasizes this hypothesis. In addition, it is noticeable that most of the carboxysomes in the TEM micrographs are pale structures, because in already available TEM images of *M. aeruginosa* (Benjamin D Rae *et al.*, 2013; Benjamin D. Rae *et al.*, 2013; Faulkner *et al.*, 2017) they always appear as dark structures. Only sporadically electron-dense carboxysomes were observed (Figure 15).

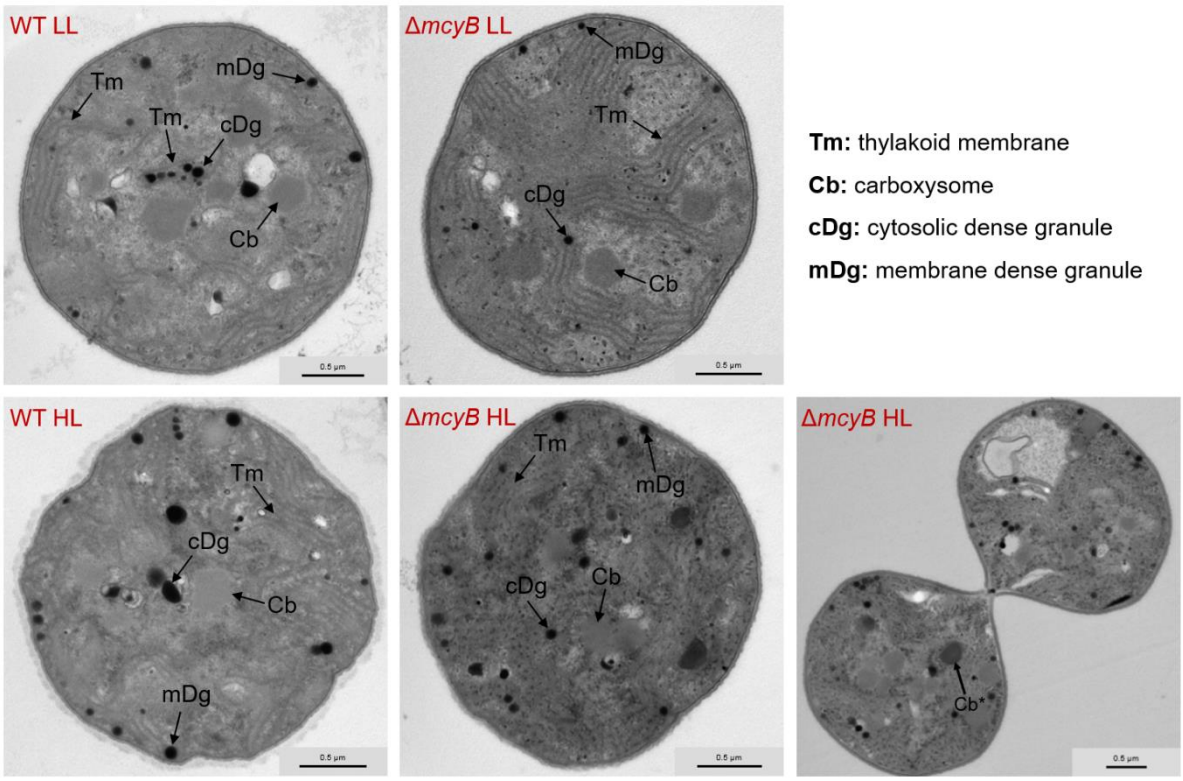

Figure 15. Transmission electron micrographs of M. aeruginosa WT and ΔmcyB. Low light-adapted cultures (LL) were illuminated with high-light (HL) for 3 h. Electron dense granules (Dg) are marked with black arrows. More granules are located underneath the cytoplasmic membrane at high-light conditions in the WT (WT HL) then in ΔmcyB (ΔmcyB HL). Carboxysomes (Cb) appear mostly as pale structures. The second TEM image of ΔmcyB under HL conditions (bottom right corner) shows an electron dense carboxysome, which is marked with an asterisk. The images were made in cooperation with Prof. Otto Baumann (University of Potsdam, Department of Zoophysiology, Institute of Biochemistry and Biology).

Until this point, only the subcellular location of RbcL was determined by IFM imaging as a parameter for RubisCO localization. Since RubisCO consists of two subunits, also the small subunit RbcS needs to be checked. The immunoblot of the light shift experiment already suggested, that both subunits of RubisCO act differently under the changing conditions. RbcS was stable in both protein fractions during the whole high-light treatment and did not show the dynamics of RbcL (Figure 10B-C). To further

examine these differences, a co-staining of high-light treated cells at higher cell density (OD_{750} 0.6) with α-RbcL and α-RbcS was performed (Figure 16). Both strains, the WT and Δ*mcyB*, show a separation of the two subunits in one cell. In the WT, RbcS in located mainly in the cytosolic matrix and at the inner layer of the thylakoid membrane. Some weak signals occurred at the cytoplasmic membrane, where it co-located with RbcL (Figure 16A). In the MC-deficient mutant Δ*mcyB*, RbcS was in the cytosol accumulating in several spots which co-located with cytoplasmic RbcL. This structures probably resemble carboxysomes (Figure 16B). It is to note, that the applied α-RbcS antibody was raised against the monomeric unit of RbcS. Therefore, it cannot be excluded that α-RbcS does not bind to hexadecameric RbcS structures during IFM hybridization, which would explain the missing signals of α-RbcS at membranes in Δ*mcyB*. Nevertheless, the co-staining with α-RbcL and α-RbcS further strengthen the observation that RbcL and RbcS are partly separated from each other in noteworthy amounts in a *M. aeruginosa* cell. The IFM imaging furthermore showed that both RubisCO subunits occur at different membranes inside of the cell under high-light conditions. RbcL relocates to the cytoplasmic membrane, RbcS is mainly found near the thylakoid membrane. Taken together immunoblotting and IFM imaging, is gets clearer that RubisCO in *M. aeruginosa* under high-light conditions deviates from the standard $RbcL_8RbcS_8$ confirmation of Form I RubisCO. Additionally, the results clearly show that the MC-producing wild type and the MC-deficient mutant do not respond equally to the light shift experiments. The response of Δ*mcyB* lags 1-2 h behind the WT and the subcellular relocalization of RubisCO is not as consequent as in the WT.

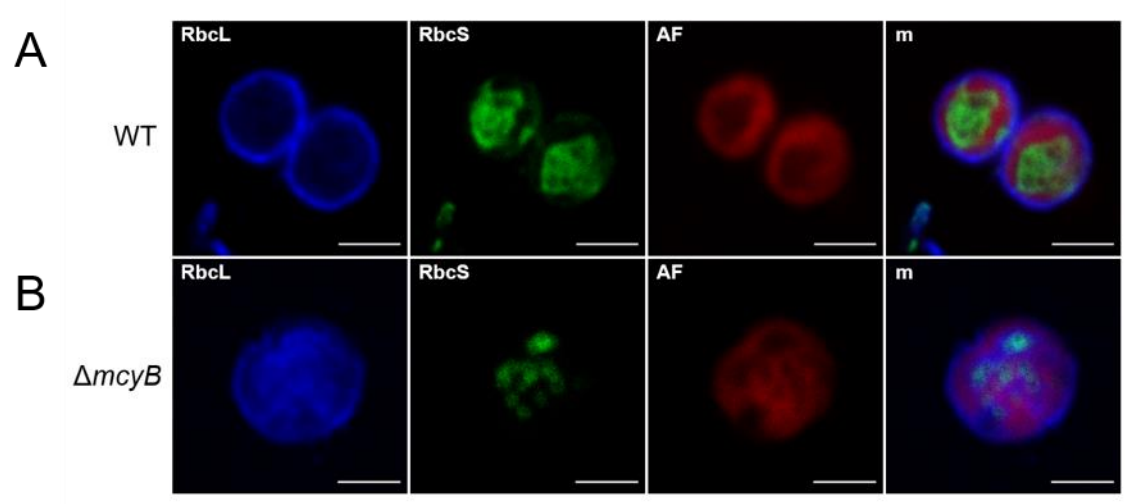

Figure 16. Co-staining of M. aeruginosa WT and ΔmcyB cells after high-light treatment with α-RbcL and α-RbcS visualized by IFM. RbcL is visible in the blue fluorescence channel, RbcS in the green fluorescence channel. The fluorescence channel is indicated in the top left corner of each image. **(A)** Co-localization of RbcL and RbcS in the WT. **(B)** Co-localization of RbcL and RbcS in ΔmcyB. AF = phycobilisome autofluorescence, m = merged image from the 3 fluorescence channels. The scale bar in all images is 2 µm.

3.3 Subcellular localization of protein bound microcystin

To further study the physiological role of MC in the high-light adaptation of *M. aeruginosa*, the subcellular localization of some MC biosynthesis proteins (McyB and McyF) and MC itself in the *M. aeruginosa* WT was examined by IFM imaging (Figure 17). McyB and McyF are both enzymes which are involved in the complex biosynthesis of MC. Specific antibodies against both McyB (a non-ribosomal synthetase) and McyF (aspartate racemase) were applied to high-light treated WT cells. Interestingly, both proteins were located exclusively at the thylakoid membrane facing the cytoplasmic space (Figure 17A-D). This leads to the assumption that the MC biosynthesis complex is anchored to the thylakoid membrane. To visualize the localization of intracellular MC a commercially available antibody against MC was used. Microcystin was primarily detected in the cytosol and at the thylakoid membranes and appeared as spots. A smaller portion of MC was also located underneath the cytoplasmic membrane. There it co-located with RbcL under high-light conditions (Figure 17E-H). However, the co-localization with RbcS was more pronounced then with RbcL. The MC aggregates in the cytosol co-located nicely with the RbcS spots, and the MC signal at the thylakoid membrane overlapped perfectly with the RbcS signal (Figure 17I-P). It needs to be noted, that the observed MC signal is the protein bound fraction of MC, because the

applied fixation dissolved the free MC pool. The results lead to the hypothesis that MC is synthesized at the thylakoid membranes into the cytoplasmic matrix where it primarily interacts with RbcS rather than RbcL as the binding partner of RubisCO.

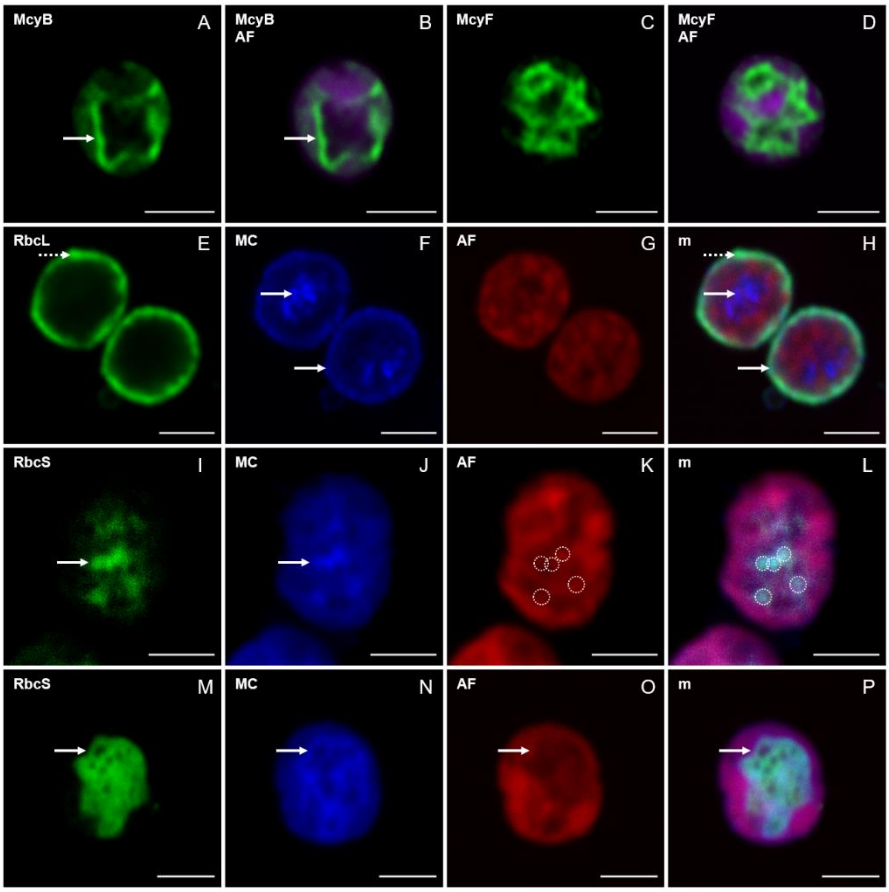

Figure 17. Location of MC and the biosynthesis enzymes McyB and McyF in high-light treated M. aeruginosa WT cells visualized by IFM. The respective fluorescence channels are indicated in the top left corner of each image. **(A-B)** Location of McyB. The green channel (McyF) is displayed alone and merged with the phycobilisome autofluorescence (AF). The arrows indicate the strong McyB signal at the thylakoid membrane. **(C-D)** Location of McyF. The green channel (McyF) is displayed alone and merged with the AF. **(E-H)** Co-staining with α-RbcL and α-MC. The green channel shows the location of RbcL, the blue channel of MC and the red channel the AF. The last image of this row is the merged image of the three channels. The continuous arrow shows the location of MC in the cytosol and underneath the cytoplasmic membrane. The dashed arrow displays RbcL located underneath the cytoplasmic membrane. **(I-P)** Co-staining with α-RbcS and α-MC. Both proteins co-locate in the cytosol (I-L) and at the thylakoid membrane (M-P). The green channel shows the location of RbcS, the blue channel of MC and the red channel of the AF. The last image in both rows is the merged image of the three channels. The arrow shows the location of MC in the cytosol (I-J) and at the thylakoid membrane (M-P). The dashed circles highlight the overlapping of both signals in the cytosol. The scale bar in all images is 2 µm.

3.4 RbcS and MC are part of a putative Calvin-Benson-Bassham cycle super complex

The previous results of this study already indicated that RubisCO in *M. aeruginosa* deviates from the canonical theory of RubisCO in cyanobacteria. Under high-light conditions RbcL and RbcS are partly separated and both accumulate in aggregates. Furthermore, the diurnal cultivation experiment showed that under higher cell densities (OD_{750} 0.6) MC bound to a high mass complex besides RbcL. To further investigate possible different RubisCO types in *M. aeruginosa* resulting from this separation and accumulation in aggregates, native protein extracts of high-light treated *M. aeruginosa* WT (OD_{750} 0.6) were analyzed (Figure 18). A high molecular mass complex was observed in both the cytosolic and the membrane protein fraction. This complex was identified as the canonical $RbcL_8RbcS_8$ confirmation of RubisCO (Liu *et al.*, 2010) through the analysis of similar treated *Synechocystis* sp. PCC 6803, which showed this mass complex as well (Figure 18A). The signal of RbcS in the membrane fraction furthermore showed that RbcS is also part of the RubisCO complex, even though RbcS rarely occurred in IFM studies at the cytoplasmic membrane. Nevertheless, RbcS was additionally detected in another high molecular mass complex which did not contain RbcL in the membrane fraction (Figure 18A). This strengthen the hypothesis of different independent RbcS species in *M. aeruginosa*. To further investigate the different high molecular mass complexes, the membrane fraction was sonicated several times to detach loosely bound proteins from the membranes. RbcL was found in the loose fraction only in the L_8S_8 confirmation, RbcS was separated into the loose fraction (only L_8S_8 type) and the tightly bound fraction, where it remained bound to the membrane. The samples were also immunoblotted against α-MC. This immunoblot revealed three major bands: one related to the RbcL-free complex and one related to the L_8S_8 RubisCO. The third band did not relate to neither RbcL nor RbcS signals. MC also appeared besides the RbcS-containing complex in all other analyzed fractions (Figure 18A).

Previous data showed that MC can bind to many enzymes of the CBB cycle. In addition, several studies suggested that cyanobacteria possess CBB enzyme super complexes like higher plants. These complexes would allow an easier and more

efficient transfer between the involved enzymes of the CBB cycle and maybe are an explanation for the efficient growth of *M. aeruginosa* under stressful conditions. MC and RbcS could be part of such a complex, since they both occur in the additional high molecular mass complex in the native protein gels. To further test the hypothesis of a CBB super complex, the presence of the Phosphoribulokinase (PRK) was checked. PRK catalyzes the transformation of Ribulose-5-phosphat to RuBP, which is the substrate for RubisCO. As expected, PRK could be found in the putative CBB super complex and corresponded perfectly to the obtained MC signals (Figure 18A). Thus, MC and PRK are likely parts of the super complex and MC acts as a linker between the different CBB cycle enzymes in this putative complex. Furthermore, PRK signals were also observed in IFM images of high-light treated *M. aeruginosa* WT cells (Figure 18C). The appearance as spots further underlines the hypothesis of a super complex and gives a possible explanation for the aggregation of RbcL in spots underneath the cytoplasmic membrane as well.

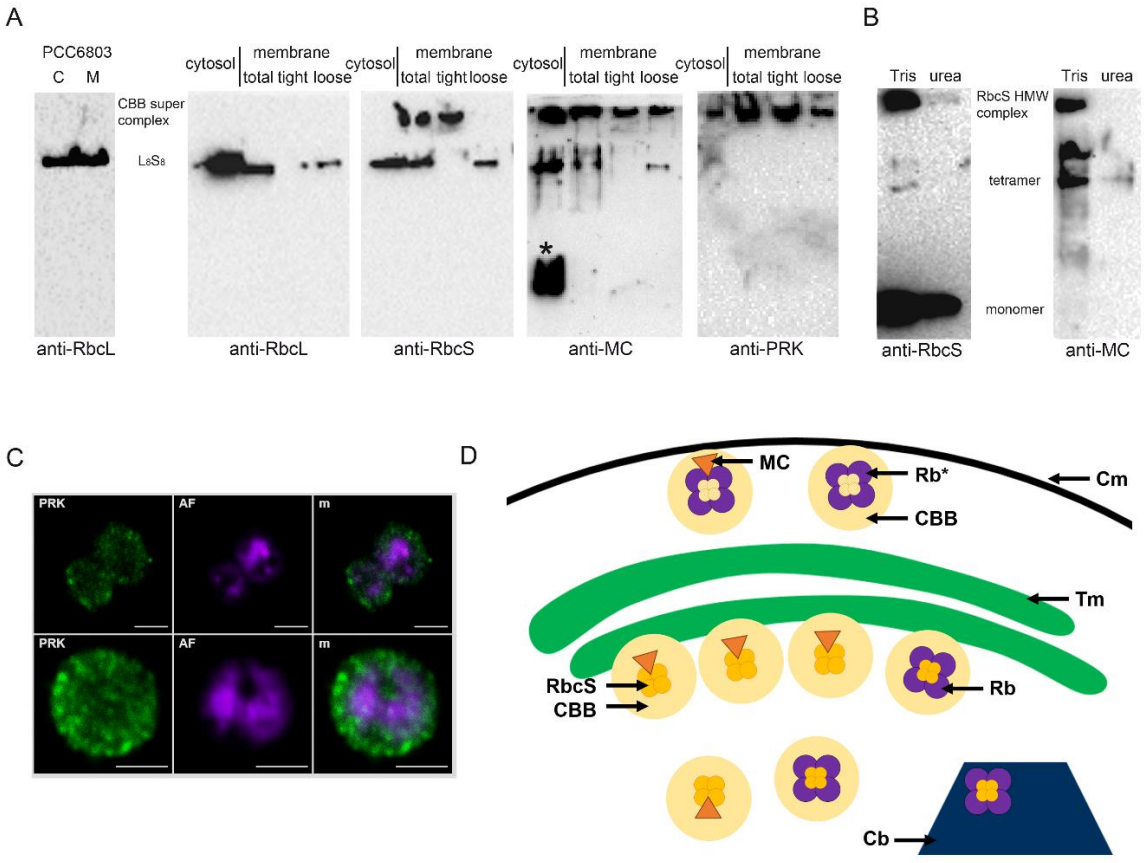

Figure 18. Native PAGE analysis of RubisCO complexes and RbcS-MC binding analysis. **(A)** Native immunoblots of Synechocystis PCC 6803 and M. aeruginosa PCC 7806 cytosolic (C) and membrane (M) protein fractions. The extracts of PCC 6803 were tested against α-RbcL (top left blot). The remaining

immunoblots with antibodies against RbcL, RbcS, MC and PRK were made with extracts of PCC 7806 only. The used antibody is indicated below each blot. The membrane protein fraction of PCC 7806 was further treated and separated into total membrane fraction, tightly bound membrane proteins (tight) and loosely bound membrane proteins (loose). To major bands were identified in all blots: A putative CBB super complex and the canonical $RbcL_8RbcS_8$ confirmation of RubisCO. The MC binding neither related to RbcL or RbcS binding is indicated with an asterisk. **(B)** Immunodetection of RbcS in RbcL-free fractions of RubisCO. The extracts were tested with antibodies against RbcS and MC (indicated below the blots) and treated with the standard SDS protocol (Tris) and with additional urea (urea). The three major bands were labelled: the putative RbcS high molecular weight complex (HMW complex), the RbcS tetramer and the RbcS monomer. **(C)** Visualization of PRK in high-light treated cells of M. aeruginosa WT by IFM imaging. The green channel indicates the location of PRK, the purple channel the phycobilisome autofluorescence (AF). The third image is the merged image of both channels (m). Two separate cells from one sample are shown. The scale bar in all images is 2 µm. **(D)** Schematic representation of cytosolic and membrane bound RubisCO (Rb) and the putative CBB cycle super complex (CBB). Rb^+ shows cytoplasmic membrane bound RubisCO, which may deviate from the canonical RubisCO confirmation. Thylakoid membrane bound RubisCO shows the canonical confirmation and additionally RbcL-free RbcS bound to MC and the CBB super complex is located there. MC is shown as orange triangles. Both types of canonical RubisCO and RbcS-containing super complex also appear in the cytosol. Cm: cytoplasmic membrane, Tm: thylakoid membrane, Cb: carboxysome. The data for this figure were made in cooperation with Dr. Arthur Guljamow (University of Potsdam, Department of Microbiology, Institute of Biochemistry & Biology).

Purified RbcL-free RbcS extracts of high cell density *M. aeruginosa* WT cultures showed an SDS stable high molecular mass complex together with the monomer of RbcS. When urea was added to the sample as a stronger denaturing agent, the complex disappeared and only the monomeric band remained. When α-MC was applied to both RbcL-free RbcS extracts (standard SDS and with urea), the MC signal of the high molecular mass complex vanished after the treatment with urea. Interestingly, no MC was found at the size of the RbcS monomer (Figure 18B). In addition, RbcS signals of approximately 55 kDa were obtained in thylakoid membrane purifications, representing tetramers of RbcS (Figure S 3). This signal was free of RbcL, which further strengthen the existence of significant amounts of RbcL-free RbcS in a *M. aeruginosa* cell. This SDS stable complexes could be dissolved with urea as well, resulting in the presence of the monomeric form of RbcS exclusively. The disappearance of the RbcS-containing high molecular mass complex under stronger denaturing conditions and the non-binding of MC to the RbcS monomer leads to the conclusion, that MC specifically binds to RbcS oligomers rather than the monomer and that this binding is of non-covalent nature.

3.5 Peptide dynamics at different cell densities

Previous experiments in this work already suggested that the observed dynamics of RubisCO, carboxysomes and the CCM in general are strongly influenced by the cell density of the population (see 3.2.2). RbcL relocates from the cytosol to the cytoplasmic membrane only at higher cell densities, at lower densities RbcL remains mainly in the cytosol and at the thylakoid membrane. This first diurnal incubation experiment furthermore proved that the observed dynamics are reversible processes which also depend on certain prerequisites like cell density. To further test this hypothesis, a full diurnal incubation experiment with the *M. aeruginosa* WT was performed to get a better understanding of the already observed dynamics. A special emphasis was put on the role of microcystin in these experiments, since previous results of this work show on the one hand a strong intracellular involvement into the CCM dynamics and on the other hand a possible role of MC as a signaling molecule.

The growth of the cultures in the diurnal cycle (16 h daytime at 55 µmol photons m^{-2} s^{-1}, 8 h nighttime without light) showed differences depending on the initial cell density. Both experiments were performed with three biological replicates, which behaved quite similarly in both experiments as well. At lower cell densities (OD_{750} 0.25) the population density increased over the whole experiment to an end point of $OD_{750} \approx 0.5$ with a short drop at the transition from the 1st day to the 2nd night (t18). The population density of the higher cell density experiment (initial OD_{750} 0.55) remained rather unchanged over the experiment (Figure 19A, D). Also, in this experiment the transition from the 1st day to the 2nd night initiated some changes in the cell density with an increase to an OD_{750} 0.6 - 0.65, but it decreased afterwards to the OD_{750} of around 0.55 in all three replicates. This first look on the growth curves revealed only a first idea about potential dynamics in a diurnal cycle, since the transitions from day to night and *vice versa* initiated some changes in the population densities.

The peptide analysis by HPLC revealed considerable differences between the two cell densities. The total intracellular peptide fraction of the low-density experiment showed only minor changes over the whole experiment. MC-LR and [D-Asp3]-LR could be detected reliably together with some unidentified compounds. The detected unidentified compounds differed between the pellet and supernatant fraction. However, the amounts of MC and the other compounds were lower in the supernatant than in

the pellet fraction, but in both fractions no strong dynamic of any compound could be detected (Figure 19E, F). Despite the growth dynamics in the higher cell density experiment, no strong dynamics in the total peptide fraction of the pellet could be detected. Besides MC-LR and [D-Asp3]-LR, four additional compounds occurred in detectable amounts (P1-4) (Figure 19B). One of these compounds could be identified as cyanopeptolin 963-A (P2). This variant of cyanopeptolin possesses a L-tyrosine at position 2 instead of arginine (Bister *et al.*, 2004). In the supernatant fraction also several compounds besides MC and cyanopeptolin 963-A were detected (P5-11), which remain unidentified (Figure 19C). In comparison with the pellet fraction, the peptides in the supernatant showed stronger dynamics. MC needs to be noted as a peptide with especially pronounced variations. Since the lower cell density experiment only shows minor changes in the peptide profile over the course of the experiment, further analyses were performed with the higher cell density samples only.

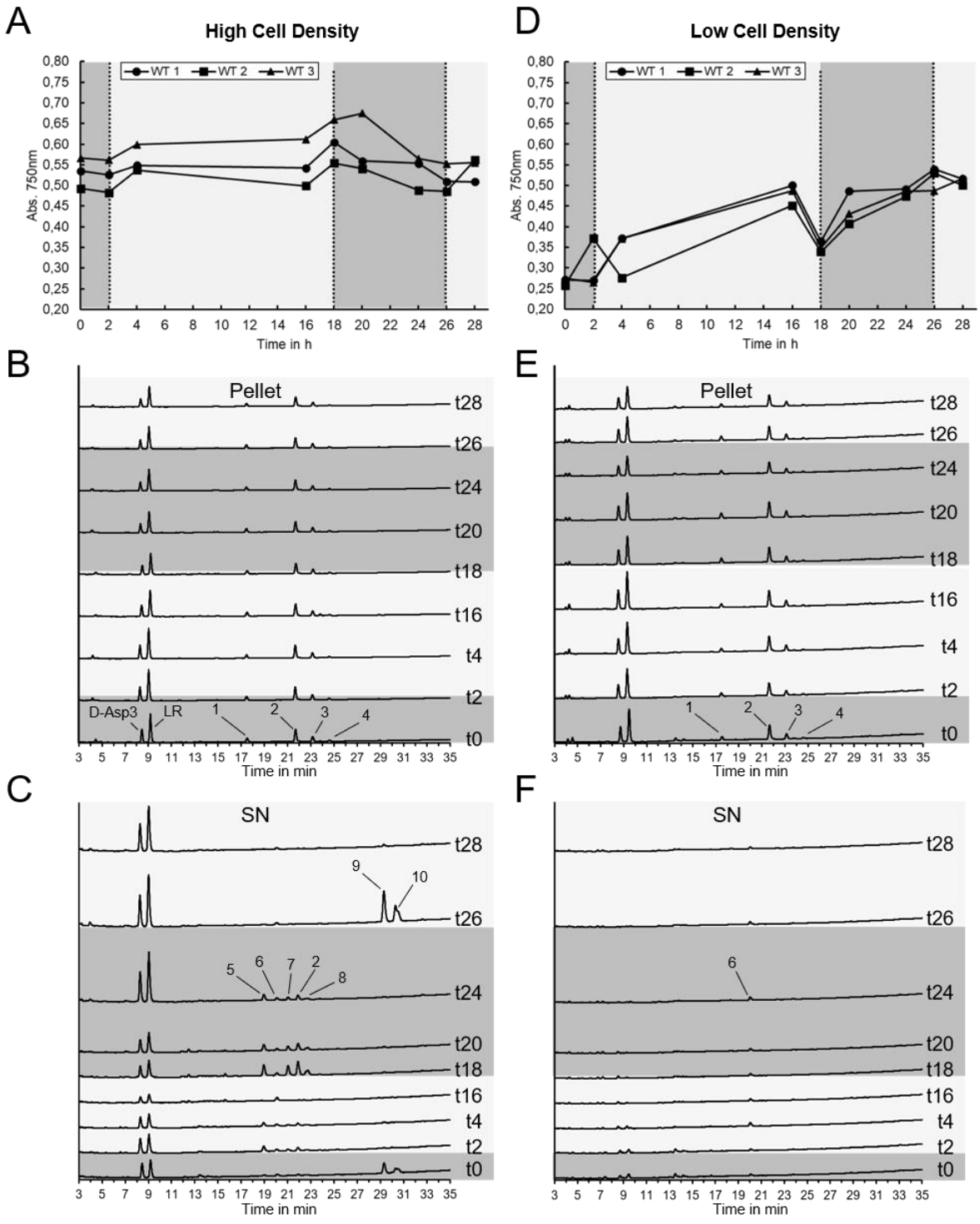

Figure 19. Growth curves and HPLC chromatograms of diurnal incubation experiment of *M. aeruginosa* WT. **(A, D)** Growth curves of three biological replicates. The optical density was measured at a wavelength of 750 nm. Daytime was 16 h (55 µmol photons m^{-2} s^{-1}; white background), nighttime 8 h (grey background). The replicates are indicated by the legend in the figure. (A) higher OD experiment with starting OD ≈ 0.55; (D) lower OD experiment with starting OD ≈ 0.25. **(B, E)** HPLC chromatograms of pellet fraction of higher OD (B) and lower OD experiment (E). The retention time is shown at the x-axis. MC-LR and D-Asp3-LR peaks are marked in figure B as an example. Visible peaks other than MC are named P1-P4 in the higher OD experiment (B). **(C, F)** HPLC chromatograms of the supernatant (SN) fraction of higher OD (C) and lower OD experiment (F). The supernatant fraction derived from the same sample as the pellet fraction. Visible peaks other than MC are named P5-P10.

3.6 Microcystin as a signaling molecule

3.6.1 Trends of intra- and extracellular microcystin and cyanopeptolin

To further asses the dynamics of MC and other peptides in the diurnal cycle of *M. aeruginosa*, steady-state levels of the identified peptides were examined. In all further results, the mean of the three replicates of the experiment was calculated and shown (Figure 20). *M. aeruginosa* PCC 7806 WT produces the MC variants -LR and -[D-Asp3]-LR. Both variants only differ in the modification of aspartate in position 3: in [D-Asp3]-LR, the aspartate lacks the methylation (Figure 20C). Otherwise these two variants are identical. However, both variants occur in different amounts in *M. aeruginosa* WT. The strain in this experiment always showed a higher concentration of MC-LR than MC-[D-Asp3]-LR, irrespective from the time point of the experiment. In the intracellular fraction, both MC variants behaved similarly, only the concentrations differed significantly (Figure 20A). The maximum point was reached at the end of the 1st night with around 450 ng/ml for MC-LR and 125 ng/ml for MC-[D-Asp3]-LR. During the 1st day, the concentration decreased continuously. This trend was sustained during the 2nd night as well and resulted in the low point of both MC variants at the end of the 2nd night (MC-LR: 250 ng/ml and [D-Asp3]: 75 ng/ml). Interestingly, the first time point into the 2nd day showed again a strong increase of MC. These results clearly show that intracellular MC is not available at all time during a diurnal cycle at the same level. It shows fluctuations in the concentration which cannot be related fully to the growth of the cultures, because the increase in cell density during the transition from the 1st day into 2nd night did not result in an increase of MC (Figure 20A).

As previous studies showed, MC can possibly act as an extracellular signaling molecule besides its intracellular effects. It influences the growth of *M. aeruginosa* and leads to a changed secondary metabolome. High amounts of MC could be detected in the supernatant of the high-density culture with a strong dynamic (Figure 20B). During the 1st day, the concentration of MC decreased slightly to a low point of around 50 ng/ml for MC-LR and around 25 ng/ml for [D-Asp3]. Interestingly, at the start of the 2nd night the amount of MC increased drastically until the end of the night and remained constant at the beginning of the next day. After this dramatic increase in the supernatant, concentrations of MC-LR of around 250 ng/ml ([D-Asp3] around 100 ng/ml) could be measured. Since the morphology of the culture and its cell density did

not indicate the lysis of big parts of the culture, an active release of MC by the *M. aeruginosa* WT is highly likely.

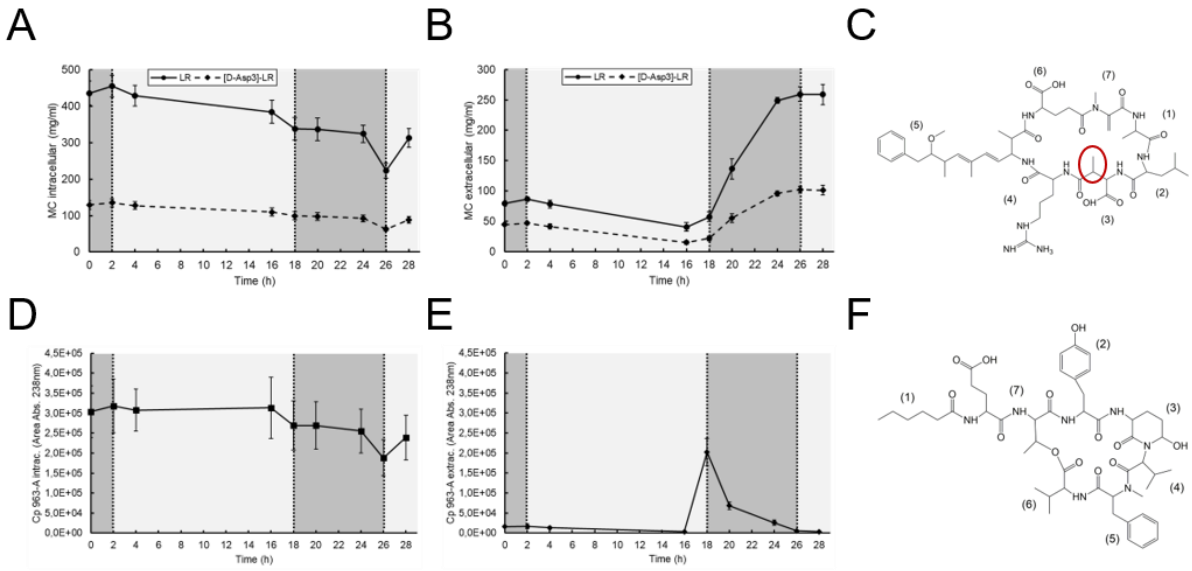

Figure 20. Quantification and trend of steady-state levels of intra- and extracellular MC and cyanopeptolin 963-A over the diurnal cycle of *M. aeruginosa* WT. **(A)** Steady-state levels of intracellular MC-LR and D-Asp3-LR during the diurnal cycle. **(B)** Steady-state levels of extracellular MC-LR and D-Asp3-LR during the diurnal cycle. **(C)** Structure of microcystin-LR. The difference between MC-LR and D-Asp3-LR is indicated with the red ellipse. In MC-D-Asp3-LR, the D-aspartate at position 3 is demethylated. (1) Ala, (2) Leu, (3) N-methyl-Asp, (4) Arg, (5) Adda, (6) Glu, (7) N-methyl-dehydro-Ala. **(D)** Steady-state levels of intracellular cyanopeptolin 963-A during the diurnal cycle. **(E)** Steady-state levels of extracellular cyanopeptolin 963-A. In all three figures, white backgrounds indicate daytime, grey background nighttime. The standard deviation of three biological replicates is displayed. The shown trends are clarified in the displayed legend. **(F)** Structure of cyanopeptolin 963-A. (1) fatty acid, (2) Tyr, (3) Ahp, (4) Leu, (5) methyl-Phe, (6) Val, (7) Thr.

Besides MC also cyanopeptolin 963-A (Figure 20F) was identified and quantified to assess possible dynamics of this oligopeptide. The intracellular fraction of cyanopeptolin showed the same trend as MC (Figure 20D). It slightly decreased over the course of the whole experiment and reached the low point at the end of the 2nd night. More interesting than the intracellular data is the extracellular trend. It was nearly not detectable at the beginning of the diurnal incubation experiment, but at the end of the 1st day (t18, transition to nighttime) there was a burst of extracellular cyanopeptolin 963-A (Figure 20E). The amount declined during the night and was hardly measurable at the beginning of the next day. These extracellular variations further strengthen the hypothesis that the oligopeptides of *M. aeruginosa* are actively secreted and fulfill extracellular functions other than inhibiting the growth of competing organisms.

3.6.2 Dynamics of protein-bound microcystin

The increase of extracellular MC is also in line with the decrease of intracellular MC. This decline of MC is reflected in the protein bound fraction of MC, detected by immunoblotting (Figure 21B). This fraction reached the highest amount in the span of 2 h before night and 2 h into the night. The constant signals of the SDS protein gels of the total protein extracts verified that the increase of MC signal cannot be explained by the increase of the amount of total proteins in the sample (Figure 21A). Afterwards, the protein bound MC dropped strongly to a very weak signal in the immunoblot together with the intracellular MC and the large gain of extracellular MC detected via HPLC analysis. Interestingly, the loss of MC as observed in the immunoblot differed from the result of the IFM imaging of MC (Figure 21C). At t28 (2h into 2nd day) MC occurred as several spots in the cytosol even though in the immunoblot the MC signal was very weak. This discrepancy could be explained by the possibility that different pools of MC are detected by the different detection methods. Due to the rather harsh and denaturing method of IFM imaging, probably only covalently protein-bound MC is detected, and the immunoblotting detects the non-covalent bound MC. Since HPLC quantification showed at any point of the diurnal incubation experiment sufficient intracellular amounts of MC (Figure 20A), the decrease of the MC signal in the immunoblot can be attributed to the loss of non-covalently bound MC intracellularly.

However, key proteins of the CCM remained rather constant in the performed immunoblotting of total protein extracts (Figure 21B). Both subunits of RubisCO, RbcL and RbcS, did not a show a significant change of their quantity unless the last time point of the experiment. 2 h into the 2nd day the RbcL signal is clearly weakened, the RbcS signal remained constant. In addition, the CcmK signal showed no strong fluctuations as well. The maximum point was reached 14 h into the 1st day, like for RbcS (Figure 21B). These immunoblotting results furthermore show that the loss of protein bound MC does not immediately lead to the decrease of RubisCO or other key proteins of the CCM in *M. aeruginosa* or at least the changes are delayed for several hours.

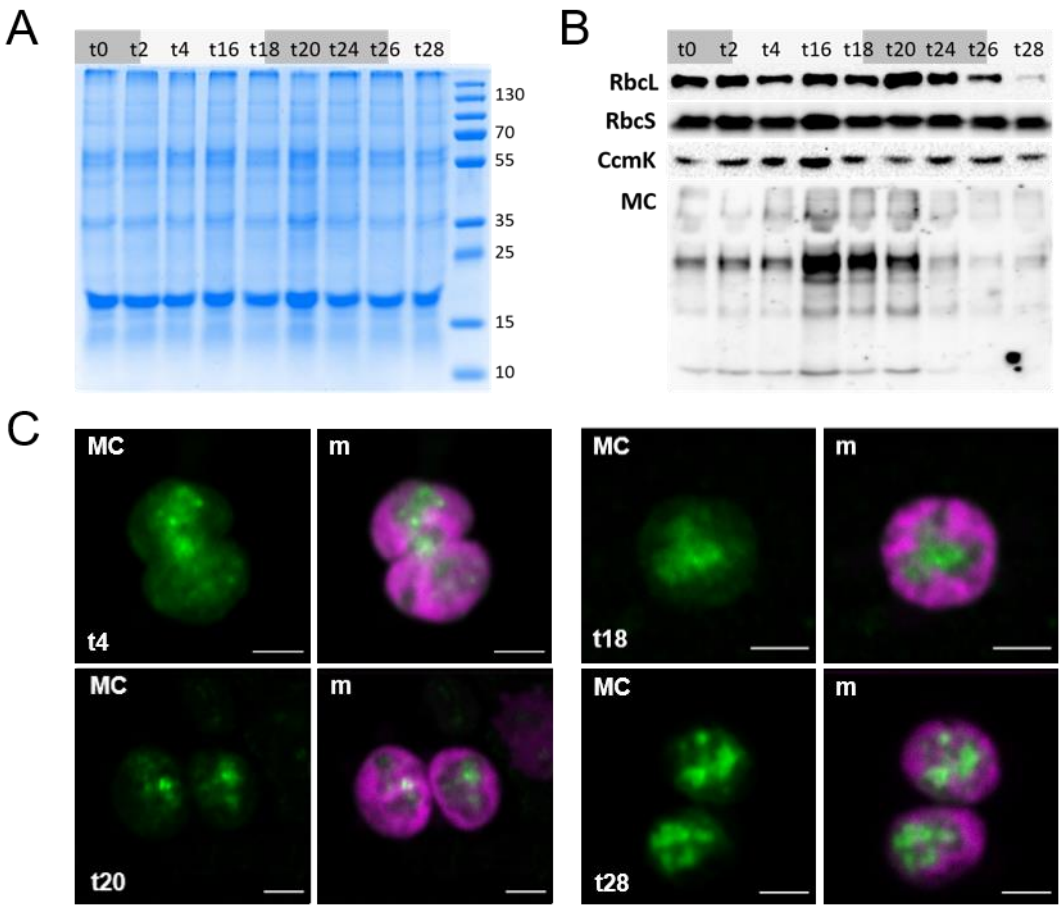

Figure 21. Immunoblot of key proteins of the CCM in *M. aeruginosa* WT and IFM imaging with MC antibody during the diurnal experiment. **(A)** SDS protein gel of total protein extracts of all samples of diurnal experiment. The displayed protein ladder is PageRuler Plus Prestained Protein Ladder (Thermo Scientific). **(B)** Immunoblot analysis of RbcL, RbcS, CcmK and MC of total protein extracts. The same samples as for (A) were used. **(C)** IFM imaging of *M. aeruginosa* WT cells from the diurnal cycle. Four time points were chosen to represent the MC localization during the transition from day to night and *vice versa*. The used time points are displayed in the bottom left corner of the image. The green channel shows the location of MC (as indicated in the top left corner) and the merged image (m) with the phycobilisome auto fluorescence (purple color) is shown. All scale bars are 2 µm.

3.7 The role of RubisCO in the diurnal cycle

Immunoblot analysis itself does not give evidence if RubisCO activity is constant during the diurnal cycle or if there are fluctuations as well. To assess the activity of RubisCO, steady-state levels of the direct fixations products of RubisCO, 3-PGA and 2-PG, were analyzed to evaluate the oxygenase and carboxylase activity of RubisCO (Figure 22A, B). Both fixation products differed in their trend over the course of the experiment. In general, amounts approximately 10 times higher of 3-PGA than 2-PG were measured intracellularly, indicating a dominance of the carboxylase over the oxygenase reaction. 3-PGA increased slightly from approx. 20 ng/ml to 25 ng/ml over the course of the 1st

day. During the night the concentration decreased to a value of approx. 17.5 ng/ml, before increasing again at the beginning of the next day (Figure 22A). This trend of intracellular 3-PGA indicates that the carboxylase activity of RubisCO is more pronounced during the day than the night. Furthermore, the strong increase of extracellular MC at the end of the 2nd night into the 2nd day appears together with the increase of intracellular 3-PGA. The extracellular 3-PGA did not follow the trend of its intracellular counterpart. The concentration fluctuated around the value of 2.5 ng/ml without strong increases or decreases over the whole incubation experiment (Figure 22A).

2-PG showed a different behavior than 3-PGA, both on an intracellular and extracellular level. The concentrations were around 10 times lower than for 3-PGA, but also showed interesting trends (Figure 22B). The intracellular portion of 2-PG showed a strong increase in the first 2 h of the day and constantly decreased afterwards during the rest of the day and into nighttime. The trend during daytime contrasts with the intracellular 3-PGA, further indicating the domination of the carboxylase reaction of RubisCO during the day. In addition, the burst of extracellular MC comes together with a strong increase of intracellular 2-PG, as seen for the intracellular 3-PGA as well (Figure 22B). In comparison to the carboxylase fixation product, the extracellular portion of 2-PG occurred in similar levels like the intracellular portion, indicating a possible more important role of extracellular 2-PG. Contrary to intracellular 2-PG, the concentration increased during the day. This oppositional behavior of both fractions suggests a secretion of 2-PG into the medium during daytime. Taken together, the diurnal incubation experiment showed that the carboxylase reaction of RubisCO is the dominant reaction over the whole diurnal cycle with some fluctuations. Interestingly, similar levels of 2-PG were found intra- and extracellularly, which suggest a possible extracellular role of 2-PG or an increase secretion of it, since photorespiration products can be toxic for the cell.

Another perspective, which need to be considered when studying RubisCO, is the subcellular localization of it. High-light shift experiments in this work already showed that the location of RubisCO is dynamic and that large portions of it are found outside of carboxysomes, associated with the thylakoid or cytoplasmic membrane. IFM imaging was used to visualize the subcellular localization of RubisCO (Figure 22C). Preliminary diurnal experiments from this study already showed that this process is

reversible. To confirm this hypothesis, several time points of the diurnal incubation experiment were checked for the subcellular localization of RubisCO by IFM imaging. Clearly, at the end of the day (t18, 16 h of daytime) large portions of RbcL were found underneath the cytoplasmic membrane, with only minor signals located in the cytosolic space together with carboxysomes. This observation changed 2 h into the night, where the largest part of RbcL was now located at the thylakoid membrane and the cytosol. The signal underneath the cytoplasmic membrane clearly faded away. After the end of the night and 2 h into the next day, nearly all RbcL signal was located together with carboxysomes (Figure 22). It seems that at least RbcL gets relocated from carboxysomes at the beginning of a day towards the cytoplasmic membrane at the end of the day. During the nighttime, it shifts towards the thylakoid membrane and finally ends up in carboxysomes again at the start of the next day. The burst of extracellular MC at the end of the experiment did not seem to influence this fluctuating process of RubisCO localization, but led to the increase of both 3-PGA and 2-PG. The amount of key proteins of the CCM was rather unchanged. Furthermore, cyanopeptolin 963-A peaked in the supernatant right before MC did but was suppressed right afterwards. Probably MC acted as a signaling molecule to influence the other oligopeptides.

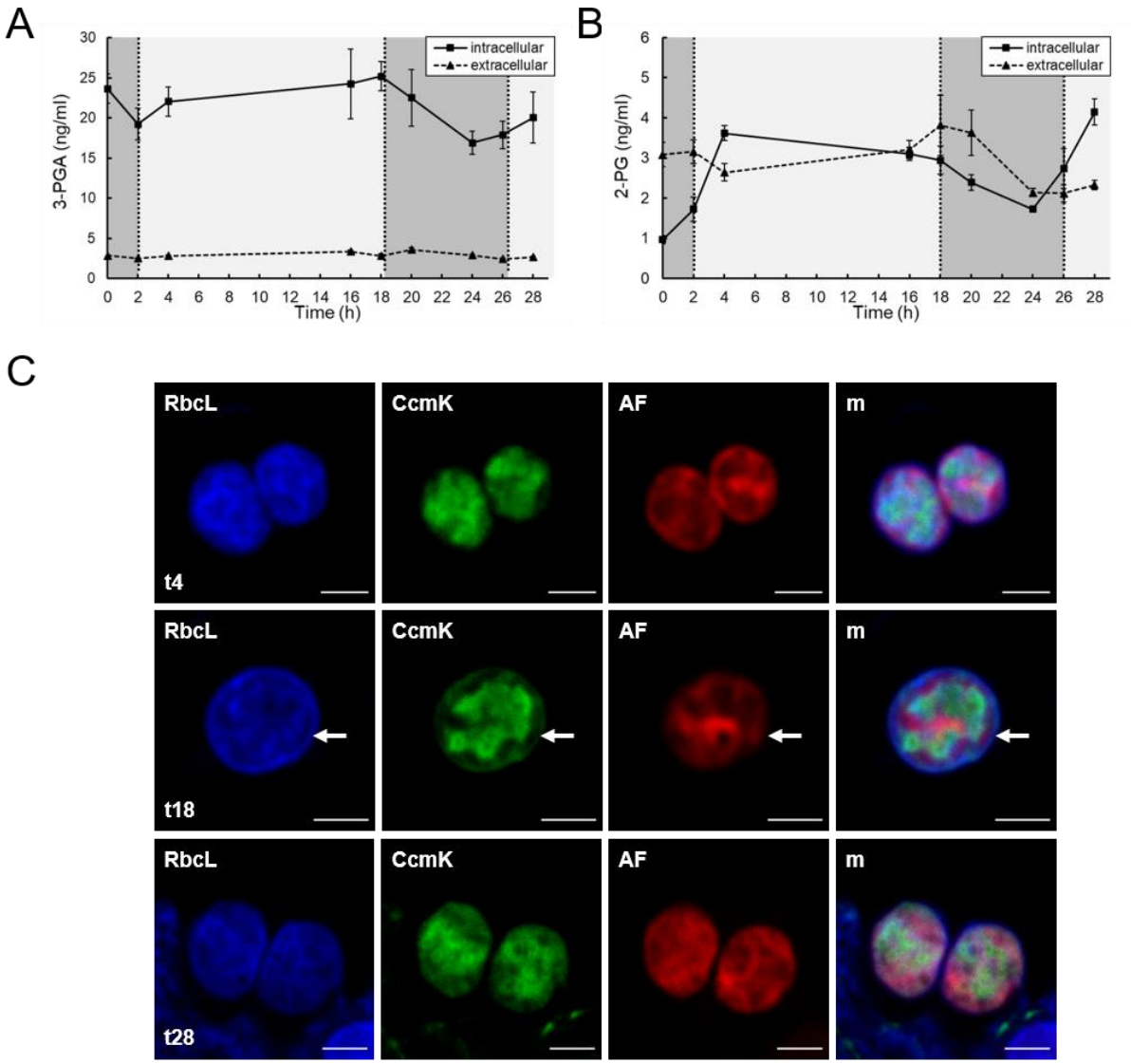

Figure 22. Steady-state levels of 3-PGA and 2-PG of *M. aeruginosa* WT during the diurnal cycle and visualization of subcellular localization of RbcL and CcmK by IFM imaging. **(A)** Steady-state levels of intra- and extracellular 3-PGA. **(B)** Steady-state levels of intra- and extracellular 2-PG. For both (A) and (B) the mean of three biological replicates and the standard deviation of it is displayed. The white background shows the daytime and the grey background the nighttime of the diurnal cycle. The shown data are displayed in the legend. **(C)** Co-hybridization of RbcL and CcmK antibody with *M. aeruginosa* WT cells of the diurnal cycle. The used sampling time points are indicated in the bottom left corner. The blue channel shows the localization of RbcL, the green channel of CcmK and the red channel of the phycobilisome auto fluorescence (AF). The merged image (m) of all three channels is displayed in the right lane. The scale bar in all images is 2 µm.

3.8 Microcystin addition experiments

To further assess to role of extracellular MC on the *M. aeruginosa* cells, addition experiments were performed. The diurnal cycle incubation experiment clearly showed that *M. aeruginosa* is capable to secrete large amounts of MC actively into the medium. This extracellular MC influences RubisCO as it leads to an increase of both fixation

products of RubisCO, 3-PGA and 2-PG. Furthermore, the signal of RubisCO in the immunoblot faded away at the end of the experiment, indicating a possible effect of the extracellular MC. Immunoblot analyses of the cytosolic and the membrane-associated protein fraction were performed to check to behavior of key proteins of the CCM after the addition of MC (Figure 23). The experiment was performed with the MC-deficient mutant Δ*mcyB* as well, to evaluate the role of MC on cells which are not capable of producing MC and by this also do not carry any intracellular MC like *M. aeruginosa* WT cells. Low-light adapted cultures of both strains were shifted to the same light conditions as in the diurnal incubation experiment (55 µmol photons m^{-2} s^{-1}). After 2 h of incubation the control cultures did not show any differences in the signal appearance of the two subunits of RubisCO (RbcL and RbcS) or the carboxysomal shell protein CcmK (Figure 23).

Two different MC concentrations were applied to the medium of the *M. aeruginosa* cultures: 10 ng/ml and 100 ng/ml. The lower concentration had only a little effect on the WT strain, since RbcL and RbcS signals appeared rather unchanged. The CcmK signal in contrast decreased clearly in comparison to the control culture. The decrease of signal was even more pronounced in the Δ*mcyB* strain. RbcL as well as RbcS showed weaker signals already after the addition of the low concentrated MC (Figure 23B). This observation was intensified in the culture with the higher concentrated MC. Interestingly, the signal intensity of all three tested proteins decreased in the cytosolic as well as in the membrane-associated protein fraction. The extracellular MC seems to influence all intracellular proteins, and not only one fraction of it. This is also in line with the previous results of this work, that MC is probably involved into a CBB super complex, which is formed outside of carboxysomes (Figure 18). These putative complexes occur in the cytosol as well as associated to the cytoplasmic and thylakoid membranes. The decrease of the CcmK signal furthermore indicates that the extracellular MC not only influences RubisCO but also the carboxysomes. Since RubisCO was found in large amounts not associated with carboxysomes in the high-light shift experiments (Figure 14), the extracellular MC is maybe another driving force of this process. It possibly acts as a signal to initiate the subcellular relocalization of RubisCO in *M. aeruginosa*. The significant role of MC besides the toxic effects on other organisms can be observed also in the *M. aeruginosa* WT culture with the higher concentrated MC added (Figure 23A). There, RubisCO and CcmK also decreased in

their amount, but the decline was not that strong as in the MC-deficient Δ*mcyB*. IFM imaging could underline this observation. The RbcL signal clearly decreased after the addition of the higher concentrated MC and no pronounced localization underneath the cytoplasmic membrane was displayed (Figure 23C). This reflects the decline of the membrane protein fraction in the immunoblot as well. The Δ*mcyB* mutant showed a similar reaction of RbcL in the IFM micrographs. Overall RbcL signal decreased as well as the specific subcellular localization underneath the cytoplasmic membrane (Figure 23D). The IFM imaging clearly supports the extracellular effects of MC to *M. aeruginosa* WT and Δ*mcyB*. The intracellular MC of the WT cells may lessen the decline of CCM-related proteins. FtsZ in the cytosolic fraction on the one hand showed the successful separation of the two protein fractions and on the other hand verified that the decline of RubisCO and CcmK cannot be attributed to the decrease of the total protein amount. This addition experiment as well as the diurnal incubation experiment clearly showed that extracellular MC influences key proteins of the CCM like RubisCO and that it may influence the secondary metabolome of *M. aeruginosa* as well.

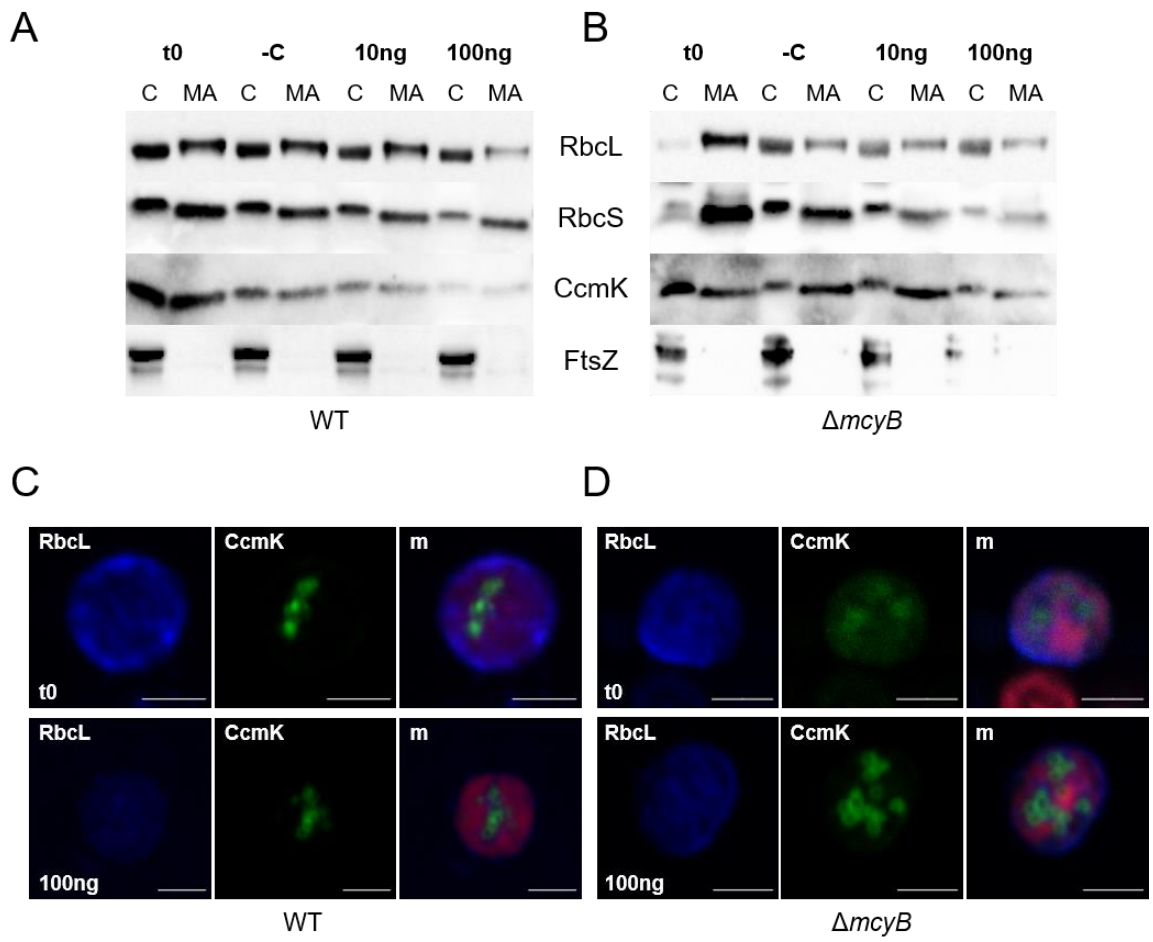

Figure 23. Immunoblot analysis of protein extracts from the MC addition experiment with the non-axenic *M. aeruginosa* WT and the MC-free Δ*mcyB* strain and representative IFM micrographs. **(A)** Immunoblots from *M. aeruginosa* WT. **(B)** Immunoblots from *M. aeruginosa* Δ*mcyB*. The experimental setup was identical for both strains. 10 ng/ml or 100 ng/ml of MC-LR was added to the low light-adapted culture or no MC was added as a negative control (-C). The cultures were shifted to higher light irradiation (55 µmol photons m^{-2} s^{-1}) at the same time. RbcL, RbcS and CcmK were checked for their occurrence and trend during the MC addition. The protein extracts were separated into cytosolic (C) and membrane-associated (MA) fraction. The success of the separation was verified by the cytosolic protein FtsZ. **(C, D)** Representative IFM micrographs of *M. aeruginosa* WT (C) and Δ*mcyB* (D) from the start of the experiment (to) and 2 h after addition of MC at a concentration of 100 ng/µl. Co-incubations with α-RbcL and α-CcmK were performed. The blue channel is the RbcL signal, the green channel the CcmK signal and the third image is the merged image (m) of the two channels and the phycobilisome auto fluorescence, seen as a red signal. The scale bar in all images is 2 µm.

4. Discussion

4.1 Subcellular localization of RubisCO in *M. aeruginosa*

Research about cyanobacteria and its primary metabolism is focused mainly on the model cyanobacteria *Synechocystis* sp. PCC 6803 and *Synechococcus elongatus* PCC 7942 (Marcus *et al.*, 2003; Hasunuma *et al.*, 2013; Jeffrey C. Cameron *et al.*, 2013; Triana *et al.*, 2014). Studies about cyanobacteria with a more complex lifestyle like *M. aeruginosa* are still underrepresented due to difficulties to replicate these lifestyles in laboratory conditions. Especially research about *M. aeruginosa* focusses mainly on the role of microcystin in the environment and the effect on other organisms (Schatz *et al.*, 2007; Huisman *et al.*, 2018; Zhang *et al.*, 2019). This study aims for a better understanding of the physiological reason behind the success of the bloom-forming cyanobacterium *M. aeruginosa* and the intracellular role of microcystin in this process.

The presented results in this study strongly suggest that *M. aeruginosa* differs from the canonical hypothesis about the subcellular localization of RubisCO (Benjamin D. Rae *et al.*, 2013). Large amounts of RubisCO could be detected outside of carboxysomes, and not associated with them. Instead, RubisCO is located mainly underneath the cytoplasmic membrane and at the thylakoid membrane as the result of a dynamic localization process. Additionally, MC seems to have at least a strong influence on the subcellular localization dynamics of RubisCO, and it may be directly involved into it. Furthermore, it plays a general role in the response of *M. aeruginosa* to changing conditions.

The results of large amounts of RubisCO outside of carboxysomes sheds new light on the ability of *M. aeruginosa* to form blooms. The relocalization of RubisCO during the light shift from low-light to high-light takes place after one to two hours of irradiation and differs between the *M. aeruginosa* WT and the MC-deficient mutant Δ*mcyB*. Comparable relocalization dynamics of RubisCO have not been reported in other single-celled cyanobacteria up to this point in literature. One of the best studied and model organisms for single-celled cyanobacteria are *Synechocystis* sp. PCC 6803 and *Synechococcus elongatus* PCC7942. Due to its easier access to genetic manipulations

in comparison to *M. aeruginosa*, they are targets of a variety of studies including research about carboxysomes (Long *et al.*, 2011; Faulkner *et al.*, 2017; Lechno-Yossef *et al.*, 2020). In *Synechocystis* sp., RubisCO is packed into the carboxysomes as part of the carbon concentrating mechanism (CCM) and does not occur in large amounts outside of carboxysomes (Burnap *et al.*, 2013; Turmo *et al.*, 2017). These studies lead to the assumption that this is the case for most of the cyanobacteria. However, this work provides evidence that not all cyanobacteria show the same subcellular localization of RubisCO. Two immunoelectron microscopy studies already located RubisCO outside of carboxysomes and directly at the thylakoid membranes of *Synechocystis* sp. PCC 6803 and *Synechocystis* UTEX 625. In addition, assembled carboxysomes were located directly at the cytoplasmic membrane and not homogeneously distributed in the cytosol under carbon limiting conditions (McKay *et al.*, 1993; Agarwal *et al.*, 2009). The different metabolic response of *Synechocystis* sp. to a high-light shift than *M. aeruginosa* is another indication for a different Ci adaptation of *M. aeruginosa*. It showed higher amounts of 2-PG, a direct product of the oxygenase activity of RubisCO, after already one hour of high-light irradiation (Meissner *et al.*, 2015). IFM studies further underlined the separation of RubisCO from carboxysomes under high-light conditions in *M. aeruginosa*. Since the growth rates of *M. aeruginosa* are not as high as for other cyanobacteria (Wilson *et al.*, 2006; El Semary, 2010) or the model enterobacterium *Escherichia coli*, this change of RubisCO cannot be explained by simple turnover of cells towards other cell configurations.

The presence of RubisCO outside of carboxysomes sheds light on the functionality of the remaining carboxysomes in the cell. IFM images and especially TEM images suggest the probability of empty carboxysomes. In several previous studies, pale carboxysomes could be observed in electron microscopy images, indicating carboxysomes do have different states of filling (Song and Qiu, 2007; Smarda and Maralek, 2008; Kinney *et al.*, 2012). Only rarely electron dense carboxysomes could be seen in the high-light treated cells. These results question the purpose of carboxysomes in *M. aeruginosa* or other cyanobacteria. Since the dynamics of assembly and disassembly of carboxysomes happen under specific conditions as high-light irradiation, this is possibly not the standard configuration of carboxysomes in cyanobacteria. Under the applied parameters in this study, carboxysomes appear as carriers for RubisCO during low-light phases before RubisCO is disassembled and

relocates underneath the cytoplasmic and associated to the thylakoid membrane. In addition, it is also very much possible that the membrane-bound RubisCO is newly synthesized under the given high-light irradiation. The assembly of such a large microcompartment as a carboxysome is a complex and time consuming process (Jeffrey C Cameron *et al.*, 2013). The results hint a faster way of adaptation to strongly changing conditions of M. aeruginosa through the dissociation of RubisCO from the carboxysomes. Furthermore, TEM studies suggest the involvement of cyanopeptides in the assembly/disassembly of carboxysomes, since they were located directly at the carboxysomes (Young *et al.*, 2008). When blooms of *M. aeruginosa* occur in natural habitats, the cells are constantly exposed to extreme conditions as nutrient limitation or high-light intensities due to direct sunlight (Park *et al.*, 2018). Empty carboxysomes could also occur in cells of the bloom to cope with these extreme conditions. They possibly serve as a reservoir for RubisCO and maybe even play a part during cell division to assure the equal distribution of RubisCO into both cells.

One major parameter for the observed dynamics of RubisCO besides the light conditions is the cell density of the population. High-light shift experiments and diurnal cycle incubation experiments in this study revealed that the relocalization of RubisCO only occurs at a certain cell density of the population. When the cell density was below an optical density of OD_{750} 0.3 RubisCO was mainly located in carboxysomes and the cytosol, independently from the time of day. In comparison, when the population was above the threshold cell density RubisCO was found mainly underneath the cytoplasmic membrane during daytime. At nighttime, it relocates back to the thylakoid membrane and the cytosol, including carboxysomes. The cell density-dependent dynamics of RubisCO suggest that these dynamics also take place in natural occurring blooms of *M. aeruginosa*. Responses and reactions of cyanobacterial communities which depend on cell densities are very well-known phenomena, even though most of the studies about cell density dependent effects in cyanobacteria are focused on the production of secondary metabolites (Sharif *et al.*, 2008; Pereira and Giani, 2014; Briand *et al.*, 2016). The result of this study suggests a possible quorum sensing effect on carbon fixation and photosynthesis in *M. aeruginosa* and possibly other cyanobacteria. The limitation of the RubisCO dynamics to higher cell densities could also be a reason why this was not observed for the model organism for unicellular cyanobacteria *Synechocystis* sp. It cannot form blooms as *M. aeruginosa*.

Interestingly, the presence of microcystin does not strongly influence the cell density effects. The MC-deficient mutant Δ*mcyB* displayed a similar behavior as the WT. MC clearly has intracellular effects on *M. aeruginosa* as shown on several studies (Dziallas and Grossart, 2011; Zilliges *et al.*, 2011; Miles *et al.*, 2016; Wei *et al.*, 2016) and will be discussed in a later chapter, but it does not seem to be the only factor or signaling molecule in this response. The mutant Δ*mcyB* showed aggregates of RbcL underneath the cytoplasmic membrane as observed in the WT after high-light treatment in IFM micrographs as well. MC may affect how fast *M. aeruginosa* reacts to shifting light intensities. The relocalization of RubisCO happened faster in the WT than in the mutant Δ*mcyB*. Furthermore, the RbcL signal in the immunoblot faded away after four hours of high-light illumination in Δ*mcyB*, underlining one of the proposed intracellular functions of MC as a protector against stresses like high-light or oxidative stress (Zilliges *et al.*, 2011; Wei *et al.*, 2016). Co-hybridizations with the RbcL and MC antibody via IFM imaging showed co-localizations of both proteins inside of the cell and suggest a direct interaction or even binding of MC to RbcL. This binding could lead to the stabilization of RbcL over longer times of high-light irradiation by preventing RbcL from degradation. It is to notice, that the Δ*mcyB* mutant was not inhibited in its growth or showed morphological signs of suffering from the possible degradation of RbcL after longer incubation at high-light conditions. The observation of the RubisCO dynamics in the diurnal incubation experiments verified that the processes are reversible and not artifacts from high-light irradiation-caused cell damages.

4.2 The dynamics of the membrane-bound RubisCO

RubisCO needs to be an amphitrophic protein to be able to interact with the hydrophilic cytosol and the hydrophobic membranes. Amphitrophic proteins harbor at least a hydrophobic and a hydrophilic domain, which allows the protein to anchor to hydrophobic membranes and interact with the hydrophilic cytoplasm at the same time. Furthermore, this enables the fast relocalization of RubisCO from the carboxysome to the membranes and *vice versa*, since it can interact with both environments. Protein binding to membranes may have different consequences. One possibility is, that the enzyme is spatially closer to the target or substrate, which leads to a higher efficiency or enables the enzyme to even process the substrate (Ghosh *et al.*, 2006). The other possibility for membrane-bound proteins is the binding to a membrane initiates a

conformational change of the protein to the active state of it (Johnson and Cornell, 1999). RubisCO seems to be attached loosely to the membranes under the tested conditions in this study, since it was only detected in the loosely bound protein fraction and the intact total membrane isolation after the application of mechanical force to the extracted proteins. The reversible form of interaction with the membrane is characterized as a non-permanent membrane interaction (Goñi, 2002). It is to note that the lack of MC did influence the distribution of RubisCO in the MC-deficient mutant Δ*mcyB*. In comparison to the WT cells, RubisCO was much more homogeneously distributed over the whole cell and fewer aggregates were observed in IFM images of high-light treated Δ*mcyB* cells.

To understand the dynamics of RubisCO in *M. aeruginosa* cells, the mode of interaction between RubisCO and the membranes to which it binds, need to be viewed. Membrane associated proteins can generally be classified into two big groups: peripheral and integral membrane proteins (Renthal, 2010; Monje-Galvan and Klauda, 2016). Integral membrane proteins are permanently bound to the respective membrane. They span through the entire membrane and are very often transporters for a variety of substrates or ions (Mouritsen and Bloom, 1993). In addition, integral membrane proteins can only be detached from the membrane by using detergents (Smith, 2017). Since RubisCO can be found in both the hydrophilic cytoplasm and the hydrophobic thylakoid or cytoplasmic membrane, it seems very unlikely that RubisCO is an integral membrane protein. The other group of membrane proteins, the peripheral membrane proteins is only attached temporarily to the membrane. This interaction with the membrane layer is achieved by certain domains of the protein, which are hydrophobic, or through a protein-protein interaction with transmembrane proteins (Johnson and Cornell, 1999; Goñi, 2002). The binding to membranes often leads to significant conformational changes of the protein and its tertiary structure, since domains may get exposed which were unfolded before or need to be rearranged for the interaction with the membrane. Many regulatory factors of transmembrane proteins function through this direct interaction. However, the majority of peripheral proteins bind non-covalently to the membrane which means it is a reversible interaction (Morozova *et al.*, 2011; Whited and Johs, 2015). It is highly likely that RubisCO in *M. aeruginosa* is a peripheral membrane protein, since it can be found associated to membranes as well as directly in the cytosol. If the binding to the membrane layers are

achieved due to hydrophobic domains or protein-protein interactions with transmembrane proteins needs to be studied further. Another possibility is, that secondary metabolites in form of lipopeptides mediate the binding of RubisCO to membranes or act at least as regulatory factors for the previously mentioned binding modes.

4.3 An alternative CCM in *M. aeruginosa*

The subcellular localization of RubisCO at the cytoplasmic membrane offers some advantages for *M. aeruginosa* over the canonical localization in carboxysomes. To be processed by RubisCO, CO_2 needs to be imported first into the *M. aeruginosa* cell and is converted into HCO_3^- while it is imported. When it is transported into the carboxysomes it is transformed back into CO_2 (Badger and Price, 2003). The localization of RubisCO at the cytoplasmic membrane circumvents the CCM, because the CO_2 needed for the photosynthesis can be fixed directly by the membrane-bound RubisCO. IFM images and the electron dense granules in the TEM images hint towards an aggregation of RubisCO at specific spots at the cytoplasmic membrane. The distribution of inorganic uptake systems over the whole cell surface could be an explanation for the RubisCO spots observed in this study. The carbonic anhydrases (CA), which are normally associated with the CO_2 importers to convert the imported CO_2 into HCO_3^-, probably perform the reverse reaction to provide RubisCO with the needed CO_2. This reaction also happens at the carboxysomal shell. It was even predicted for all *Microcystis* strains, that they possess two homologues of the periplasmatic CAs, EcaA and EcaB. These CA would enrich CO_2 in the periplasm, but the experimental verification is still missing (Sandrini *et al.*, 2014). For another unicellular cyanobacterium as *M. aeruginosa*, *Cyanothece* ATCC 51142, high amounts and activities of extracellular EcaA and EcaB homologues were shown (Kupriyanova *et al.*, 2019). In addition, RubisCO may also fix CO_2 which enters the cell via passive diffusion (Mangan and Brenner, 2014). Both possible ways to assimilate CO_2 have the same motive: a higher availability of the substrate through spatial limitation of the way the substrate need to take until it reaches the targeted enzyme.

The membrane-bound RubisCO could be part of an alternative and not yet characterized CCM in cyanobacteria. In this putative alternative CCM CO_2 is

concentrated right after its import into the cell without the need to transfer it through the cell in form of HCO_3^- towards the carboxysomes. Furthermore, it gives a possible explanation why *M. aeruginosa* can cope with the high rate of photorespiration. The localization outside of carboxysomes favor the fixation of O_2 by RubisCO, since it is directly exposed to oxygen in the cytosol (Marcus *et al.*, 1992; Abernathy *et al.*, 2019). Simultaneously, the fast response of *M. aeruginosa* to changing light conditions achieved by RubisCO binding to the cytoplasmic membrane excels the negative effects of photorespiration. The direct localization of RubisCO at its substrates CO_2 and O_2 leads to a faster conversion of them as well. Hence, RubisCO is exposed to higher amounts of O_2, but also it can process incoming CO_2 even faster when it is directly located at or around the inorganic carbon uptake systems. This is a common strategy in nature in the enzyme-substrate interaction. The minimization of the physical distance between the two partners results in a higher metabolization rate (Ghosh *et al.*, 2006; Kuzmak *et al.*, 2019). The carboxysomal CCM would take more time and is more energy consuming when a low light-adapted cell is immediately exposed to high-light intensities. The fixation of CO_2 by RubisCO is not the only possible pathway for cyanobacteria to assimilate inorganic carbon. Besides the C_3 photosynthetic pathway (RubisCO and CBB cycle), they can assimilate inorganic carbon as C_4 acids. Instead of reversing the imported HCO_3^- back to CO_2 in the carboxysomes, it is fixed directly through the activity of the phosphoenolpyruvate (PEP) carboxylase. It catalyzes the irreversible carboxylation of PEP to form oxaloacetate by using HCO_3^- and inorganic phosphorus. Oxaloacetate can be transformed to aspartate or malate. Since cyanobacteria have a modified tricarboxylic acid (TCA) cycle, aspartate and malate cannot be used for energy gain as for the TCA cycle of other bacterial groups or eukaryotic cells. Instead the TCA cycle in cyanobacteria serves for biosynthetic reactions (Zhang and Bryant, 2011). Furthermore, the C_4 acids fixed by the PEP carboxylase may supply carbon for the synthesis of cytochromes, chlorophyll a and phycobilins (Shylajanaciyar *et al.*, 2015). The proposed alternative CCM would be another pathway of inorganic carbon assimilation in cyanobacteria.

In addition, RubisCO is directly located at the cytoplasmic membrane and could also explain why similar amounts of 2-PG were found inside and outside of the cells. Studies of *Synechococcus* and *Synechocystis* lacking carboxysomes due to the genetic deletion of it, displayed an increased rate of photorespiration since RubisCO cannot

be packed into carboxysomes to be shielded from O_2 (Marcus *et al.*, 1992; Abernathy *et al.*, 2019). Photorespiration products are considered to be toxic and that organisms want to avoid generating them (Colman, 1989). Since the observed RubisCO system in *M. aeruginosa* is prone to higher rates of the oxygenase reaction than other cyanobacteria, a strategy is needed to detoxify the products or to cope with the generated products in another way. The detected extracellular amounts of 2-PG strongly suggest that it is secreted directly into the surrounding medium after production. The secretion of photorespiration products lowers the amount of possible harmful compounds inside of the cell as shown for *Synechococcus lividus* in a cyanobacterial mat. It secreted large amounts of glycolate, the subsequent product of 2-PG (Bateson and Ward, 1988). Another study showed that the *M. aeruginosa* WT and MC-deficient mutant release higher amounts of glycolate to the surrounding medium than *Synechocystis* PCC6803 under high-light conditions (Meissner *et al.*, 2015). This clear difference between *M. aeruginosa* and model organisms is another hint towards an alternative CCM in *M. aeruginosa* under high-light conditions. The carboxysomal CCM generates only extremely low amounts of extracellular glycolate, since RubisCO is packed into carboxysomes. Consequently, the oxygenase reaction as well as the rate of glycolate production is lowered. The putative membranous CCM generates more glycolate due to its location directly at the cytoplasmic membrane and the missing physical separation of RubisCO from the rest of the cell. The remaining amount of 2-PG after secretion of photorespiratory products is low enough that the cell can detoxify it or use it for other metabolic pathways. The secretion of products in the later steps of photorespiration suggests that this happens maybe not only because of detoxification, since this could be achieved faster by secreting 2-PG directly after the fixation of O_2. The secretion of glycolate may serve another purpose for *M. aeruginosa*. It could be an energy or carbon source for surrounding heterotrophic bacteria. Studies with *Synechococcus* showed the development of stable cyanobacterium – heterotroph populations maintained by the secretion of sucrose as a carbon source through the cyanobacterium to feed the heterotroph (Beliaev *et al.*, 2014; Weiss *et al.*, 2017). The interaction of cyanobacteria with each other or with heterotrophic bacteria is a complex network. Most often interactions are taking place in the form of cross-feeding. One or several interaction partners secrete a certain compound, which is taken up by the other non-producing organisms of this particular compound, resulting in positive growth

effects of the receiver. In turn the receiver secretes other compounds, from which the other partners benefit. The secretion of carbon sources in the cyanobacterium – heterotroph interaction could be beneficial for both organisms: the heterotroph can use glycolate as a nutrient and in turn it provides *M. aeruginosa* with other growth promoting factors or performs needed metabolic steps for the cyanobacterium as the fixation of nitrogen. The interaction with heterotrophic partners supports *M. aeruginosa* biomass production to establish and maintain a bloom. They invest and thus effectively loose carbon to the heterotrophs to benefit at the end from the interaction.

4.4 The Calvin-Benson-Bassham cycle super complex

The fact, that RubisCO is the only enzyme of the CBB cycle which is relocated under changing light conditions seems not likely. Immunoblot analyses showed that RbcS (small subunit of RubisCO) appeared in a high molecular weight alongside MC, besides the fully assembled RubisCO. This observation was supported by IFM imaging, where both RbcS and MC co-located at the cytoplasmic membrane. These are already strong indicators that MC binds under high-light irradiation to RbcS. It was already shown that MC acts as a protector of proteins under stressful conditions (Zilliges *et al.*, 2011; Wei *et al.*, 2016). Possibly, RbcS is stabilized by the bound MC under these circumstances and is stable enough to act without any bound RbcL. However, it is remarkably interesting that another enzyme of the CBB cycle can be found in this high molecular mass complex: the phosphoribulokinase (PRK). It occurs together with RbcS and MC in the immunoblots and in distinct spots during IFM imaging. The occurrence of CBB cycle super complexes is already known from higher plants and was hypothesized for cyanobacteria as well (Süss *et al.*, 1993; Agarwal *et al.*, 2009). Spinach and *Nicotiana tabacum* chloroplast extractions showed a five-enzyme complex, containing RubisCO as well as PRK (Gontero *et al.*, 1988; Jebanathirajah and Coleman, 1998). Such a super complex of all or even only a few enzymes of the CBB cycle would allow a faster metabolization of incoming substrates. With the existence of such a super complex it is not necessary to transport intermediates to different parts of the cell. The accumulation of enzymes saves time and energy. In addition, the putative super complex could also explain why RubisCO was observed through TEM and IFM imaging as distinct spots and not as a homogeneous signal at the cytoplasmic membrane. The membrane surface likely acts

as a regulator of the formation of such protein condensates (Snead and Gladfelter, 2019). RubisCO accumulates in carboxysomes in the canonical CCM as well as RubisCO accumulates at the cytoplasmic and thylakoid membrane in the alternative CCM.

However, there it is not packed into a bacterial microcompartment, instead RubisCO is part of an enzyme cluster. The experimental data suggest, that the complex is not a permanent construct. It assembles and disassembles in a fast rate, since the aggregates appear already after 1 h of high-light treatment and mainly disappear during nighttime. Despite these dynamics, the super complex seems to be stable and functional. Furthermore, the cystathione β-synthase (CBS)-chloroplast protein (CP12), a regulator of photosynthesis in a variety of cyanobacteria (Hackenberg *et al.*, 2018), was detected at the cytoplasmic membrane as well. The existence of such regulatory proteins further strengthens the hypothesis of a CBB super complex. The stability of the complex is achieved possibly due to the involvement of MC in the complex and its assembly. Since RbcS is only one of the two subunits of RubisCO, it should not be active solely when bound to membranes. Furthermore, the exposure of a single protein or subunit to such stressful conditions without any protection seems unlikely, especially if this protein is part of a key enzyme of photosynthesis and the carbon uptake mechanism. However, the fact that MC is detected also in the putative CBB complex in immunoblot analyses expands the role of MC its function as a protector. MC can bind to a variety of enzymes of the CBB cycle, including PRK (Zilliges *et al.*, 2011; Wei *et al.*, 2016). After MC binds to RbcS at the cytoplasmic membrane and prevents from degradation, MC could possibly act as a mediator for the assembly of the CBB complex by binding to the other involved enzymes as well. The stability and fast assembly of the complex is likely achieved due to the involvement of MC, which is in line with previous studies about the intracellular role of MC (Dziallas and Grossart, 2011; Zilliges *et al.*, 2011; Wei *et al.*, 2016).

In comparison to carboxysomes, which need time to assemble and by this are not feasible for fast responses of a cell to drastic changes (Faulkner *et al.*, 2017; Sutter *et al.*, 2019), the putative super complex seems to be a fast response mechanism of *M. aeruginosa* to high-light shifts. It is important to note, that these dynamics of RubisCO do not take place in all cells of the population in the performed experiments. It is likely that the separation of different cell types and states can be found in blooms as well.

The cells which are on top of the bloom, directly at the air-water interface, are exposed to the high intensities of the direct sunlight (Ibelings and Maberly, 1998; Sommaruga *et al.*, 2009). The fast response could give an advantage over other cyanobacteria. Hypothetically, it enables *M. aeruginosa* to establish the bloom and generate biomass quickly to outcompete other organisms and be more robust against external factors. Cells which are inside of the bloom or in deeper water layers face totally different conditions than the cells on top of the bloom (Kromkamp and Mur, 1984; Ibelings *et al.*, 1991). Due to the high cell density, CO_2 access is extremely limited for these cells and the light intensity is much lower through shading effects generated by the dense bloom itself. These cells in the deeper layers of the bloom perform likely the canonical CCM with RubisCO located in the carboxysomes (Figure 24). The results of this study suggest that the obtained results about the RubisCO dynamics under changing light conditions may provide a possibility for a rapid adaptation to extreme conditions by *M. aeruginosa*, giving a certain portion of its bloom a growth advantage.

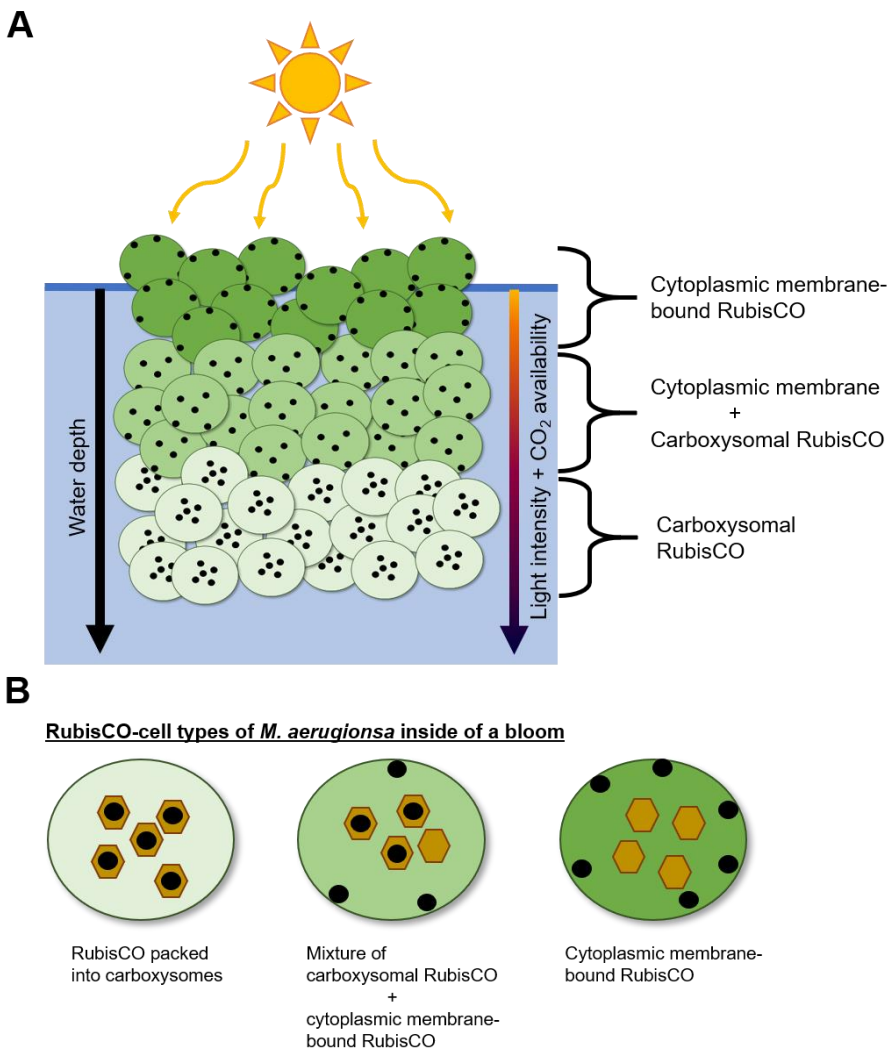

Figure 24. Model of an *M. aeruginosa* bloom exposed to the sunlight. **(A)** The different layers of a *M. aeruginosa* bloom under high-light conditions. On top the bloom (dark green cells) at the water-air interphase are cells, where RubisCO (black dots) is located almost exclusively underneath the cytoplasmic membrane. Underneath in the middle layer (light green cells) are cells with a mixture of RubisCO locations. One portion is located underneath the cytoplasmic membrane and the other portion is located in carboxysomes. The bottom layer (pale green cells) are cells, where RubisCO is almost exclusively located inside of the carboxysomes. Light intensity and CO_2 availability are decreasing with the depth of the bloom. **(B)** More detailed representation of the cell types from (A) in terms of the subcellular localization of RubisCO inside of a *M. aeruginosa* bloom.

4.5 Microcystin binds to RubisCO and the CBB super complex

In water management, the biggest concern about a *M. aeruginosa* bloom is the presence of cyanotoxins and especially microcystin (Huisman *et al.*, 2018). The fast and robust growth of these blooms due to the quick adaptation of *M. aeruginosa* to changing light conditions and differing CO_2 and O_2 availabilities by subcellular RubisCO relocalization, promotes the production of high amounts of MC. Several studies on the functional role of MC suggest (Miller *et al.*, 2010; Chen *et al.*, 2016) that,

the toxic effect on other organisms is only one of a variety of functions for the producing *M. aeruginosa*. IFM images from this work showed that two enzymes of the MC biosynthesis pathway, McyB and McyF, are located at the inner layer of the thylakoid membrane, which is facing the cytosol. McyB is the microcystin synthetase and McyF an aspartate racemase, and both are part of the MC gene cluster in *M. aeruginosa* (Tillett *et al.*, 2000). Since both enzymes could be detected only at the inner layer of the thylakoid membrane, it is highly likely that the whole MC biosynthesis is located there and thus being a membrane-bound pathway. McyH, an ABC transporter, harbors a membrane domain and could serve as a membrane scaffold for the whole biosynthesis complex (Pearson *et al.*, 2004). This observation is also in line with the hypothesis of the CBB super complexes at the cytoplasmic and thylakoid membranes in *M. aeruginosa*, where MC seems to play a major role in the establishment and stability of the whole complex. MC is synthesized at the membrane and can directly bind to membrane-bound proteins as RubisCO or other enzymes of the CBB cycle. Another factor which strengthens the hypothesis of the thylakoid membrane-bound MC biosynthesis complex is the presence of the ATP synthase at the thylakoid membrane. The MC biosynthesis consumes a lot of energy and could benefit from the proximity to the ATP synthase. In *Synechocystis* PCC6803 CBB cycle enzymes were already co-located with the ATP synthase (Agarwal *et al.*, 2009). RbcS showed a strong co-localization with MC under high-light conditions, in comparison to RbcL. Hence, it is highly likely that RbcS is the main interaction partner of MC when it binds to RubisCO. The thylakoid-bound RbcS possibly serves as a pool for the assembly of the functional RubisCO enzyme with RbcL during nighttime or when forming the CBB super complex, although an evolutionary study about RbcL suggests that it can be functional without RbcS (Banda *et al.*, 2020). MC prevents RbcS from degradation and probably mediates the binding to RbcL and other enzymes of the CBB cycle. The excessive MC in the cell either directly binds to proteins as RbcS or PRK or is secreted into the surrounding medium as observed in the diurnal incubation experiment.

Intracellular MC can be divided into two pools: the bound MC pool and the free MC pool (Meissner *et al.*, 2013). Both pools can show totally different amounts of MC and do not necessary develop similar in the same conditions or the performed experiment. The diurnal incubation experiment conducted in this work, is a perfect example for the difference of the two MC pools. Intracellular MC examined by HPLC analysis showed

a decrease of concentration during the 1st day and into the 2nd night, with the low point at the end of the 2nd night. With the start of the 2nd day, the concentration increased again. The MC measured by HPLC analysis represents the free intracellular MC pool, since MC bound to different proteins would not be detectable through the assessed analysis method. However, when examining the immunoblot analysis of MC of the same experiment, it suggests another dynamic of MC during the diurnal cycle. The maximum points were reached at the transition from the 1st day to the 2nd night. Afterwards, MC dramatically drops and is only detectable in low amounts. The MC signals obtained in this immunoblot analysis represent the bound MC pool, more precisely the protein-bound pool. The decrease of the free MC pool over the course of the 1st day and the simultaneous increase of protein-bound MC strengthen the hypothesis that excessive MC is binding to proteins including RubisCO to form CBB complexes, lowering the free MC level constantly. RbcL clearly re-locates from the thylakoid membrane towards the cytoplasmic membrane at the end of the 1st day, where several spots of the RbcL signal are visible in the IFM imaging.

The cytosolic RbcL signal is fading over the course of the same time span. In turn, the CcmK signal did not change dramatically, further underlining the independent behavior of RubisCO from the carboxysomes under high-light conditions. The discrepancy between the signal strength of immunoblot analyses and IFM imaging over the course of the experiment can be explained by the different analyzed MC pools. The harsh treatment of cells during IFM preparation possibly leads to the non-covalently bound MC dissolving and not being detected by the IFM imaging method. Furthermore, the native immunoblot analyses about the putative CBB complex suggest that MC mainly binds to RbcS instead of RbcL. Microcystin and RbcS perfectly co-localized during treatment with high-light, and in contrast, MC only rarely co-localized with RbcL. Immunoblots of thylakoid membrane preparations from high-light treated *M. aeruginosa* cultures showed RbcS as the main interaction partner of MC as well. Since in immunoblot analyses no protein binding of microcystin to the monomeric form of RbcS could be observed, it is highly likely that MC binds only to aggregate conformations of RbcS monomers. When sufficient amounts of RbcS monomers are bound to membranes, and especially thylakoid membranes, MC will bind to it as well, possibly mediating the formation of fully assembled RubisCO molecules or even the CBB super complex. Besides the binding of excessive MC to other proteins in the cell,

it is also possible that *M. aeruginosa* actively secretes MC into the surrounding medium.

4.6 The extracellular signaling peptide microcystin

Extracellular MC, and more precisely dissolved MC, is typically present in low amounts in a M. aeruginosa bloom. Most of the total MC of a bloom is found intracellularly. Several studies identified cell lysis as the main factor for the release of MC into the water (Park *et al.*, 1998; Dong *et al.*, 2016; Wang *et al.*, 2018). This cell lysis is caused besides normal cell death and nutrient limitations, most likely in large parts due to the activity of phages in *M. aeruginosa* bloom (Yoshida *et al.*, 2006; Stough *et al.*, 2017). In addition, the presented results in this study about microcystin being a possible key protein for the stabilization of photosynthesis enzymes including RubisCO, suggest that *M. aeruginosa* cells would avoid the loss of MC in large amounts. However, some studies also reported active release mechanisms of MC in *M. aeruginosa* (Cordeiro-Araújo and Bittencourt-Oliveira, 2013; Rastogi *et al.*, 2014). The growth of the WT cultures during the analyzed diurnal cycle did not suggest the presence of harmful growth conditions. Cell lysis as the main reason for the burst of extracellular MC can be eliminated, especially since it started together with an increase of the cell density. Furthermore, only MC could be detected in large amounts in the medium and no other peptides, which would be expected if the cell lyses.

The presence of such high concentrations of microcystin in the medium of the *M. aeruginosa* culture without any abnormal cell lysis suggests an active secretion mechanism of MC The effect of heavily increasing extracellular concentrations of MC was observed as the RbcL signal decreased in the immunoblot. The subcellular localization of RubisCO was not affected since its dynamics were still present. The shift from the cytosol and thylakoid membranes towards the cytoplasmic membrane and *vice versa* happened independent from the level of extracellular MC. However, the signal of RbcL in IFM micrographs clearly diminished at the end of the analyzed time span, supporting the results obtained from the immunoblot analysis. To investigate further the role of extracellular MC in *M. aeruginosa*, MC addition experiments were performed. Both subunits of RubisCO, RbcL and RbcS, as well as CcmK showed a decrease of the signal the higher the applied concentration of MC-LR was. This was

true for the *M. aeruginosa* WT as well as the MC-free mutant Δ*mcyB*. That the effect occurred in both strains is another evidence for an extracellular function of MC. The Δ*mcyB* mutant cannot produce MC, thus it is interesting that the addition induced the same response as the WT, underlining the hypothesized extracellular role. Furthermore, this experiment also proved that the added MC had an effect on the WT cells despite the presence of intracellular MC in even higher concentrations than the surrounding medium. Hence, the diminishing of key proteins of the CBB cycle is caused most likely by the presence of MC in the surrounding medium of the cell. It appears to be a concentration-based response, since the decrease of RubisCO and CcmK was less pronounced with less MC added to the cell culture.

The dependence of the cellular response on a certain extracellular compound concentration gives strong evidence, that the observed process is a quorum sensing (QS) or QS-like mechanism. When the concentration of MC in the medium reaches a certain threshold, the diminishing of photosynthetic enzymes is induced. This mechanism could serve as a controlling function of the overall photosynthetic performance of the bloom in its collectivity. *M. aeruginosa* is possibly using microcystin as marker for the cell density of the whole population. The reduction of photosynthetic enzymes and thus the photosynthesis rate itself per single cell could lead to the saving of energy when the whole bloom is taken into consideration. Due to the high-light intensities, to which the cells are exposed, RubisCO is fragmented because of the saturation with light (Kokubun *et al.*, 2002). The degradation prevents the cell from the generation of too many photorespiratory products. Possibly, the PEP carboxylase is taking over to be the main enzyme for CO2 fixation under these conditions, since it cannot fix O2 to generate toxic compounds. Furthermore, the degraded RubisCO could serve as a sulfur-rich amino acid source, when photosynthesis is downregulated as reported for the green algae *Chlamydomonas reinhardtii* (Majeran *et al.*, 2019). That a QS system can affect the expression of RubisCO was already reported for the cyanobacterium *Gloeothece* PCC6909 (Sharif *et al.*, 2008). The postulated model of a heterogeneous bloom in terms of subcellular localization of RubisCO can be expanded with the involvement of MC as an indicator of cell density (Figure 24). Cells in the upper levels of a bloom, near to the surface, are exposed to extremely strong light intensities. The high-light induces the subcellular relocalization of RubisCO from the carboxysomes towards the cytoplasmic membrane as part of the alternative CCM. In

addition, the raising level of MC in the surroundings of the cell can lead to the reduction of RubisCO and other enzymes involved into photosynthesis. These two mechanisms do not act against each other; they are adaptations to cope with different challenges of a bloom. Cells in the lower levels of the bloom are facing the same raising level of extracellular MC, resulting in the reduction of RubisCO packed into carboxysomes as well. The presented results are in line with previous studies, that the main function of MC for *M. aeruginosa* is not the inhibition or killing of other organisms like antibiotics do (Zilliges *et al.*, 2011; Makower, Schuurmans, Groth, Zilliges, Hans C.P. Matthijs, *et al.*, 2015; Meissner *et al.*, 2015). Instead, it is used possibly as a QS molecule to indicate the cell density of a bloom and induce a collective response from which the population is benefitting. This function is strengthened also by the fact that only exceedingly small amounts of MC were found in the supernatant of the lower cell density populations in the diurnal incubation experiment. At this low population densities, it is not necessary to down-regulate RubisCO, thus only low amounts of MC are secreted into the medium. Furthermore, the induction of the diminishing of RubisCO in the MC-deficient mutant Δ*mcyB* suggests that the intracellular response is not depending on the cell even to be able to produce MC. It is possibly a global signaling molecule (Federle and Bassler, 2003; Lowery *et al.*, 2008; Kwan *et al.*, 2011).

The response of the Δ*mcyB* mutant to the high-light treatment raises the possibility of the involvement of other cyanopeptides as extracellular signals as well. RbcL clearly diminished after 4 h of high-light treatment without any MC present inside of the cells or in the surrounding medium. The decrease of the RbcL signal is probably linked to cyanopeptolin. The diurnal incubation of the WT showed a burst of its extracellular portion. It is also known that in the Δ*mcyB* mutant higher amounts of aeruginosin and cyanopeptolin are measured in comparison to the WT at similar conditions (Briand *et al.*, 2016). Probably, the other cyanopeptides have similar functions as microcystin in MC-free *M. aeruginosa* cells or cell cultures. The presence of high amounts of cyanopeptolin in a drinking water treatment plant is at least a hint about a possible extracellular role of cyanopeptolin (Beversdorf *et al.*, 2018). To discuss more detailed about the possible influences of cyanopeptolin or aeruginosin on the producing *M. aeruginosa*, further studies are needed. Addition experiments with cyanopeptolin instead of microcystin would provide helpful information about the extracellular role of it and would be good starting point for an in-depth study about its physiological role.

Since the MC-deficient mutant Δ*mcyB* showed very similar RubisCO relocalization dynamics under high-light illumination, it is very likely that this process is not linked solely to microcystin as the mediating peptide and cyanopeptolin and aeruginosin are at least small parts of the whole process.

Taken together all the results obtained in this study, it appears quite clear, that *M. aeruginosa* PCC7806 deviates from the canonical knowledge about the CCM of cyanobacteria. This study suggests the presence of an alternative membrane-located CCM in cyanobacteria, which enables bloom-forming cyanobacteria like *M. aeruginosa* to adapt to the harsh conditions inside of a dense bloom. The formation of a CBB cycle super complex is part of this mechanism and is a time and energy saving alternative to the canonical carboxysome-based CCM. IFM images from this work suggest the involvement of microcystin into this process by binding to the RubisCO subunits or other CBB cycle enzymes to prevent them from degradation. An possible effect on the assembly of the enzyme complex through its binding needs to be studied further. Microcystin addition and diurnal incubation experiments furthermore suggest a key role of MC as a population density-based signaling molecule to induce collective responses of the *M. aeruginosa* bloom.

5. References

Abed, R.M.M., Dobretsov, S., and Sudesh, K. (2009) Applications of cyanobacteria in biotechnology. *J Appl Microbiol* **106**: 1–12.

Abernathy, M.H., Czajka, J.J., Allen, D.K., Hill, N.C., Cameron, J.C., and Tang, Y.J. (2019) Cyanobacterial carboxysome mutant analysis reveals the influence of enzyme compartmentalization on cellular metabolism and metabolic network rigidity. *Metab Eng* **54**: 222–231.

Abisado, R.G., Benomar, S., Klaus, J.R., Dandekar, A.A., and Chandler, J.R. (2018) Bacterial quorum sensing and microbial community interactions. *MBio* **9**: 1-13.

Agarwal, R., Ortleb, S., Sainis, J.K., and Melzer, M. (2009) Immunoelectron microscopy for locating Calvin cycle enzymes in the thylakoids of synechocystis 6803. *Mol Plant* **2**: 32–42.

Al-Haj, L., Lui, Y., Abed, R., Gomaa, M., and Purton, S. (2016) Cyanobacteria as Chassis for Industrial Biotechnology: Progress and Prospects. *Life* **6**: 42.

des Aulnois, M.G., Roux, P., Caruana, A., Réveillon, D., Briand, E., Hervé, F., et al. (2019) Physiological and metabolic responses of freshwater and brackish-water strains of Microcystis aeruginosa acclimated to a salinity gradient: Insight into salt tolerance. *Appl Environ Microbiol* **85**: 1-15.

Badger, M.R., Hanson, D., and Price, G.D. (2002) Evolution and diversity of CO2 concentrating mechanisms in cyanobacteria. *Functional Plant Biology* **29**:161–173.

Badger, M.R. and Price, G.D. (2003) CO2 concentrating mechanisms in cyanobacteria: Molecular components, their diversity and evolution. *J Exp Bot* **54**: 609–622.

Banda, D.M., Pereira, J.H., Liu, A.K., Orr, D.J., Hammel, M., He, C., et al. (2020) Novel bacterial clade reveals origin of form I Rubisco. *Nat Plants* **6**: 1158-1166.

Bateson, M.M. and Ward, D.M. (1988) Photoexcretion and Fate of Glycolate in a Hot

Spring Cyanobacterial Mat. *Appl Environ Microbiol* **54**: 1738–1743.

Beliaev, A.S., Romine, M.F., Serres, M., Bernstein, H.C., Linggi, B.E., Markillie, L.M., et al. (2014) Inference of interactions in cyanobacterial-heterotrophic co-cultures via transcriptome sequencing. *ISME J* **8**: 2243–2255.

Berg, Katri A., Lyra, C., Sivonen, K., Paulin, L., Suomalainen, S., Tuomi, P., and Rapala, J. (2009) High diversity of cultivable heterotrophic bacteria in association with cyanobacterial water blooms. *ISME J* **3**: 314–325.

Berg, Katri A, Lyra, C., Sivonen, K., Paulin, L., Suomalainen, S., Tuomi, P., and Rapala, J. (2009) High diversity of cultivable heterotrophic bacteria in association with cyanobacterial water blooms. *ISME J* **3**: 314–325.

Beversdorf, L.J., Rude, K., Weirich, C.A., Bartlett, S.L., Seaman, M., Kozik, C., et al. (2018) Analysis of cyanobacterial metabolites in surface and raw drinking waters reveals more than microcystin. *Water Res* **140**: 280–290.

Bister, B., Keller, S., Baumann, H.I., Nicholson, G., Weist, S., Jung, G., et al. (2004) Cyanopeptolin 963A, a chymotrypsin inhibitor of Microcystis PCC 7806. *J Nat Prod* **67**: 1755–1757.

Bittencourt-Oliveira, M. do C., Chia, M.A., de Oliveira, H.S.B., Cordeiro Araújo, M.K., Molica, R.J.R., and Dias, C.T.S. (2014) Allelopathic interactions between microcystin-producing and non-microcystin-producing cyanobacteria and green microalgae: implications for microcystins production. *J Appl Phycol* **27**: 275–284.

Bloom, A.J., Burger, M., Asensio, J.S.R., and Cousins, A.B. (2010) Carbon dioxide enrichment inhibits nitrate assimilation in wheat and arabidopsis. *Science* **328**: 899–903.

Briand, E., Bormans, M., Gugger, M., Dorrestein, P.C., and Gerwick, W.H. (2016) Changes in secondary metabolic profiles of Microcystis aeruginosa strains in response to intraspecific interactions. *Environ Microbiol* **18**: 384–400.

Burnap, R.L., Nambudiri, R., and Holland, S. (2013) Regulation of the carbon-concentrating mechanism in the cyanobacterium Synechocystis sp. PCC6803 in response to changing light intensity and inorganic carbon availability. *Photosynth Res* **118**: 115–124.

Cameron, Jeffrey C, Wilson, S.C., Bernstein, S.L., and Kerfeld, C.A. (2013) Biogenesis of a bacterial organelle: The carboxysome assembly pathway. *Cell* **155**: 1131–1140.

Cameron, Jeffrey C., Wilson, S.C., Bernstein, S.L., and Kerfeld, C.A. (2013) Biogenesis of a bacterial organelle: The carboxysome assembly pathway. *Cell* **155**: 1131-1140.

Campbell, W.J. and Ogren, W.L. (1990) Glyoxylate inhibition of ribulosebisphosphate carboxylase/oxygenase activation in intact, lysed, and reconstituted chloroplasts. *Photosynth Res* **23**: 257–268.

Carmichael, W.W. (2001) Health effects of toxin-producing cyanobacteria: “The CyanoHABs.” *Hum Ecol Risk Assess* **7**: 1393–1407.

Carmichael, W.W., Beasley, V., Bunner, D.L., Eloff, J.N., Falconer, I., Gorham, P., et al. (1988) Naming of cyclic heptapeptide toxins of cyanobacteria (blue-green algae). *Toxicon* **26**: 971–973.

Chen, L., Chen, J., Zhang, X., and Xie, P. (2016) A review of reproductive toxicity of microcystins. *J Hazard Mater* **301**: 381–399.

Christiansen, G., Fastner, J., Erhard, M., Börner, T., and Dittmann, E. (2003) Microcystin biosynthesis in Planktothrix: Genes, evolution, and manipulation. *J Bacteriol* **185**: 564–572.

Colman, B. (1989) Photosynthetic carbon assimilation and the suppression of photorespiration in the cyanobacteria. *Aquat Bot* **34**: 211–231.

Cook, K. V., Li, C., Cai, H., Krumholz, L.R., Hambright, K.D., Paerl, H.W., et al. (2020) The global Microcystis interactome. *Limnol Oceanogr* **65**: S194–S207.

Cordeiro-Araújo, M.K. and Bittencourt-Oliveira, M. do C. (2013) Active release of microcystins controlled by an endogenous rhythm in the cyanobacterium Microcystis aeruginosa. *Phycol Res* **61**: 1–6.

Cossar, J.D., Rowell, P., Darling, A.J., Murray, S., Codd, G.A., and Stewart, W.D.P. (1985) Localization of ribulose 1,5-bisphosphate carboxylase/oxygenase in the N2-fixing cyanobacterium Anabaena cylindrica. *FEMS Microbiol Lett* **28**: 65–68.

Cot, S.S.W., So, A.K.C., and Espie, G.S. (2008) A multiprotein bicarbonate dehydration complex essential to carboxysome function in cyanobacteria. *J Bacteriol* **190**: 936–945.

Dittmann, E., Neilan, B.A., Erhard, M., Von Döhren, H., and Börner, T. (1997) Insertional mutagenesis of a peptide synthetase gene that is responsible for hepatotoxin production in the cyanobacterium Microcystis aeruginosa PCC 7806. *Mol Microbiol* **26**: 779–787.

Dong, X., Zeng, S., Bai, F., Li, D., and He, M. (2016) Extracellular microcystin prediction based on toxigenic Microcystis detection in a eutrophic lake. *Sci Rep* **6**: 1–8.

Dziallas, C. and Grossart, H.P. (2011) Increasing oxygen radicals and water temperature select for toxic microcystis sp. *PLoS One* **6**: e25569.

Von Elert, E., Oberer, L., Merkel, P., Huhn, T., and Blom, J.F. (2005) Cyanopeptolin 954, a chlorine-containing chymotrypsin inhibitor of Microcystis aeruginosa NIVA Cya 43. *J Nat Prod* **68**: 1324–1327.

Ellis, R.J. (1979) The most abundant protein in the world. *Trends Biochem Sci* **4**: 241–244.

Faltermann, S., Zucchi, S., Kohler, E., Blom, J.F., Pernthaler, J., and Fent, K. (2014) Molecular effects of the cyanobacterial toxin cyanopeptolin (CP1020) occurring in algal blooms: Global transcriptome analysis in zebrafish embryos. *Aquat Toxicol* **149**: 33–39.

Farazdaghi, H. (2009) Modeling the Kinetics of Activation and Reaction of Rubisco from Gas Exchange. Springer, Dordrecht, pp. 275–294.

Faulkner, M., Rodriguez-Ramos, J., Dykes, G.F., Owen, S. V., Casella, S., Simpson, D.M., et al. (2017) Direct characterization of the native structure and mechanics of cyanobacterial carboxysomes. *Nanoscale* **9**: 10662–10673.

Federle, M.J. and Bassler, B.L. (2003) Interspecies communication in bacteria. *J Clin Invest* **112**: 1291–1299.

Flores, C. and Caixach, J. (2015) An integrated strategy for rapid and accurate determination of free and cell-bound microcystins and related peptides in natural

blooms by liquid chromatography-electrospray-high resolution mass spectrometry and matrix-assisted laser desorption/ionization time-of-flight/time-of-flight mass spectrometry using both positive and negative ionization modes. *J Chromatogr A* **1407**: 76–89.

Foyer, C.H., Bloom, A.J., Queval, G., and Noctor, G. (2009) Photorespiratory Metabolism: Genes, Mutants, Energetics, and Redox Signaling. *Annu Rev Plant Biol* **60**: 455–484.

Frangeul, L., Quillardet, P., Castets, A.M., Humbert, J.F., Matthijs, H.C.P., Cortez, D., et al. (2008) Highly plastic genome of Microcystis aeruginosa PCC 7806, a ubiquitous toxic freshwater cyanobacterium. *BMC Genomics* **9**: 274.

Gademann, K., Portmann, C., Blom, J.F., Zeder, M., and Jüttner, F. (2010) Multiple toxin production in the cyanobacterium Microcystis: Isolation of the toxic protease inhibitor cyanopeptolin 1020. *J Nat Prod* **73**: 980–984.

Gandini, C., Schmidt, S.B., Husted, S., Schneider, A., and Leister, D. (2017) The transporter SynPAM71 is located in the plasma membrane and thylakoids, and mediates manganese tolerance in Synechocystis PCC6803. *New Phytol* **215**: 256–268.

Gaysina, L.A., Saraf, A., and Singh, P. (2018) Cyanobacteria in Diverse Habitats. In, *Cyanobacteria: From Basic Science to Applications*. Elsevier, pp. 1–28.

Ghosh, M., Tucker, D.E., Burchett, S.A., and Leslie, C.C. (2006) Properties of the Group IV phospholipase A2 family. *Prog Lipid Res* **45**: 487–510.

Goñi, F.M. (2002) Non-permanent proteins in membranes: When proteins come as visitors (review). *Mol Membr Biol* **19**: 237–245.

Gontero, B., CÁRDENAS, M.L., and RICARD, J. (1988) A functional five-enzyme complex of chloroplasts involved in the Calvin cycle. *Eur J Biochem* **173**: 437–443.

Hackenberg, C., Hakanpää, J., Cai, F., Antonyuk, S., Eigner, C., Meissner, S., et al. (2018) Structural and functional insights into the unique CBS–CP12 fusion protein family in cyanobacteria. *Proc Natl Acad Sci U S A* **115**: 7141–7146.

Hackenberg, C., Huege, J., Engelhardt, A., Wittink, F., Laue, M., Matthijs, H.C.P., et al. (2012) Low-carbon acclimation in carboxysome-less and photorespiratory mutants of the cyanobacterium synechocystis sp. strain PCC 6803. *Microbiology* **158**: 398–413.

Hagemann, M., Fernie, A.R., Espie, G.S., Kern, R., Eisenhut, M., Reumann, S., et al. (2013) Evolution of the biochemistry of the photorespiratory C2 cycle. *Plant Biol* **15**: 639–647.

Hanson, T.E. and Tabita, F.R. (2001) A ribulose-1,5-bisphosphate carboxylase/oxygenase (RubisCO)-like protein from Chlorobium tepidum that is involved with sulfur metabolism and the response to oxidative stress. *Proc Natl Acad Sci U S A* **98**: 4397–4402.

Hasunuma, T., Kikuyama, F., Matsuda, M., Aikawa, S., Izumi, Y., and Kondo, A. (2013) Dynamic metabolic profiling of cyanobacterial glycogen biosynthesis under conditions of nitrate depletion. *J Exp Bot* **64**: 2943–2954.

Heinhorst, S., Cannon, G.C., and Shively, J.M. (2006) Carboxysomes and Carboxysome-like Inclusions. Springer, Berlin, Heidelberg, pp. 141–165.

Hohmann-Marriott, M.F. and Blankenship, R.E. (2011) Evolution of Photosynthesis. *Annu Rev Plant Biol* **62**: 515–548.

Huisman, J., Codd, G.A., Paerl, H.W., Ibelings, B.W., Verspagen, J.M.H., and Visser, P.M. (2018) Cyanobacterial blooms. *Nat Rev Microbiol* **16**: 471–483.

Husic, D.W., Husic, H.D., Tolbert, N.E., and Black, C.C. (1987) The oxidative photosynthetic carbon cycle or c2 cycle. *CRC Crit Rev Plant Sci* **5**: 45–100.

Ibelings, B.W. and Maberly, S.C. (1998) Photoinhibition and the availability of inorganic carbon restrict photosynthesis by surface blooms of cyanobacteria. *Limnol Oceanogr* **43**: 408–419.

Ibelings, B.W., Mur, L.R., and Walsby, A.E. (1991) Diurnal changes in buoyancy and vertical distribution in populations of Microcystisin two shallow lakes. *J Plankton Res* **13**: 419–436.

Igamberdiev, A.U. and Kleczkowski, L.A. (1977) Glyoxylate metabolism during photorespiration - A cytosol connection. *Handb Photosynth*, New York, 269–279.

Ishida, K., Okita, Y., Matsuda, H., Okino, T., and Murakami, M. (1999) Aeruginosins, protease inhibitors from the cyanobacterium Microcystis aeruginosa. *Tetrahedron* **55**: 10971–10988.

Jähnichen, S., Ihle, T., Petzoldt, T., and Benndorf, J. (2007) Impact of inorganic carbon availability on microcystin production by Microcystis aeruginosa PCC 7806. *Appl Environ Microbiol* **73**: 6994–7002.

Jaki, B., Heilmann, J., and Sticher, O. (2000) New antibacterial metabolites from the cyanobacterium Nostoc commune (EAWAG 122b). *J Nat Prod* **63**: 1283–1285.

Janssen, E.M.L. (2019) Cyanobacterial peptides beyond microcystins – A review on co-occurrence, toxicity, and challenges for risk assessment. *Water Res* **151**: 488–499.

Jebanathirajah, J.A. and Coleman, J.R. (1998) Association of carbonic anhydrase with a Calvin cycle enzyme complex in Nicotiana tabacum. *Planta* **204**: 177–182.

Johnson, J.E. and Cornell, R.B. (1999) Amphitropic proteins: Regulation by reversible membrane interactions. *Mol Membr Biol* **16**: 217–235.

Kajiyama, S.I., Kanzaki, H., Kawazu, K., and Kobayashi, A. (1998) Nostofungicidine, an antifungal lipopeptide from the field-grown terrestrial blue-green alga Nostoc commune. *Tetrahedron Lett* **39**: 3737–3740.

Kaplan, A., Harel, M., Kaplan-Levy, R.N., Hadas, O., Sukenik, A., and Dittmann, E. (2012) The languages spoken in the water body (or the biological role of cyanobacterial toxins). *Front Microbiol* **3**: 138.

Keatinge-Clay, A.T. (2017) Polyketide Synthase Modules Redefined. *Angew Chemie - Int Ed* **56**: 4658–4660.

Kerfeld, C.A., Aussignargues, C., Zarzycki, J., Cai, F., and Sutter, M. (2018) Bacterial microcompartments. *Nat Rev Microbiol* **16**: 277–290.

Kim, M., Shin, B., Lee, J., Park, H.Y., and Park, W. (2019) Culture-independent and culture-dependent analyses of the bacterial community in the phycosphere of cyanobloom-forming Microcystis aeruginosa. *Sci Rep* **9**: 1–13.

Kinney, J.N., Salmeen, A., Cai, F., and Kerfeld, C.A. (2012) Elucidating essential role

of conserved carboxysomal protein CcmN reveals common feature of bacterial microcompartment assembly. *J Biol Chem* **287**: 17729–17736.

Kodani, S., Ishida, K., and Murakami, M. (1998) Aeruginosin 103-A, a thrombin inhibitor from the cyanobacterium Microcystis viridis. *J Nat Prod* **61**: 1046–1048.

Kokubun, N., Ishida, H., Makino, A., and Mae, T. (2002) The degradation of the large subunit of ribulose-1,5-bisphosphate carboxylase/oxygenase into the 44-kDa fragment in the lysates of chloroplasts incubated in darkness. *Plant Cell Physiol* **43**: 1390–1394.

Kromkamp, J.C. and Mur, L.R. (1984) Buoyant density changes in the cyanobacterium Microcystis aeruginosa due to changes in the cellular carbohydrate content. *FEMS Microbiol Lett* **25**: 105–109.

Kupriyanova, E. V., Sinetova, M.A., Mironov, K.S., Novikova, G. V., Dykman, L.A., Rodionova, M. V., et al. (2019) Highly active extracellular α-class carbonic anhydrase of Cyanothece sp. ATCC 51142. *Biochimie* **160**: 200–209.

Kuzmak, A., Carmali, S., von Lieres, E., Russell, A.J., and Kondrat, S. (2019) Can enzyme proximity accelerate cascade reactions? *Sci Rep* **9**: 1–7.

Kwan, J.C., Meickle, T., Ladwa, D., Teplitski, M., Paul, V., and Luesch, H. (2011) Lyngbyoic acid, a “tagged” fatty acid from a marine cyanobacterium, disrupts quorum sensing in Pseudomonas aeruginosa. *Mol Biosyst* **7**: 1205–1216.

Lechno-Yossef, S., Rohnke, B.A., Belza, A.C.O., Melnicki, M.R., Montgomery, B.L., and Kerfeld, C.A. (2020) Cyanobacterial carboxysomes contain an unique rubisco-activase-like protein. *New Phytol* **225**: 793–806.

Li, Q., Lin, F., Yang, C., Wang, J., Lin, Y., Shen, M., et al. (2018) A large-scale comparative metagenomic study reveals the functional interactions in six bloom-forming Microcystis-epibiont communities. *Front Microbiol* **9**: 746.

Liu, C., Young, A.L., Starling-Windhof, A., Bracher, A., Saschenbrecker, S., Rao, B.V., et al. (2010) Coupled chaperone action in folding and assembly of hexadecameric Rubisco. *Nature* **463**: 197–202.

Long, B.M., Rae, B.D., Badger, M.R., and Price, G.D. (2011) Over-expression of the β-carboxysomal CcmM protein in Synechococcus PCC7942 reveals a tight co-

regulation of carboxysomal carbonic anhydrase (CcaA) and M58 content. In, *Photosynthesis Research*. Springer, pp. 33–45.

Lowery, C.A., Dickerson, T.J., and Janda, K.D. (2008) Interspecies and interkingdom communication mediated by bacterial quorum sensing. *Chem Soc Rev* **37**: 1337–1346.

Maeda, S.I., Badger, M.R., and Price, G.D. (2002) Novel gene products associated with NdhD3/D4-containing NDH-1 complexes are involved in photosynthetic CO2 hydration in the cyanobacterium, Synechococcus sp. PCC7942. *Mol Microbiol* **43**: 425–435.

Majeran, W., Wostrikoff, K., Wollman, F.A., and Vallon, O. (2019) Role of ClpP in the biogenesis and degradation of RuBisCO and ATP synthase in Chlamydomonas reinhardtii. *Plants* **8**: 191.

Makower, A.K., Schuurmans, J.M., Groth, D., Zilliges, Y., Matthijs, Hans C P, and Dittmann, E. (2015) Transcriptomics-aided dissection of the intracellular and extracellular roles of microcystin in Microcystis aeruginosa PCC 7806. *Appl Environ Microbiol* **81**: 544–554.

Makower, A.K., Schuurmans, J.M., Groth, D., Zilliges, Y., Matthijs, Hans C.P., and Dittmann, E. (2015) Transcriptomics-aided dissection of the intracellular and extracellular roles of microcystin in Microcystis aeruginosa PCC 7806. *Appl Environ Microbiol* **81**: 544–554.

Mangan, N. and Brenner, M. (2014) Systems analysis of the CO2 concentrating mechanism in cyanobacteria. *Elife* **2014**: e02043.

Marcus, Y., Altman-Gueta, H., Finkler, A., and Gurevitz, M. (2003) Dual role of cysteine 172 in redox regulation of ribulose 1,5-bisphosphate carboxylase/oxygenase activity and degradation. *J Bacteriol* **185**: 1509–1517.

Marcus, Y., Berry, J.A., and Pierce, J. (1992) Photosynthesis and photorespiration in a mutant of the cyanobacterium Synechocystis PCC 6803 lacking carboxysomes. *Planta* **187**: 511–516.

McFadden, G.I. (1999) Endosymbiosis and evolution of the plant cell. *Curr Opin Plant Biol* **2**: 513–519.

McKay, R.M.L., Gibbs, S.P., and Espie, G.S. (1993) Effect of dissolved inorganic carbon on the expression of carboxysomes, localization of Rubisco and the mode of inorganic carbon transport in cells of the cyanobacterium Synechococcus UTEX 625. *Arch Microbiol* **159**: 21–29.

Meissner, S., Fastner, J., and Dittmann, E. (2013) Microcystin production revisited: Conjugate formation makes a major contribution. *Environ Microbiol* **15**: 1810–1820.

Meissner, S., Steinhauser, D., and Dittmann, E. (2015) Metabolomic analysis indicates a pivotal role of the hepatotoxin microcystin in high light adaptation of Microcystis. *Environ Microbiol* **17**: 1497–1509.

Miles, C.O., Sandvik, M., Nonga, H.E., Ballot, A., Wilkins, A.L., Rise, F., et al. (2016) Conjugation of Microcystins with Thiols Is Reversible: Base-Catalyzed Deconjugation for Chemical Analysis. *Chem Res Toxicol* **29**: 860–870.

Miller, M.A., Kudela, R.M., Mekebri, A., Crane, D., Oates, S.C., Tinker, M.T., et al. (2010) Evidence for a novel marine harmful algal bloom: Cyanotoxin (microcystin) transfer from land to sea otters. *PLoS One* **5**: 1–11.

Monje-Galvan, V. and Klauda, J.B. (2016) Peripheral membrane proteins: Tying the knot between experiment and computation. *Biochim Biophys Acta - Biomembr* **1858**: 1584–1593.

Van Mooy, B.A.S., Hmelo, L.R., Sofen, L.E., Campagna, S.R., May, A.L., Dyhrman, S.T., et al. (2012) Quorum sensing control of phosphorus acquisition in Trichodesmium consortia. *ISME J* **6**: 422–429.

Morozova, D., Guigas, G., and Weiss, M. (2011) Dynamic structure formation of peripheral membrane proteins. *PLoS Comput Biol* **7**: 1002067.

Morse, D., Salois, P., Markovic, P., and Hastings, J.W. (1995) A nuclear-encoded form II RuBisCO in dinoflagellates. *Science (80-)* **268**: 1622–1624.

Mouritsen, O.G. and Bloom, M. (1993) Models of lipid-protein interactions in membranes. *Annu Rev Biophys Biomol Struct* **22**: 145–171.

Murakami, M., Okita, Y., Matsuda, H., Okino, T., and Yamaguchi, K. (1994) Aeruginosin 298-A, a thrombin and trypsin inhibitor from the blue-green alga

Microcystis aeruginosa (NIES-298). *Tetrahedron Lett* **35**: 3129–3132.

Ng, W.-L. and Bassler, B.L. (2009) Bacterial Quorum-Sensing Network Architectures. *Annu Rev Genet* **43**: 197–222.

Omata, T., Takahashi, Y., Yamaguchi, O., and Nishimura, T. (2002) Structure, function and regulation of the cyanobacterial high-affinity bicarbonate transporter, BCT1. In, *Functional Plant Biology*. CSIRO PUBLISHING, pp. 151–159.

Orf, I., Timm, S., Bauwe, H., Fernie, A.R., Hagemann, M., Kopka, J., and Nikoloski, Z. (2016) Can cyanobacteria serve as a model of plant photorespiration? - A comparative meta-analysis of metabolite profiles. *J Exp Bot* **67**: 2941–2952.

Park, B.S., Li, Z., Kang, Y.H., Shin, H.H., Joo, J.H., and Han, M.S. (2018) Distinct Bloom Dynamics of Toxic and Non-toxic Microcystis (Cyanobacteria) Subpopulations in Hoedong Reservoir (Korea). *Microb Ecol* **75**: 163–173.

Park, H.D., Iwami, C., Watanabe, M.F., Harada, K.I., Okino, T., and Hayashi, H. (1998) Temporal variabilities of the concentrations of intra- and extracellular microcystin and toxic microcystis species in a hypertrophie lake, Lake Suwa, Japan (1991-1994). *Environ Toxicol Water Qual* **13**: 61–72.

Pearson, L.A., Hisbergues, M., Börner, T., Dittmann, E., Neilan, B.A., Pearson, L.A., et al. (2004) Inactivation of an ABC Transporter Gene , mcyH , Results in Loss of Microcystin Production in the Cyanobacterium Microcystis aeruginosa PCC 7806 Inactivation of an ABC Transporter Gene , mcyH , Results in Loss of Microcystin Production in the Cyanobacteri. *Appl Environ Microbiol* **70**: 6370–6378.

Pereira, D.A. and Giani, A. (2014) Cell density-dependent oligopeptide production in cyanobacterial strains. *FEMS Microbiol Ecol* **88**: 175–183.

Price, G.D. and Howitt, S.M. (2011) The cyanobacterial bicarbonate transporter BicA: Its physiological role and the implications of structural similarities with human SLC26 transporters. *Biochem Cell Biol* **89**: 178–188.

Price, G.D., Shelden, M.C., and Howitt, S.M. (2011) Membrane topology of the cyanobacterial bicarbonate transporter, SbtA, and identification of potential regulatory loops. *Mol Membr Biol* **28**: 265–275.

Rabalais, N.N., Díaz, R.J., Levin, L.A., Turner, R.E., Gilbert, D., and Zhang, J. (2010)

Dynamics and distribution of natural and human-caused hypoxia. *Biogeosciences* **7**: 585–619.

Rachmilevitch, S., Cousins, A.B., and Bloom, A.J. (2004) Nitrate assimilation in plant shoots depends on photorespiration. *Proc Natl Acad Sci U S A* **101**: 11506–11510.

Rae, Benjamin D, Long, B.M., Badger, M.R., and Price, G.D. (2013) Functions, compositions, and evolution of the two types of carboxysomes: polyhedral microcompartments that facilitate CO2 fixation in cyanobacteria and some proteobacteria. *Microbiol Mol Biol Rev* **77**: 357–379.

Rae, B. D., Long, B.M., Badger, M.R., and Price, G.D. (2013) Functions, Compositions, and Evolution of the Two Types of Carboxysomes: Polyhedral Microcompartments That Facilitate CO2 Fixation in Cyanobacteria and Some Proteobacteria. *Microbiol Mol Biol Rev* **77**: 357–379.

Rae, Benjamin D., Long, B.M., Whitehead, L.F., Förster, B., Badger, M.R., and Price, G.D. (2013) Cyanobacterial carboxysomes: Microcompartments that facilitate CO 2 fixation. *J Mol Microbiol Biotechnol* **23**: 300–307.

Raines, C.A. (2003) The Calvin cycle revisited. *Photosynth Res* **75**: 1–10.

Rantala, A., Fewer, D.P., Hisbergues, M., Rouhiainen, L., Vaitomaa, J., Börner, T., and Sivonen, K. (2004) Phylogenetic evidence for the early evolution of microcystin synthesis. *Proc Natl Acad Sci U S A* **101**: 568–573.

Rastogi, R.P., Sinha, R.P., and Incharoensakdi, A. (2014) The cyanotoxin-microcystins: Current overview. *Rev Environ Sci Biotechnol* **13**: 215–249.

Renthal, R. (2010) Helix insertion into bilayers and the evolution of membrane proteins. *Cell Mol Life Sci* **67**: 1077–1088.

Rippka, R., Deruelles, J., Waterbury, J.B., Herdman, M., and Stanier, R.Y. (1979) Generic Assignments, Strain Histories and Properties of Pure Cultures of Cyanobacteria. *Microbiology* **111**: 1–61.

Rounge, T.B., Rohrlack, T., Tooming-Klunderud, A., Kristensen, T., and Jakobsen, K.S. (2007) Comparison of cyanopeptolin genes in Planktothrix, Microcystis, and Anabaena strains: Evidence for independent evolution within each genus. *Appl Environ Microbiol* **73**: 7322–7330.

Sandrini, G., Jakupovic, D., Matthijs, H.C.P., and Huisman, J. (2015) Strains of the harmful cyanobacterium Microcystis aeruginosa differ in gene expression and activity of inorganic carbon uptake systems at elevated CO2 levels. *Appl Environ Microbiol* **81**: 7730–7739.

Sandrini, G., Matthijs, H.C.P., Verspagen, J.M.H., Muyzer, G., and Huisman, J. (2014) Genetic diversity of inorganic carbon uptake systems causes variation in CO2 response of the cyanobacterium Microcystis. *ISME J* **8**: 589–600.

Schatz, D., Keren, Y., Vardi, A., Sukenik, A., Carmeli, S., Börner, T., et al. (2007) Towards clarification of the biological role of microcystins, a family of cyanobacterial toxins. *Environ Microbiol* **9**: 965–970.

Schirrmeister, B.E., Sanchez-Baracaldo, P., and Wacey, D. (2016) Cyanobacterial evolution during the Precambrian. *Int J Astrobiol* **15**: 187–204.

El Semary, N.A. (2010) Investigating factors affecting growth and cellular mcyB transcripts of Microcystis aeruginosa PCC 7806 using real-time PCR. *Ann Microbiol* **60**: 181–188.

Sharif, D.I., Gallon, J., Smith, C.J., and Dudley, E. (2008) Quorum sensing in Cyanobacteria: N-octanoyl-homoserine lactone release and response, by the epilithic colonial cyanobacterium Gloeothece PCC6909. *ISME J* **2**: 1171–1182.

Shibata, M., Ohkawa, H., Kaneko, T., Fukuzawa, H., Tabata, S., Kaplan, A., and Ogawa, T. (2001) Distinct constitutive and low-CO2-induced CO2 uptake systems in cyanobacteria: Genes involved and their phylogenetic relationship with homologous genes in other organisms. *Proc Natl Acad Sci U S A* **98**: 11789–11794.

Shih, P.M., Hemp, J., Ward, L.M., Matzke, N.J., and Fischer, W.W. (2017) Crown group Oxyphotobacteria postdate the rise of oxygen. *Geobiology* **15**: 19–29.

Shylajanaciyar, M., Dineshbabu, G., Rajalakshmi, R., Subramanian, G., Prabaharan, D., and Uma, L. (2015) Analysis and Elucidation of Phosphoenolpyruvate Carboxylase in Cyanobacteria. *Protein J* **34**: 73–81.

Smarda, J. and Maršalek, B. (2008) Microcystis aeruginosa (Cyanobacteria): ultrastructure in a pelagic and in a benthic ecosystem. *Arch Hydrobiol Suppl Algol*

Stud **126**: 73–86.

Smith, S.M. (2017) Strategies for the purification of membrane proteins. In, *Methods in Molecular Biology*. Humana Press Inc., pp. 389–400.

Snead, W.T. and Gladfelter, A.S. (2019) The Control Centers of Biomolecular Phase Separation: How Membrane Surfaces, PTMs, and Active Processes Regulate Condensation. *Mol Cell* **76**: 295–305.

Sommaruga, R., Chen, Y., and Liu, Z. (2009) Multiple strategies of bloom-forming microcystis to minimize damage by solar ultraviolet radiation in surface waters. *Microb Ecol* **57**: 667–674.

Song, H., Lavoie, M., Fan, X., Tan, H., Liu, G., Xu, P., et al. (2017) Allelopathic interactions of linoleic acid and nitric oxide increase the competitive ability of Microcystis aeruginosa. *ISME J* **11**: 1865–1876.

Song, Y. and Qiu, B. (2007) The CO2-concentrating mechanism in the bloom-forming cyanobacterium Microcystis aeruginosa (Cyanophyceae) and effects of UVB radiation on its operation. *J Phycol* **43**: 957–964.

Stough, J.M.A., Tang, X., Krausfeldt, L.E., Steffen, M.M., Gao, G., Boyer, G.L., and Wilhelm, S.W. (2017) Molecular prediction of lytic vs lysogenic states for Microcystis phage: Metatranscriptomic evidence of lysogeny during large bloom events. *PLoS One* **12**: e0184146.

Straub, C., Quillardet, P., Vergalli, J., de Marsac, N.T., and Humbert, J.-F. (2011) A Day in the Life of Microcystis aeruginosa Strain PCC 7806 as Revealed by a Transcriptomic Analysis. *PLoS One* **6**: e16208.

Süss, K.H., Arkona, C., Manteuffel, R., and Adler, K. (1993) Calvin cycle multienzyme complexes are bound to chloroplast thylakoid membranes of higher plants in situ. *Proc Natl Acad Sci U S A* **90**: 5514–5518.

Süssmuth, R.D. and Mainz, A. (2017) Nonribosomal Peptide Synthesis—Principles and Prospects. *Angew Chemie - Int Ed* **56**: 3770–3821.

Sutter, M., Laughlin, T.G., Sloan, N.B., Serwas, D., Davies, K.M., and Kerfeld, C.A. (2019) Structure of a Synthetic β-Carboxysome Shell. *Plant Physiol* **181**: 1050–1058.

Tabita, F.R., Hanson, T.E., Li, H., Satagopan, S., Singh, J., and Chan, S. (2007) Function, Structure, and Evolution of the RubisCO-Like Proteins and Their RubisCO Homologs. *Microbiol Mol Biol Rev* **71**: 576–599.

Tanabe, Y., Hodoki, Y., Sano, T., Tada, K., and Watanabe, M.M. (2018) Adaptation of the Freshwater Bloom-Forming Cyanobacterium Microcystis aeruginosa to Brackish Water Is Driven by Recent Horizontal Transfer of Sucrose Genes. *Front Microbiol* **9**: 1150.

Tillett, D., Dittmann, E., Erhard, M., von Döhren, H., Börner, T., and Neilan, B.A. (2000) Structural organisation of microcystin biosynthesis in Microcystis aeruginosa PCC7806: an integrated peptide-polyketide synthetase system. *Chem Biol* **7**: 753–764.

Tonk, L., Welker, M., Huisman, J., and Visser, P.M. (2009) Production of cyanopeptolins, anabaenopeptins, and microcystins by the harmful cyanobacteria Anabaena 90 and Microcystis PCC 7806. *Harmful Algae* **8**: 219–224.

Tooming-Klunderud, A., Rohrlack, T., Shalchian-Tabrizi, K., Kristensen, T., and Jakobsen, K.S. (2007) Structural analysis of a non-ribosomal halogenated cyclic peptide and its putative operon from Microcystis: implications for evolution of cyanopeptolins. *Microbiology* **153**: 1382–1393.

Towbin, H., Staehelin, T., and Gordon, J. (1979) Electrophoretic transfer of proteins from polyacrylamide gels to nitrocellulose sheets: procedure and some applications. *Proc Natl Acad Sci* **76**: 4350–4354.

Triana, J., Montagud, A., Siurana, M., Fuente, D., Urchueguía, A., Gamermann, D., et al. (2014) Generation and Evaluation of a Genome-Scale Metabolic Network Model of Synechococcus elongatus PCC7942. *Metabolites* **4**: 680–698.

Turmo, A., Gonzalez-Esquer, C.R., and Kerfeld, C.A. (2017) Carboxysomes: metabolic modules for CO2 fixation. *FEMS Microbiol Lett* **364**: 176.

Van De Waal, D.B., Verspagen, J.M.H., Finke, J.F., Vournazou, V., Immers, A.K., Kardinaal, W.E.A., et al. (2011) Reversal in competitive dominance of a toxic versus non-toxic cyanobacterium in response to rising CO 2. *ISME J* **5**: 1438–1450.

Walsby, A.E. (1994) Gas vesicles. *Microbiol Rev* **58**: 94–144.

Wang, Z., Chen, Q., Hu, L., and Wang, M. (2018) Combined effects of binary antibiotic mixture on growth, microcystin production, and extracellular release of Microcystis aeruginosa: application of response surface methodology. *Environ Sci Pollut Res* **25**: 736–748.

Wei, N., Hu, L., Song, L.R., and Gan, N.Q. (2016) Microcystin-bound protein patterns in different cultures of Microcystis aeruginosa and field samples. *Toxins (Basel)* **8**: 293.

Weiss, T.L., Young, E.J., and Ducat, D.C. (2017) A synthetic, light-driven consortium of cyanobacteria and heterotrophic bacteria enables stable polyhydroxybutyrate production. *Metab Eng* **44**: 236–245.

West, S.A., Griffin, A.S., Gardner, A., and Diggle, S.P. (2006) Social evolution theory for microorganisms. *Nat Rev Microbiol* **4**: 597–607.

Whited, A.M. and Johs, A. (2015) The interactions of peripheral membrane proteins with biological membranes. *Chem Phys Lipids* **192**: 51–59.

Whitton, B.A. and Potts, M. (2006) Introduction to the Cyanobacteria. In, *The Ecology of Cyanobacteria*. Kluwer Academic Publishers, pp. 1–11.

Williams, B.P., Johnston, I.G., Covshoff, S., and Hibberd, J.M. (2013) Phenotypic landscape inference reveals multiple evolutionary paths to C4 photosynthesis. *Elife* **2**: e00991.

Wilson, A.E., Wilson, W.A., and Hay, M.E. (2006) Intraspecific variation in growth and morphology of the bloom-forming cyanobacterium Microcystis aeruginosa. *Appl Environ Microbiol* **72**: 7386–7389.

Woodhouse, J.N., Ziegler, J., Grossart, H.P., and Neilan, B.A. (2018) Cyanobacterial community composition and bacteria-bacteria interactions promote the stable occurrence of particle-associated bacteria. *Front Microbiol* **9**: 777.

Xiao, M., Li, M., and Reynolds, C.S. (2018) Colony formation in the cyanobacterium Microcystis. *Biol Rev* **93**: 1399–1420.

Xu, H., Paerl, H.W., Zhu, G., Qin, B., Hall, N.S., and Zhu, M. (2017) Long-term nutrient

trends and harmful cyanobacterial bloom potential in hypertrophic Lake Taihu, China. *Hydrobiologia* **787**: 229–242.

Xu, Z., Jiang, Y., and Zhou, G. (2015) Response and adaptation of photosynthesis, respiration, and antioxidant systems to elevated CO2 with environmental stress in plants. *Front Plant Sci* **6**: 701.

Yamano, T. and Fukuzawa, H. (2009) Carbon-concentrating mechanism in a green alga, Chlamydomonas reinhardtii, revealed by transcriptome analyses. *J Basic Microbiol* **49**: 42–51.

Yoshida, T., Takashima, Y., Tomaru, Y., Shirai, Y., Takao, Y., Hiroishi, S., and Nagasaki, K. (2006) Isolation and characterization of a cyanophage infecting the toxic cyanobacterium Microcystis aeruginosa. *Appl Environ Microbiol* **72**: 1239–1247.

Young, F.M., Morrison, L.F., James, J., and Codd, G.A. (2008) Quantification and localization of microcystins in colonies of a laboratory strain of Microcystis (Cyanobacteria) using immunological methods. *Eur J Phycol* **43**: 217–225.

Zhai, C., Zhang, P., Shen, F., Zhou, C., and Liu, C. (2012) Does Microcystis aeruginosa have quorum sensing? *FEMS Microbiol Lett* **336**: 38–44.

Zhang, M., Lu, T., Paerl, H.W., Chen, Y., Zhang, Z., Zhou, Z., and Qian, H. (2019) Feedback regulation between aquatic microorganisms and the bloom-forming cyanobacterium Microcystis aeruginosa. *Appl Environ Microbiol* **85**: e01362-19.

Zhang, S. and Bryant, D.A. (2011) The tricarboxylic acid cycle in cyanobacteria. *Science (80-)* **334**: 1551–1553.

Zheng, Q., Wang, Y., Lu, J., Lin, W., Chen, F., and Jiao, N. (2020) Metagenomic and Metaproteomic Insights into Photoautotrophic and Heterotrophic Interactions in a Synechococcus Culture. *MBio* **11**: 1–18.

Zilliges, Y., Kehr, J.C., Meissner, S., Ishida, K., Mikkat, S., Hagemann, M., et al. (2011) The cyanobacterial hepatotoxin microcystin binds to proteins and increases the fitness of Microcystis under oxidative stress conditions. *PLoS One* **6**: e17615.

6. Supplemental Information

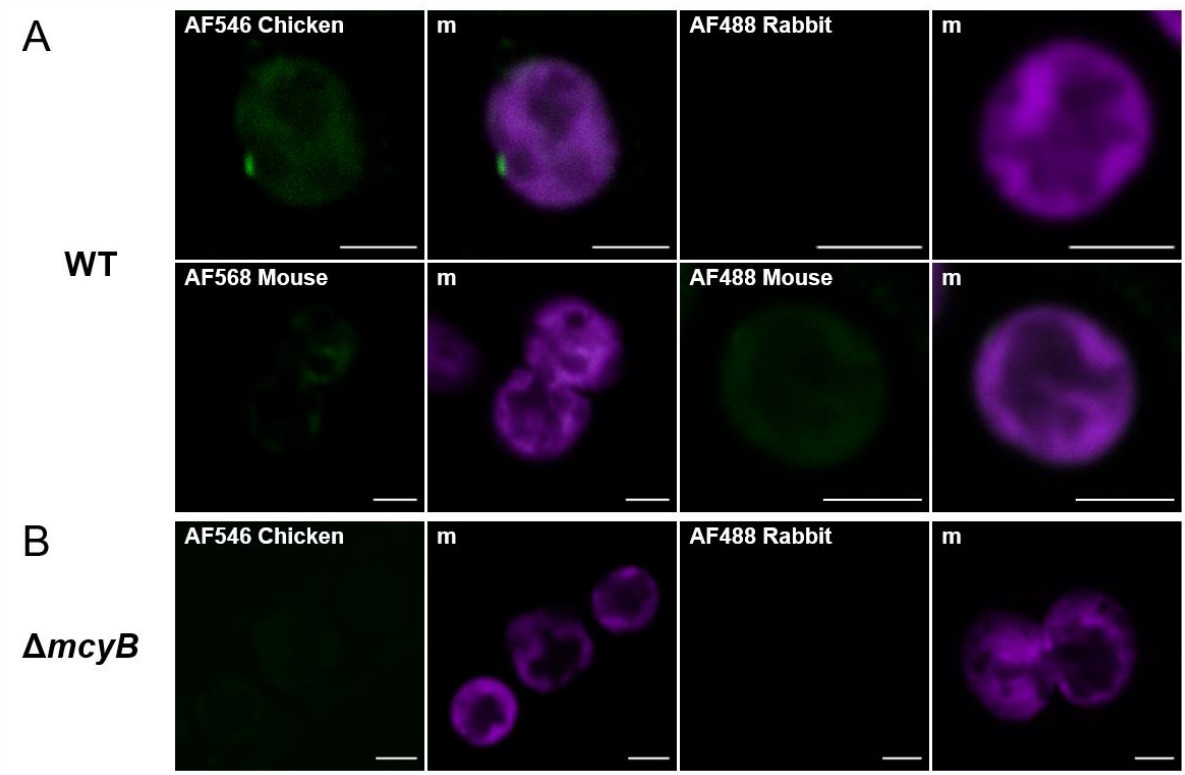

Figure S 1. Immunofluorescence micrographs (IFM) showing the controls of the used secondary antibodies in *M. aeruginosa* wild type (WT) and Δ*mcyB* mutant IFM studies. **A:** Controls for *M. aeruginosa* WT show no specific signals when only the secondary antibodies are applied. Alexa Fluor 546 anti-Chicken was used as the secondary antibody for the visualization of RbcL. Alexa Fluor 488 anti-Rabbit was used as the secondary antibody for the visualization of RbcS, CcmK, McyB and McyF. Alexa Fluor 568 - and 488 anti-Mouse were used as the secondary antibodies for the visualization of microcystin. m: merged image. **B:** Controls for *M. aeruginosa* Δ*mcyB* mutant show no specific signals when only the secondary antibodies are applied. Alexa Fluor 546 anti-Chicken was used as the secondary antibody for the visualization of RbcL. Alexa Fluor 488 anti-Rabbit was used as the secondary antibody for the visualization of RbcS and CcmK. m: merged image. Scale bar in all images: 2µm.

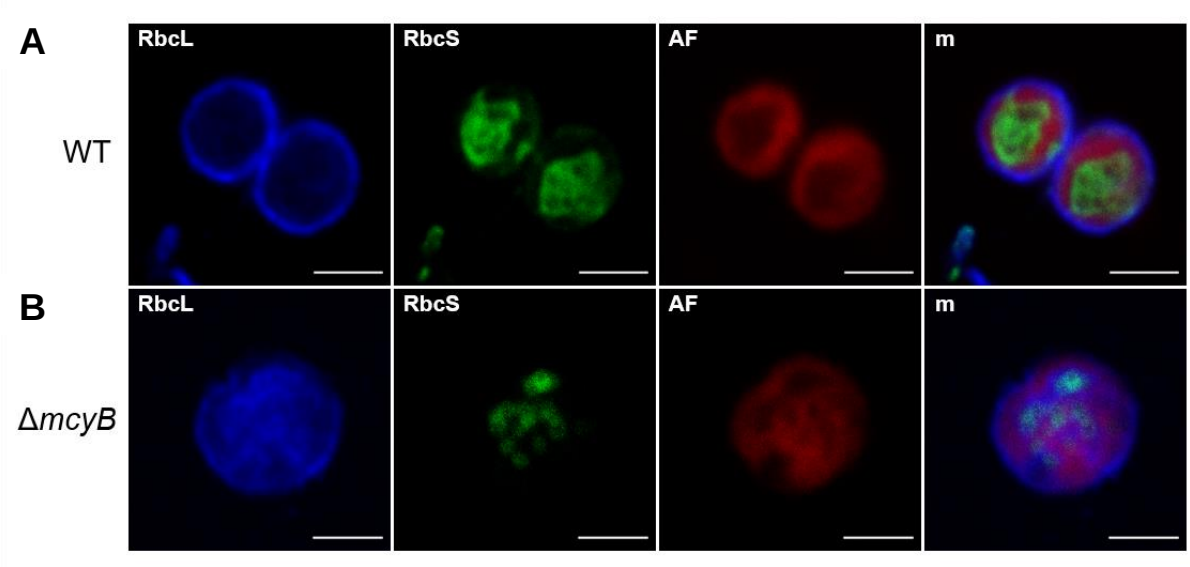

Figure S 2. Co-Hybridization of high-light treated cells of **(A)** *M. aeruginosa* WT and **(B)** Δ*mcyB* with RbcL and RbcS antibodies (OD_{750}: 0.6). RbcL is visible in the blue fluorescence channel and RbcS is visible in the green fluorescence channel. The fluorescence channel is indicated in the top left corner of each image. AF=phycobilisome auto fluorescence, m=merged image from the 3 fluorescence channels. The scale bar is 2 µm.

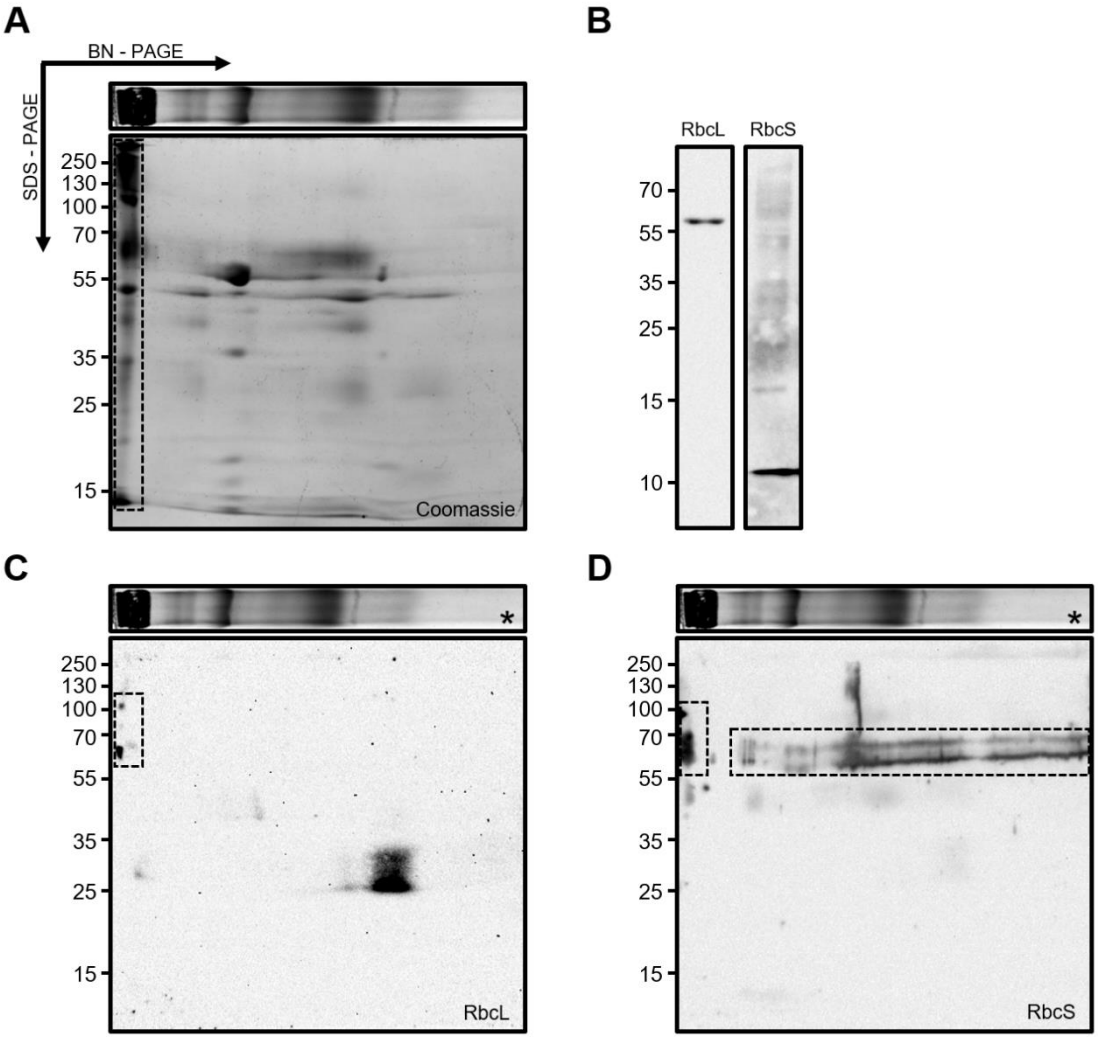

Figure S 3. Blue-Native (BN)-SDS-PAGE analysis of thylakoid membrane preparations from *M. aeruginos*a PCC 7806 WT. A) Proteins were separated by BN-PAGE and SDS-PAGE analysis in the first and second dimension, respectively. B) One-dimensional SDS-PAGE analysis of thylakoid membrane protein fractions treated with 4M urea reveals presence of monomeric RbcS along with lower amounts of RbcL. C) 2D-Western Blot with anti-RbcL antibody reveals presence of RbcL in a high-molecular weight complex along with degraded RbcL in smaller size fraction. D) 2D-Western Blot with anti-RbcS antibody reveals presence of oligomeric SDS-stable RbcS in high molecular weight complex (HMW) along with oligomeric RbcS in various size fractions suggesting that RbcS sticks unspecific to the membrane beside of its involvement in the HMW complex. The HMW complex comprising both RbcL and RbcS and RbcL-free RbcS fractions are highlighted with frames. The Coomassie-stained copy of the first-dimension gel shown in Fig. 2A that was run in parallel with the BN gel stripes used for Figs. 2C and D is shown for orientation and indicated with an asterisk. Note that thylakoid membrane preparations may also contain proteins associated with the cytoplasmic membrane.

7. Deutsche Zusammenfassung

Cyanobakterien können weltweit in einer Vielzahl von ökologischen Nischen gefunden werden. Sie stellen eine Gefahr für Eukaryoten wie Fische oder Säugetiere dar, und können auch die Nutzung von Seen oder Flüssen zu Erholungszwecken oder als Trinkwasserquelle beeinträchtigen, wenn sie an der Wasser-Luft Interphase Blüten bilden. Einer der häufigsten blütenbildenden Cyanobakterien ist der Stamm *M. aeruginosa* PCC7806, welcher in Cyanobakterienblüten auf der ganzen Welt gefunden werden kann.

Im ersten Teil dieser Arbeit wurde die Funktion und mögliche Dynamiken von RubisCO während der Bildung und Aufrechterhaltung von dicht gewachsenen Blüten untersucht. Dafür wurden Schwachlicht-adaptierte *M. aeruginosa* Zellkulturen Starklicht ausgesetzt und deren Reaktion auf dem Protein- und Peptidlevel analysiert. Verwendete Analysemethoden waren Western Blots, Immunofluoreszenz-mikroskopie und Hochleistungsflüssigkeitschromatografie (HPLC). Es konnte aufgezeigt werden, dass unter der angewendeten Starklichtbehandlung große Mengen RubisCO außerhalb der Carboxysomen lokalisiert waren. Dabei konnte RubisCO hauptsächlich direkt unterhalb der zytoplasmatischen Membran in Form von Aggregaten nachgewiesen werden. Diese Aggregate sind möglicherweise Teil eines hypothetischen Calvin-Benson-Bassham Zyklus (CBB) Superkomplexes zusammen mit anderen Enzymen aus der Photosynthese. Dieser Komplex könnte Teil eines alternativen Kohlenstoff-Konzentrationsmechanismus in *M. aeruginosa* sein, welcher eine schnellere und energiesparendere Anpassung der Cyanobakterienblüte an Starklichtstress ermöglicht.

Weiterhin erfolgte die Relokalisation von RubisCO in der Microcystin-freien Mutante Δ*mcyB* verzögert und RubisCO war homogener in der Zelle verteilt im Vergleich zum Wildtyp. Die Ergebnisse dieser Arbeit sind im Einklang mit vorherigen Publikationen zu der Funktion von Microcystin als Schutz gegen Proteinabbau in Folge der Bindung von Microcystin an das jeweilige Protein. Da Δ*mcyB* im Wachstum nicht eingeschränkt war, scheint es möglich, dass andere Cyanopeptoline wie Aeruginosin oder Cyanopeptolin die stabilisierende Funktion von Microcystin gegenüber RubisCO und

den hypothetischen CBB Komplex übernehmen, vor allem in der Microcystin-freien Mutante.

Im zweiten Teil dieser Arbeit wurde die mögliche extrazelluläre Funktion von Microcystin untersucht. HPLC-Analysen zeigen eine starke Zunahme an extrazellulärem Microcystin im Wildtyp als die Zellkultur in die Nachtphase übergegangen ist. Dieser Trend hat sich auch in den folgenden Tag hinein fortgesetzt. Zusammen mit der Zunahme an extrazellulärem Microcystin wurde eine starke Abnahme an proteingebundenem intrazellulärem Microcystin festgestellt, anhand von Western Blot-Untersuchungen. Interessanterweise verringerte sich die Signalstärke der großen Untereinheit von RubisCO (RbcL) im selben Zeitraum im Western Blot. Microcystin Zugabe-Experimente zu *M. aeruginosa* WT und Δ*mcyB* unterstützen diese Beobachtung, da das Western Blot-Signal für sowohl beide Untereinheiten von RubisCO als auch CcmK, ein Hüllenprotein der Carboxysomen, nach der Zugabe von Microcystin stark abnahm. Zusätzlich weist die Fluktuation des Cyanopeptolin-Signals während des Tag-Nacht Zyklus auf eine wichtigere Funktion von Cyanopeptiden abseits von Microcystin hin; als Signalpeptide, sowohl intrazellulär als auch extrazellulär.

Diese Dissertation gibt neue Einsichten in Adaptionsprozesse von *M. aeruginosa* an Starklicht-Bedingungen. Der postulierte alternative Kohlenstoff-Konzentrations-mechanismus, welcher direkt unterhalb der zytoplasmatischen Membran stattfindet, gibt *M. aeruginosa* einen Vorteil gegenüber anderen Cyanobakterien, welche nur den in der Literatur anerkannten Carboxysomen-basierten Kohlenstoff-Konzentrations-mechanismus besitzen. Des Weiteren stärkt die vorliegende Arbeit die Hypothese, dass die eigentliche extrazelluläre Funktion von Microcystin die eines Signalstoffes ist, und nicht die eines antibiotischen Stoffes.

8. Acknowledgements

Als Erstes möchte ich meinen Eltern danken. Mama und Papa, ihr unterstützt mich seitdem ich denken kann. Ihr steht immer mit Rat und Tat zur Seite und steht hinter mir, bei allem was ich mache und angehe. Diese Arbeit wäre ohne eure Unterstützung nicht zustande gekommen.

Danke an meinen Bruder Daniel, für die etlichen Online-Stunden am Nachmittag oder Abend, bei denen ich den Kopf immer wieder frei bekommen habe. Diese Zeit hat mich noch fokussierter für die Arbeit gemacht und war somit auch ein essentieller Teil dieser Arbeit.

Ein ganz besonderer Dank gehört auch Linh. Ohne deine Motivation und Unterstützung wäre die Arbeit nicht in dieser Form zustande gekommen. Vor allem im Schreibprozess warst du mein Anker. Du hast immer die passenden Worte gefunden um mich zu motivieren und ohne dich hätte ich den Corona-Shutdown nicht so gut überstanden. Deine emotionale Unterstützung war und ist Gold wert.

Ein riesiges Dankeschön natürlich auch an Elke und Arthur. Ich hätte mir keine bessere Arbeitsumgebung vorstellen können. Das Projekt hat mich von Anfang an gepackt und hat mich bis zum Ende motiviert, es gut abzuschließen. Ihr habt immer extrem hilfreiches Feedback gegeben, habt immer die positiven Seiten gesehen und dadurch konnte ich mich immer vollkommen auf die Arbeit konzentrieren.

Vielen Dank auch an die gesamte Mibi-Gruppe. Ihr habt eine Arbeitsatmosphäre geschaffen, in der ich mich von Anfang an wohlgefühlt habe. Die gegenseitige Unterstützung habe ich enorm wertgeschätzt. Ihr habt das Labor lebendig und zu einem Ort gemacht, in dem ich gerne Zeit verbracht habe und somit erst die Ergebnisse erhalten konnte, die am Ende diese Arbeit ausmachen.

Ein letzter Dank gehört Otto Baumann und auch den Kollegen aus Rostock, für die durchgeführten Experimente und Analysen und die fachliche Unterstützung zu jeder Zeit.